

Helical Polyacetylene: Asymmetric Polymerization in a Chiral Liquid-Crystal Field

Kazuo Akagi*

Department of Polymer Chemistry, Kyoto University, Katsura, Kyoto 615-8510, Japan

Received May 19, 2009

Contents

1. Introduction	5354	7.1. Chiral Dopants of Crown Ether-Type Binaphthyl Derivatives	5382
1.1. Prologue	5354	7.1.1. Synthesis of CEBDs	5382
1.2. Background of Polyacetylene (PA)	5355	7.1.2. Twisting Power and Specific Rotation of the CEBDs	5383
1.3. Origin of Helical PA (H-PA)	5357	7.1.3. Spiral Morphologies of N*-LCs and H-PAs	5384
Part 1. Chiral Liquid-Crystal Field	5358	8. Control of the Helical Sense	5385
1.		8.1. Chiral Dopants of Bridged- and Nonbridged-Type Binaphthyl Derivatives	5385
2. Asymmetric Reaction Field	5358	8.1.1. Synthesis and Characterization of Chiral Binaphthyl Derivatives	5386
2.1. Chiral Dopants and Chiral Nematic Liquid Crystals (N*-LCs)	5358	8.1.2. Characterization of the N*-LC	5387
2.2. Acetylene Polymerization in N*-LC	5360	8.2. Helical Twisting Directions of N*-LCs and H-PAs	5388
2.3. Characterization of H-PA Film	5360	9. Control of the Helical Twisting Power and Helical Sense	5389
3. Advances in N*-LC Reaction Field	5363	9.1. Chiral Dopants of Double Chirality-Based Binaphthyl Derivatives	5389
3.1. Liquid-Crystalline Binaphthyl Derivatives	5363	9.1.1. Synthesis of Double Chirality-Based Binaphthyl Derivatives	5390
3.1.1. Mesomorphic Properties of Chiral Dopants	5364	9.1.2. Preparation of the N*-LC	5390
3.1.2. Amplification of HTP	5364	9.1.3. Temperature Dependence of N*-LCs	5391
3.1.3. Role of Liquid Crystallinity of Chiral Dopant in Induction of N*-LC	5364	9.2. H-PAs in Helical Pitch and Helical Sense-Controllable N*-LCs	5393
Part 2. Control of the Morphology	5366	9.2.1. Helical Pitch-Controllable N*-LC	5393
2.		9.2.2. Helical Sense-Controllable N*-LCs	5393
4. Control of the Fibril Morphology	5366	Part 4. Extension	5395
4.1. Bundle-Free Fibril Morphology of H-PA	5366	4.	
4.1.1. Highly Twisted Chiral Dopants and N*-LCs	5368	10. Extension of H-PA	5395
4.1.2. Contribution of the HTP and Miscibility of a Chiral Dopant in the Helical Pitch of the N*-LC	5368	10.1. Morphology-Retaining Carbonization for Helical Graphite	5395
4.1.3. Asymmetric Reaction Field Constructed with the N*-LC	5369	11. Conclusions	5397
4.1.4. Synthesis of HP with Bundle-Free Morphology	5370	16. Acknowledgments	5398
5. Orientation-Controllable N*-LC Field	5372	17. References	5398
5.1. Aligned H-PA Synthesized in N*-LC Using Orientation Dopant	5372		
5.1.1. Comprehensive Description of N*-LC Fields and Resultant Products	5372		
5.1.2. Horizontal and Vertical Alignments of N*-LC and H-PA	5375		
5.2. Aligned H-PA Synthesized in a N*-LC under a Magnetic Field	5377		
6. Extension in the N*-LC Reaction Field	5378		
6.1. Polymerization in a N*-LC Including an Asymmetric Center-Type Chiral Dopant	5378		
6.2. Chiral Titanium Catalysts	5380		
Part 3. Control of Helicity	5382		
3.			
7. Control of the Helical Twisting Power	5382		

* E-mail: akagi@star.polym.kyoto-u.ac.jp.

1. Introduction

1.1. Prologue

Because the synthesis of polyacetylene (PA) thin film and the discovery of chemical doping disclosed the uncultivated field of conductive polymers,^{1–3} conductive polymers have been extensively investigated and widely used in such products as electrolytic capacitors and secondary batteries.^{4–6} Today, polymers have become essential for lightweight, high-performance batteries used in notebook computers, cellular phones, and other portable equipment. Much research and development has also been conducted on polymer light-emitting diodes, organic solar cells that are anticipated for



Kazuo Akagi is a Professor of the Department of Polymer Chemistry at Kyoto University with expertise in functional conjugated polymers. His research interests have involved electrically conducting polymers and liquid-crystalline, luminescent, and photoresponsive conjugated polymers, with works focused on the synthesis of helical polyacetylene in the chiral nematic liquid-crystal field. He has also been engaged in development of liquid-crystalline aromatic conjugated polymers with linearly and circularly polarized optoelectronic properties. He graduated from the Department of Hydrocarbon Chemistry of the Faculty of Engineering at Kyoto University and obtained a doctoral degree in 1980. He became a Research Associate at Fukui University in 1982. He became an Assistant Professor in the Institute of Materials Science at University of Tsukuba in 1984 and then was promoted to an Associate Professor in 1991 and a Professor in 1998. He became a Director of Tsukuba Research Center of Interdisciplinary Materials Science in 2003 and a Professor of the Graduate School of Pure and Applied Sciences in 2004. He moved to the present department at Kyoto University in 2006. He was awarded The Divisional Award of The Chemical Society of Japan (1999), NISSAN Science Prize (2000), The Award of the Japanese Liquid Crystal Society for Outstanding Paper (2000), Tsukuba Prize (2001), The Award of the Society of Polymer Science, Japan (2002), and The Commendation for Science and Technology by the Minister of Education, Culture, Sports, Science and Technology, Prizes for Science and Technology (2005). He was awarded the title of Professor Emeritus from the University of Tsukuba (2009). He has been a Head Investigator of Scientific Research in Priority Area entitled "Control of Super-Hierarchical Structures and Innovative Functions of Next-Generation Conjugated Polymers", Grants-in-Aids for Scientific Research in Japan, from 2005 to 2009.

use in next-generation displays, and energy sources.⁶ Conductive polymers are also being studied for their use as materials in molecular devices, called the ultimate electronic devices.⁷ Thus, although many conductive polymers have been developed for various applications, PA is still the highest conductive polymer, showing an electrical conductivity of 10^5 S/cm after iodine doping.^{8,9}

Helical PA (H-PA) is a unique conductive polymer because it has a superhierarchical helical structure forming a spiral morphology, and it is synthesized in an asymmetric reaction field consisting of a chiral nematic liquid crystal, even though an acetylene monomer has no chiral moiety.¹⁰ Despite the helical structure, the relatively high conductivity of 10^3 S/cm allowed us to anticipate that H-PA might be a prototype exhibiting novel electromagnetism properties such as a nanosize polymer solenoid. It is intriguing to elucidate H-PA from an interdisciplinary viewpoint between polymers, liquid crystals (LCs), and synthetic metals.

The purpose of this review is to delineate the current progress of H-PA and the chiral liquid-crystal reaction field for asymmetric polymerization. The goal of this review is to develop a promising method for precise helicity-controllable helical conjugated polymers and also to expand the possibility of application of helical conjugated polymers such as helical graphites.

The review is organized as follows. Section 1 shows a general introduction concerning the background of PA and the origin of H-PA. Part 1, consisting of sections 2 and 3, describes the asymmetric reaction field constructed with a chiral nematic liquid crystal (N*-LC) for synthesizing H-PA. Part 2, consisting of sections 4, 5, and 6, focuses on the control of fibril structure and orientation of the morphology of H-PA. Part 3, consisting of sections 7, 8, and 9, deals with the control of the helical twisting power and helical sense of the N*-LC and H-PA. Part 4, consisting of sections 10 and 11, describes the extension of H-PA, perspective of the N*-LC, and conclusions. The literature cited in the text has been chosen for didactical purposes and cannot reflect the chronology of the research field nor does it claim completeness. The interested reader is referred to the vast amount of quality papers published in this field during the past decade.

1.2. Background of Polyacetylene (PA)

PA is the simplest linear conjugated macromolecule and is representative of conducting polymers.¹¹ Pristine PA is a typical semiconductor, but its electrical conductivity can be varied by over 14 orders of magnitude through doping.^{12,13} The maximum conductivity reported to date is more than 10^5 S/cm, which is comparable to that of copper and gold.^{8,9} Strong interchain interactions give rise to a fibrillar crystal consisting of rigidly π -stacked polymer chains.^{14–16} This makes PA infusible and insoluble in any kind of solvent. This means that the solid-state structure and morphology of PA are determined during polymerization, which is not the case for substituted PAs.^{17–20} The fibril morphology of PA film is randomly oriented, as shown in Figure 1a. The random morphology, as usually encountered in ordinary polymers, depresses the inherent one-dimensionality of the conductive polymer. Several polymerization methods for the macroscopic alignment of the polymer have been developed to achieve higher electrical conductivity with its anisotropic nature.

One approach is the mechanical stretching of an as-grown PA film.^{8,9,21–27} The conductivity of the film is enhanced through a uniaxial alignment of the fibrils associated with the mechanical stretching of the film. It is therefore desirable to develop highly stretchable PA films with high-modulus and high-tensile properties that might prevent the cleavage of fibrils and/or of PA chains during mechanical stretching. In other words, profound mechanical strengths such as Young's modulus and tensile strength are responsible for the uniaxial alignment and hence the electrical conductivity of the stretched film.

Actually, Naarmann and co-workers^{8,29} synthesized highly stretchable PA films using a high-temperature aged Ziegler-Natta catalyst, $\text{Ti}(\text{O}-n\text{-Bu})_4$ and AlEt_3 , dissolved in viscous silicone oil or toluene, and reported high conductivities of 10^5 S/cm after iodine doping. Tsukamoto et al.⁹ modified Naarmann's method using a higher temperature aged catalyst dissolved in decaline and employing acetylene gas under low pressure, and obtained conductivities of higher than 1.2×10^5 S/cm. Akagi et al.^{21,28} developed two solvent-free acetylene polymerization methods: a solvent evacuation method and an intrinsic nonsolvent (INS) one. In the former, cumene, used as a solvent, is evacuated after the high-temperature aging of the catalyst. In the latter, no solvent is used from the preparation and high-temperature aging of the catalyst to the polymerization. PA films synthesized by these

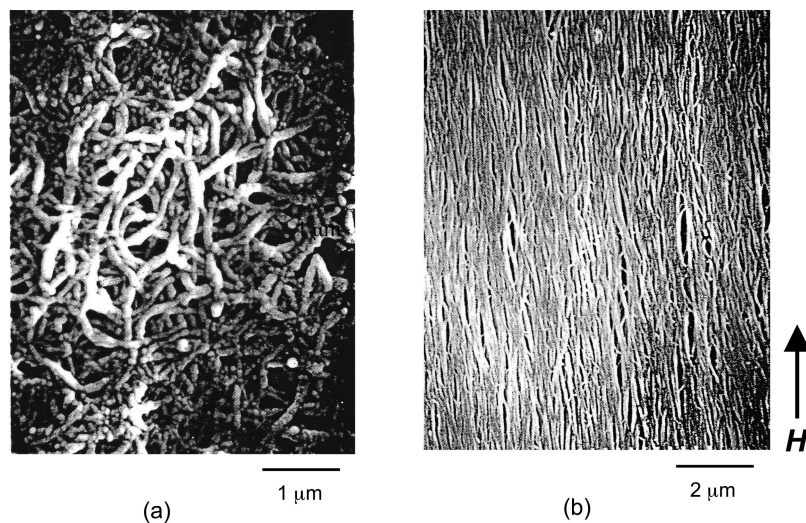


Figure 1. Random fibril morphology of PA film synthesized in toluene (a) and aligned PA film synthesized in nematic LC under magnetic field (b).

methods exhibit extremely high mechanical strengths characterized by a Young's modulus of 100 GPa and a tensile strength of 2.1 GPa, in addition to a high bulk density of more than 1.0 g/cm^3 . The films show reproducible and high conductivities of $2.0\text{--}4.0 \times 10^4 \text{ S/cm}$, which are enhanced by the uniaxial alignment of polymer chains associated with a mechanical stretching of eight to nine times. It can be remarked from these results that the high mechanical strength is a prerequisite for the achievement of high electrical conductivity, and that in the INS polymerization, the co-catalyst of AlR_3 , by virtue of its liquidity, plays the role of a solvent toward catalytically active complexes formed between $\text{Ti}(\text{OR})_4$ and AlR_3 , which guarantees the homogeneity of the catalyst system in spite of the absence of solvent.

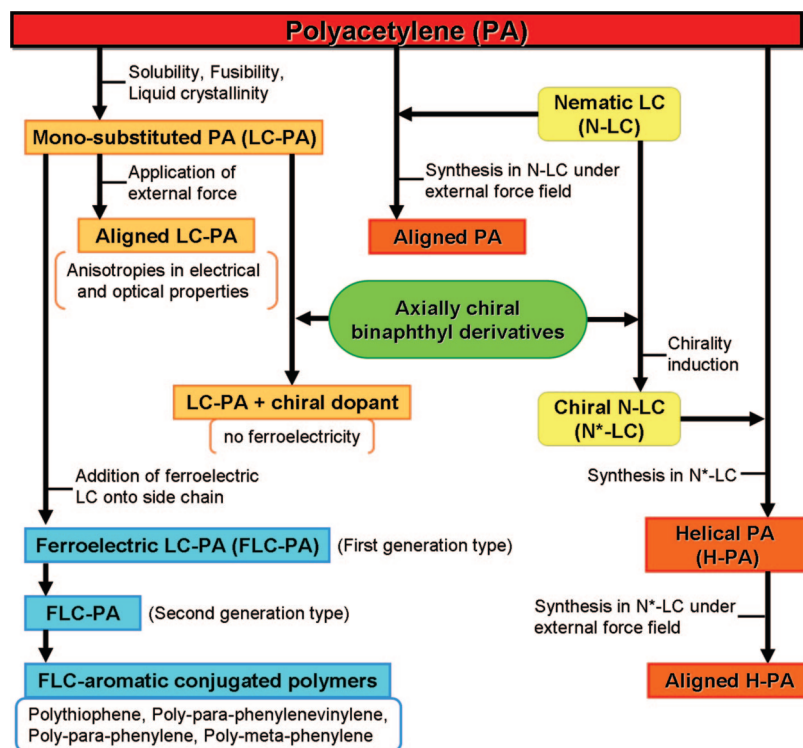
Another approach is to introduce a liquid-crystal (LC) group into the side chain and then to align the LC-substituted polymer under an external force such as shear stress, rubbing, or a magnetic field.^{30–43} Although PA is the most conducting polymer, it is insoluble and infusible. This prevents us from explicitly evaluating its molecular weight and conjugation length and also processing it in solution, as in casting. The introduction of alkyl or aromatic substituents into a PA chain makes the polymer soluble in organic solvents when the alkyl chain length is long enough, i.e., with hexyl, pentyl, and octyl groups. However, the main chain of the polymer is still randomly oriented even in substituted PA, which further depresses the observed electrical conductivity of this polymer.

If the substituent is a LC group, the polymer not only is soluble in organic solvents but also can be aligned by spontaneous orientation of the LC group. Besides, it can be macroscopically oriented by an external perturbation, such as shear stress, an electric field, or a magnetic force field. As a result, the main chain is aligned following the orientation of the LC side chain. This means that a monodomain structure of the LC phase is constructed at the macroscopic level. Under such a circumstance, the polymer is expected to show higher electrical conductivity than with a random orientation. At the same time, one can control the macroscopic orientation and, hence, the electrical conductivity of the polymers by an external force. The LC PA derivatives were synthesized using both a Fe-based Ziegler–Natta catalyst and a Mo-based metathesis catalyst.^{30–34,37–39} The polymers showed an enantiotropic smectic A phase, by virtue of the spontaneous orientation of LC side chains

composed of phenylcyclohexyl or biphenyl mesogenic moieties. The electrical conductivities of the polymers were $10^{-8}\text{--}10^{-7} \text{ S/cm}$ upon iodine doping of the cast films. The alignment of the polymer chain, accompanied by the side-chain orientation in an external magnetic force of $0.7\text{--}1.0 \text{ T}$, increased the conductivities to 10^{-6} S/cm and gave rise to notable electrical anisotropies. It should be remarked that the substituted PAs, including LC ones, have lower electrical conductivities than nonsubstituted PA. The large difference in conductivity between the substituted and nonsubstituted PAs can be rationalized by taking account of two factors such as intrachain and interchain conductivities. In cases of the substituted PAs, the smaller degree of coplanarity of the main chain arising from steric repulsions between substituents results in a higher ionization potential and a lower electron affinity. This situation leads to an increase of the band gap (a decrease in generation of charge carrier such as a hole) and a narrowing of the π -electron valence band (a decrease of mobility of the charge carrier due to an increased localization), which makes the intrachain conductivity of the substituted PA much lower than that of nonsubstituted PA. Besides, the main chains of the substituted PA are more largely separated from each other because of the substituents being side chains compared to those of the nonsubstituted PA, which suppresses an interchain hopping of the charge carriers to cause a lowering in interchain conductivity.

The third approach is a direct alignment of the film using a liquid crystal as an anisotropic solvent for acetylene polymerization under an external perturbation such as gravity flow and magnetic force field.^{44–48} This approach affords an alignment of even ultrathin films with semitransparency that is suitable for measurements of nonlinear optics.⁴⁹ The macroscopically aligned PA films prepared in a nematic liquid crystal under the gravity flow and magnetic field show high conductivities of 10^4 S/cm after iodine doping, and anisotropies of ca. 5 defined as a ratio of parallel-to-perpendicular to the aligned fibril direction (Figure 1b). The unexpectedly small anisotropy is attributed to the relatively high conductivity in the perpendicular direction. This is because the aligned film has highly condensed fibril morphology and hence the interchain and even interfibril hopping of the charged carrier are largely enhanced. The degree of alignment of the film is governed by that of the liquid crystal used as the solvent. That is, the morphology and therefore

Scheme 1. Overview of the Origins of H-PA as Well as the Related Conjugated Polymers



the macroscopic properties of the film are crucially dependent on the anisotropic polymerization field.^{50,51} This situation is common to an epitaxial polymerization, where acetylene polymerization is carried out on the substrate crystal with a homologous isomorphous compound such as naphthalene, anthracene, biphenyl, or terphenyl.⁵² The fibril orientation is strongly dependent on the lattice matching between PA and the substrate crystals.

1.3. Origin of Helical PA (H-PA)

It has been generally accepted that PA has a planar structure, irrespective of the *cis* and *trans* forms, because of the π -conjugation between the sp^2 hybridized carbon atoms in the polymer chain.¹¹ If it were possible to modify such a planar structure of PA into a helical one,⁵³ one might expect novel magnetic and optical properties.^{54–56} Here, we review the polymerization of acetylene in an asymmetric reaction field constructed with N^* -LCs and show that it is possible to synthesize PA films formed by helical chains and fibrils.^{10,57–59} The polymerization mechanism giving helical structure from primary to higher order and hierarchical spiral morphology is also discussed. It is useful to first give an accounting of the initial synthesis of H-PA that is anecdotal in nature. The overview of the origins of H-PA, as well as the related conjugated polymers, is shown in Scheme 1.

In the early 1990s, new types of conjugated polymers bearing liquid-crystalline groups in side chains were synthesized. The polymers synthesized first were monosubstituted PAs with liquid crystallinity and were abbreviated as LC-PAs.^{30–43} The LC-PAs were soluble in organic solvents and fusible, and they showed thermotropically smectic phases with an enantiotropic nature. Subsequently, the LC-PAs were macroscopically aligned through shear stress, rubbing, or a magnetic force field under LC phases.^{60,61} The aligned LC-PAs exhibited anisotropies in electrical conductivities and optical properties. However, the macroscopic alignment of

the polymers was time-consuming because of their high viscosities, which was inevitable for macromolecules and polymers. This made it difficult to achieve control of the alignment or the dynamic switching of anisotropic conductivities and linearly polarized optical properties by means of external forces.

One of the promising approaches to solve this problem was to add ferroelectricity to the LC-PAs since this should enable a quick response to the electric field by virtue of the strong interaction between the spontaneous polarization and the electric field. Thus, the ferroelectric LC (FLC) group was designed and synthesized, where an asymmetric carbon was neighbored to a polarized moiety composed of a carbonyl group with a mesogenic biphenyl group core. The FLC-PA derivative, bearing the FLC group in the side chain, showed a chiral smectic C (SmC^*) phase necessary for generation of the ferroelectricity.⁶² However, the temperature region giving the SmC^* phase was 5 °C, i.e., from 95 to 100 °C. Such a narrow temperature region was less practical for the achievement of the macroscopic alignment and the dynamic switching using an electric force field under the SmC^* phase.

It should be noted that FLC-PA with a wider temperature region of SmC^* phase was successfully synthesized afterward by using a novel FLC group, which replaced the carbonyl group with a highly polarized fluorine moiety and three-membered phenylene rings for a rigid mesogenic core.^{63,64} Other FLC conjugated polymers such as polythiophene,^{65–67} poly-*para*-phenylenevinylene,⁶⁸ and poly-*para*-phenylene or poly-*meta*-phenylene⁶⁹ followed the synthetic development of the FLC-PA.

An alternative attempt to prepare the FLC-PA was made by adding a chiral compound to the LC-PA to induce chirality since it has been known that the FLC compound could be easily prepared by the addition of small amounts of a chiral inducer (chiral dopant). To do this, novel axially chiral binaphthyl derivatives with highly helical twisted

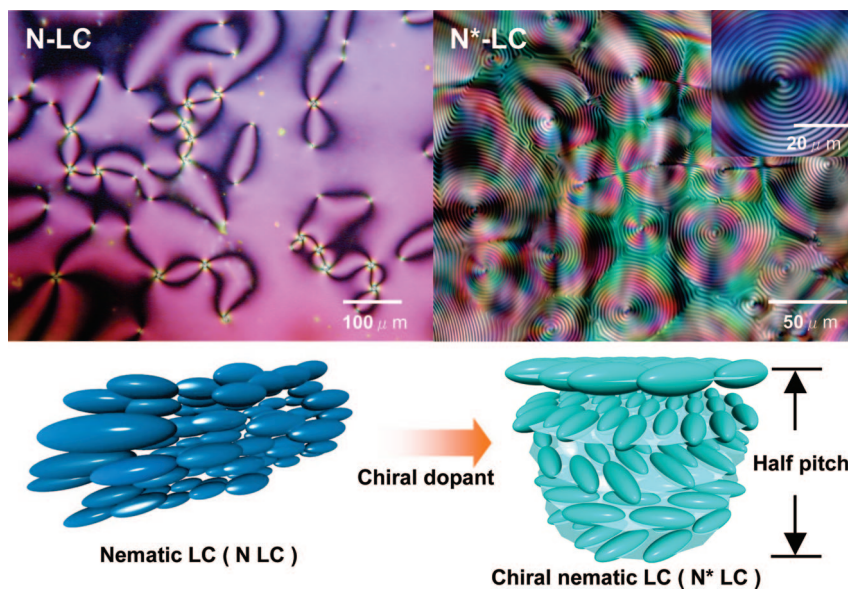


Figure 2. N*-LC induced by an addition of chiral dopant into nematic LC. Schlieren texture (left) and fingerprint texture (right) are observed for nematic and N*-LCs, respectively, in a polarized optical microscope.

powers were synthesized by introducing LC groups composed of phenylcyclohexyl (PCH) mesogenic cores into the 2- and 2'-positions of the binaphthyl rings, as will be mentioned later. The chiral binaphthyl derivative was added as a chiral dopant (chiral inducer) to the LC-PA. However, the prepared mixture failed to show the SmC* phase necessary for the generation of ferroelectricity. This is because the chirality induction giving the SmC* phase is possible only when the parent LC compound has a SmC phase, and LC-PA has a SmA rather than a SmC phase.

At this point, it was required to consider another possibility for the usage of the chiral binaphthyl derivative. It was helpful to remember that the highly aligned PA film was synthesized through acetylene polymerization in macroscopically oriented nematic liquid crystal (N-LC) used as an anisotropic solvent.^{44–48} It has been elucidated that the formation of directly aligned PA is due to a so-called epitaxial growth,⁵² where acetylene is interfacially polymerized through duplication of the macroscopically oriented morphology of the N-LC. Taking into account the above experimental results, one can hypothesize that if the N-LC could be twisted in a one-handed direction, as seen in a chiral nematic (N*) or a cholesteric LC, the PA synthesized therein might also be twisted or screwed to form a peculiar structure.

Thus, the chiral binaphthyl derivative was used as a chiral dopant (chiral inducer) and added to the N-LC to prepare an induced N*-LC that might be available for asymmetric reaction field. The PA film synthesized in the N*-LC was examined with a scanning electron microscope (SEM). Very interestingly, it was found that the PA fibrils in certain regions of the film are loosely bundled and slightly twisted to form swirls, though those in the main region of the film show a randomly oriented fibril morphology as usually seen in ordinary films synthesized in organic solvent. The finding of the slightly twisted and swirled fibrils in a SEM photograph became a starting point to pursue the H-PA. More than 1 year was required to optimize the experimental conditions that make it reproducible to synthesize the H-PA film with well-controlled spiral morphology in each domain.

Part 1. Chiral Liquid-Crystal Field

2. Asymmetric Reaction Field

2.1. Chiral Dopants and Chiral Nematic Liquid Crystals (N*-LCs)

The N*-LC to be used as an asymmetric solvent is prepared by adding a small amount of chiral compound, as a chiral dopant, into N-LC (Figure 2). The formation of N*-LC is recognized when a Schlieren texture characteristic of nematic LC changes into a striated Schlieren or a fingerprint texture in viewing with a polarized optical microscope (POM). The distance between the striae corresponds to a half helical pitch of the N*-LC. Note that as the degree of twist in the N*-LC increases, the helical pitch observed in POM decreases.

The helical pitch of the N*-LC can be adjusted by two methods: (i) changing the concentration or (ii) the twisting power of the chiral dopant.⁷⁰ However, the mesophase temperature region of the N*-LC is affected by changing the concentration of the chiral dopant. That is, it becomes narrow as the concentration increases, and finally, the mesophase is destroyed when the concentration approaches a critical value.^{71–74} Owing to the limitation of the concentration method, an alternative approach of utilizing the chiral compound with large twisting power was adopted. Axially chiral binaphthyl derivatives were used as chiral dopants as they have been reported to possess larger twisting powers than asymmetric carbon-containing chiral compounds. The N*-LCs using the latter chiral compounds will be presented later.

(*R*)- and (*S*)-1,1'-binaphthyl-2,2'-di[*para*-(*trans*-4-*n*-pentylcyclohexyl)phenoxy-1-hexyl]ether were synthesized through the Williamson etherification reactions of chiroptical (*R*)-(+)- and (*S*)-(–)-1,1'-bi-2-naphthols, respectively, with phenylcyclohexyl derivatives. The products will be hereafter abbreviated as (*R*)- and (*S*)-PCH506-Binol (Figure 3). The substituent is composed of phenylcyclohexyl (PCH) moiety, *n*-pentyl group (the number of carbons, 5), and hexameth-

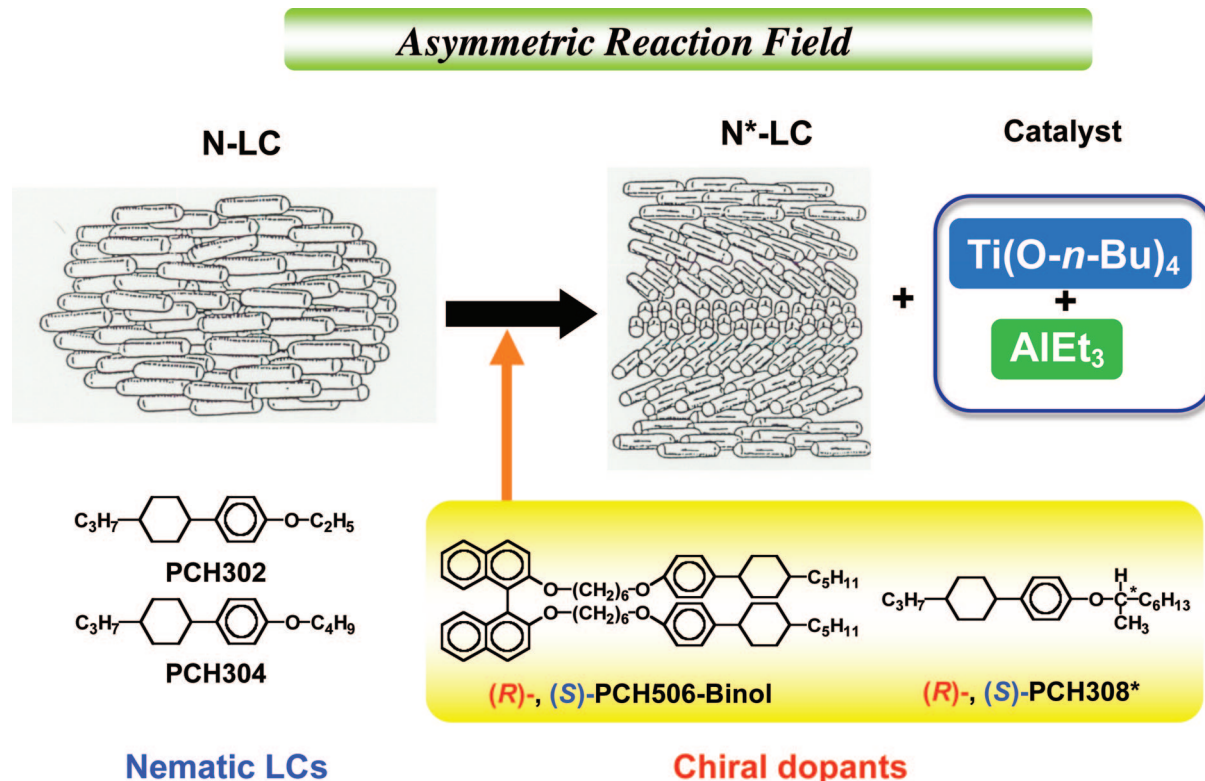


Figure 3. Asymmetric reaction field for acetylene polymerization prepared by dissolving Ziegler–Natta catalyst, $\text{Ti}(\text{O}-n\text{-Bu})_4\text{-AlEt}_3$, into the $\text{N}^*\text{-LC}$. The $\text{N}^*\text{-LC}$ includes an axially chiral binaphthyl derivative, or asymmetric carbon-containing chiral compound.

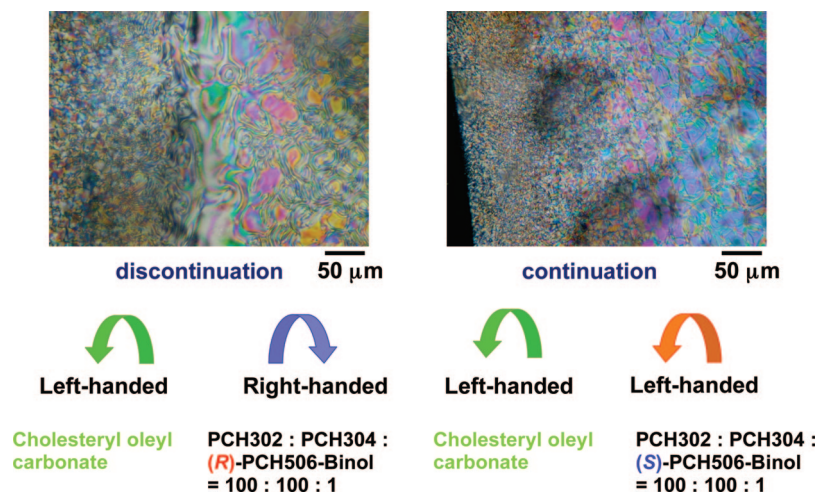


Figure 4. Miscibility test between the $\text{N}^*\text{-LC}$ induced by (*R*-) or (*S*-)PCH506-Binol and the standard LC, cholesteryl oleyl carbonate of left-handed screw direction.

ylene chain linked with an ether-type oxygen atom, $[-(\text{CH}_2)_6\text{O}-, 06]$, and thus abbreviated as PCH506.

To prepare an induced $\text{N}^*\text{-LC}$, 5–14 wt % of (*R*-) or (*S*-)PCH506-Binol was added as a chiral dopant to the equimolar mixture of the nematic LCs 4-(*trans*-4-*n*-propylcyclohexyl)ethoxybenzene (PCH302) and 4-(*trans*-4-*n*-propylcyclohexyl)butoxybenzene (PCH304). The PCH506 substituent group in the (*R*-) and (*S*-)PCH506-Binol enhances the miscibility between the nematic LC mixture and the binaphthyl derivative used as the chiral dopant. Usage of similar substituent with a shorter methylene spacer such as PCH503 or normal alkyl substituent gave insufficient miscibility, yielding no chiral nematic phase.

In polarizing optical micrographs of the mixture of PCH302, PCH304, and (*R*-)PCH506-Binol (abbreviated as

(*R*-1) and that of PCH302, PCH304, and (*S*-)PCH506-Binol (abbreviated as (*S*-1), a striated Schlieren or fingerprinted texture characteristic of $\text{N}^*\text{-LC}$ phases is observed (Figure 2). Cholesteryl oleyl carbonate is known to be a left-handed $\text{N}^*\text{-LC}$, and therefore it is available as a standard LC for a miscibility test with the present LCs. The miscibility test method is based on the observation of the mixing area between the $\text{N}^*\text{-LC}$ and the standard LC in POM, where the screw direction of the standard LC is known. If the screw direction of the $\text{N}^*\text{-LC}$ is the same as that of the standard LC, the mixing area will be continuous. Otherwise, it will be discontinuous as a Schlieren texture of the $\text{N}^*\text{-LC}$.

As shown in Figure 4, the mixture of ((*R*-1)- $\text{N}^*\text{-LC}$ and cholesteryl oleyl carbonate lost the striae characteristic of a chiral nematic phase in the POM, yielding instead features

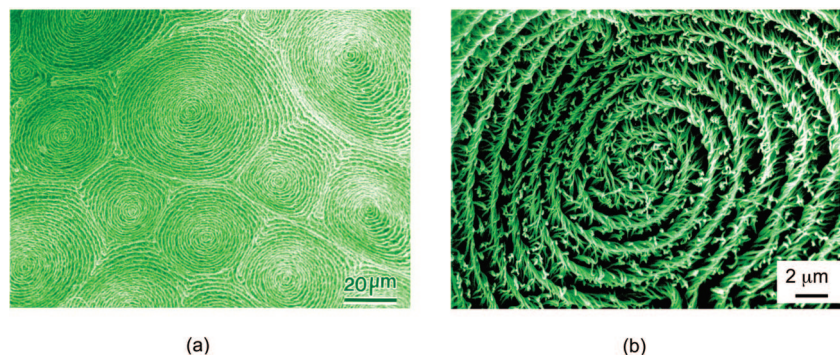


Figure 5. Hierarchical spiral morphologies of H-PA film. Parts (a) and (b) show scanning electron microscope (SEM) photographs of multidomain spiral morphology and left-handed screwed bundles of fibrils in a domain, respectively.

corresponding to an ordinary nematic phase. In contrast, the mixture of ((*S*)-1)-N*-LC and cholesteryl oleyl carbonate showed no change in optical texture, keeping a chiral nematic phase. The results demonstrate that the screw directions of the ((*R*)-1)- and ((*S*)-1)-N*-LCs are opposite to and the same as that of cholesteryl oleyl carbonate, respectively. Namely, they are right-handed and left-handed N*-LCs, respectively.

2.2. Acetylene Polymerization in N*-LC

First, it should be noted that although each component (PCH302 or PCH304) shows a LC phase, the LC temperature region is very narrow, i.e., less than 1–2 °C. This is not suitable for acetylene polymerization in an N or N*-LC reaction field because the exothermal heat evoked during the acetylene polymerization would raise the temperature inside a Schlenk flask and easily destroy the LC phase, becoming an isotropic one. Hence, the LC mixture is prepared by mixing two equimolar LC components. In the LC mixture, the nematic–isotropic temperature, T_{N-I} , and the crystalline–nematic temperature, T_{C-N} , might be raised and lowered, respectively. In fact, the mixture exhibited the LC phase in the region from 20 to 35 °C. Subsequently, the change of T_{N-I} upon an addition of $\text{Ti}(\text{O}-n\text{-Bu})_4\text{-AlEt}_3$ catalyst was examined through differential scanning calorimeter (DSC) measurement. Taking into account the effect of supercooling for LCs, the catalyst solution consisting of the LC mixture and the chiral dopant was found available for room temperature polymerization ranging from 5 to 25 °C. This sufficiently wide temperature region enabled us to perform the acetylene polymerization in the N*-LC phase.

The Ziegler–Natta catalyst consisting of $\text{Ti}(\text{O}-n\text{-Bu})_4$ and AlEt_3 was prepared using the ((*R*)-1)- or ((*S*)-1)-N*-LC as a solvent (Figure 3). The concentration of $\text{Ti}(\text{O}-n\text{-Bu})_4$ was 15 mmol/L, and the mole ratio of the cocatalyst-to-catalyst, $[\text{AlEt}_3]/[\text{Ti}(\text{O}-n\text{-Bu})_4]$, was 4.0. The catalyst solution was aged for 0.5 h at room temperature. During the aging, the N*-LC containing the catalyst showed no noticeable change in optical texture, and only a slight lowering of the transition temperature by 2–5 °C: The transition temperature between the solid and chiral nematic phases was 16–17 °C, and that between the chiral nematic and isotropic ones was 30–31 °C. No solidification was observed down to –7 °C as a result of supercooling. Thus, the ((*R*)-1)- and ((*S*)-1)-N*-LCs are confirmed to be chemically stable to the catalyst. These LCs can therefore be used as asymmetric solvents for acetylene polymerization.

Acetylene gas of six-nine grade (99.9999% in purity) was used without further purification. The apparatus and procedure employed were similar to those in earlier studies,^{44–48}

except for the polymerization temperature. Here, the polymerization temperature was kept between 17 and 18 °C to maintain the chiral nematic phase, by circulating cooled ethanol through an outer flask enveloping the Schlenk flask. The initial acetylene pressure was 11.6–22.6 Torr and the polymerization time was 10–43 min. After polymerization, PA films were carefully stripped from the container and washed with toluene several times under argon gas at room temperature. The films were dried through vacuum pumping on a Teflon sheet and stored in a freezer at –20 °C.

2.3. Characterization of H-PA Film

SEM images of PA films show that multidomains of spiral morphology are formed (Figure 5a), and each domain is composed of a helical structure of a bundle of fibrils with a one-handed screwed direction (Figure 5b). The multidomain-type fibril morphology of PA seems to replicate that of the N*-LC during the interfacial acetylene polymerization.

A closer observation of SEM images indicates that H-PAs synthesized in the ((*R*)-1)- and ((*S*)-1)-N*-LCs form the screwed bundles of fibrils and even screwed fibrils with left-handed and right-handed directions, respectively (Figure 6). This result implies that the screw direction of H-PA is controllable by choosing the helicity, i.e., optical configuration of the chiral dopant, so far as the N*-LC induced by the chiral dopant is employed as an asymmetric polymerization solvent. Besides, it is of keen interest that the screw directions of bundle and fibrils are opposite to those of the ((*R*)-1)- and ((*S*)-1)-N*-LCs used as solvents (see Figure 4). This is an unexpected and even surprising result, requiring a sound interpretation, which will be discussed below.

The helical pitch of the N*-LC depends on the helical twisting power of the chiral dopant, and also its concentration and optical purity. This means that the helical pitch of the PA chain can also be varied by changing the helical twisting power of the chiral dopant. Another axially chiral dopant, (*R*)- or (*S*)-6,6'-PCH506-2,2'-Et-Binol, abbreviated as (*R*)- or (*S*)-2 (Scheme 2),^{75,76} gave a shorter helical pitch of N*-LC by 0.3 μm than the corresponding (*R*)- or (*S*)-PCH506-Binol. Acetylene polymerizations using these sorts of highly twisted N*-LCs, designated ((*R*)-2)- and ((*S*)-2)-N*-LCs, afforded clearer spiral morphologies consisting of helical bundles of fibrils (Figure 7). Namely, these bundles are aligned parallel to each other in the microscopic regime, and form spiral morphologies in the macroscopic regime. It is noteworthy that the hierarchical higher order structures observed in Figure 7 resemble the helical self-assembled microstructure of biological molecules such as lipids,⁷⁷ but they, as well as those of Figure 5, are rarely formed in

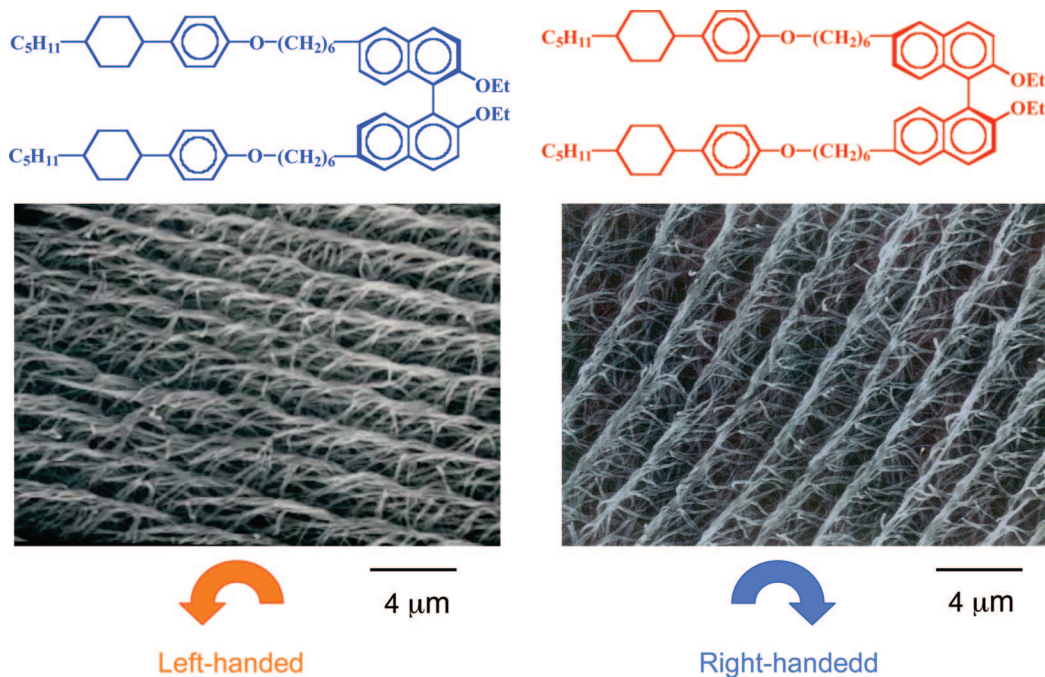
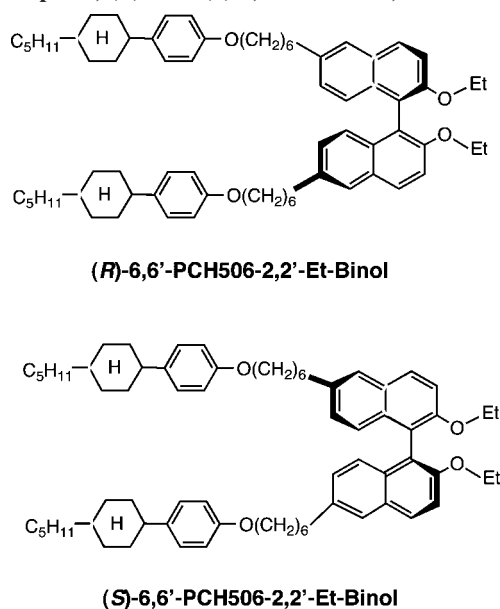


Figure 6. SEM photographs of H-PA films synthesized in the N^* -LCs including (*R*)- and (*S*)-PCH506-Et-Binol. The left- and right-handed screw directions of H-PAs are determined by the chirality of the chiral dopants with (*R*)- and (*S*)-configurations, respectively.

Scheme 2. Axially Chiral Binaphthyl Derivatives Used as Chiral Dopants, (*R*)- and (*S*)-6,6'-PCH506-2,2'-Et-Binol



synthetic polymers. This indicates a validity of N^* -LC as a template polymerization medium for controlling a higher order structure of synthetic polymer.

The bundles of fibrils for H-PAs synthesized in the ((*R*)-2)- and ((*S*)-2)- N^* -LCs are screwed left-handed and right-handed, respectively: The screw directions of H-PA are opposite to those of the corresponding ((*R*)-2)- and ((*S*)-2)- N^* -LCs whose directions are confirmed to be right-handed and left-handed, respectively, through the miscibility test with cholesteryl oleyl carbonate. This is the same situation as the case of the ((*R*)-1)- and ((*S*)-1)- N^* -LCs including (*R*)- and (*S*)-PCH506-Binol.

It has been elucidated so far that the PA chains propagate along the director (an averaged direction for the LC molecules within a domain) of the N^* -LC. Since the helical

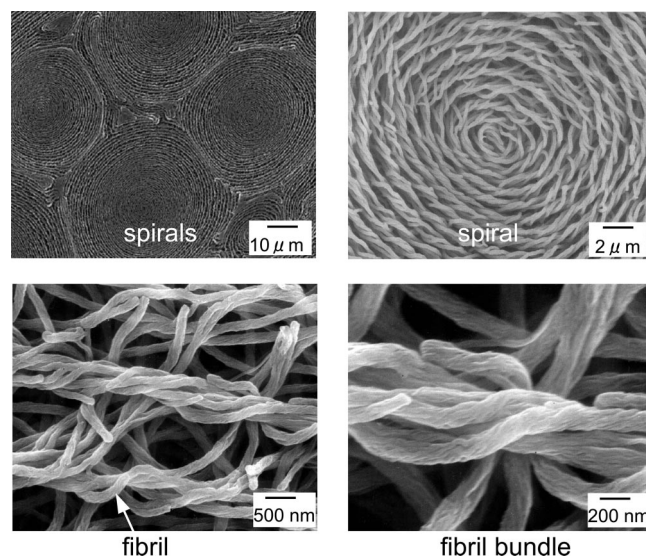


Figure 7. SEM photographs showing hierarchical spiral morphology of H-PA film synthesized in the N^* -LCs including (*R*)-6,6'-PCH506-2,2'-Et-Binol. The multidomain spiral morphology consists of one-handed screwed bundles of fibrils. The bundle is composed of helically twisted fibrils.

axis of PA is parallel to the PA chain, and the director of the N^* -LC is perpendicular to the helical axis of N^* -LC, the helical axis of PA is perpendicular to that of N^* -LC. Taking these aspects into account, one can describe a plausible mechanism for interfacial acetylene polymerization in the N^* -LC, as shown in Figure 8. In the case of a right-handed N^* -LC, for instance, the PA chain would propagate with a left-handed manner, starting from the catalytic species, but not with a right-handed one. This is because the PA chains with the opposite screw direction to that of the N^* -LC could propagate along the LC molecules, but those with the same direction as that of the N^* -LC would encounter LC molecules, making the propagation stereospecifically impossible. The detailed mechanism of acetylene polymerization in N^* -LC has to be elucidated.

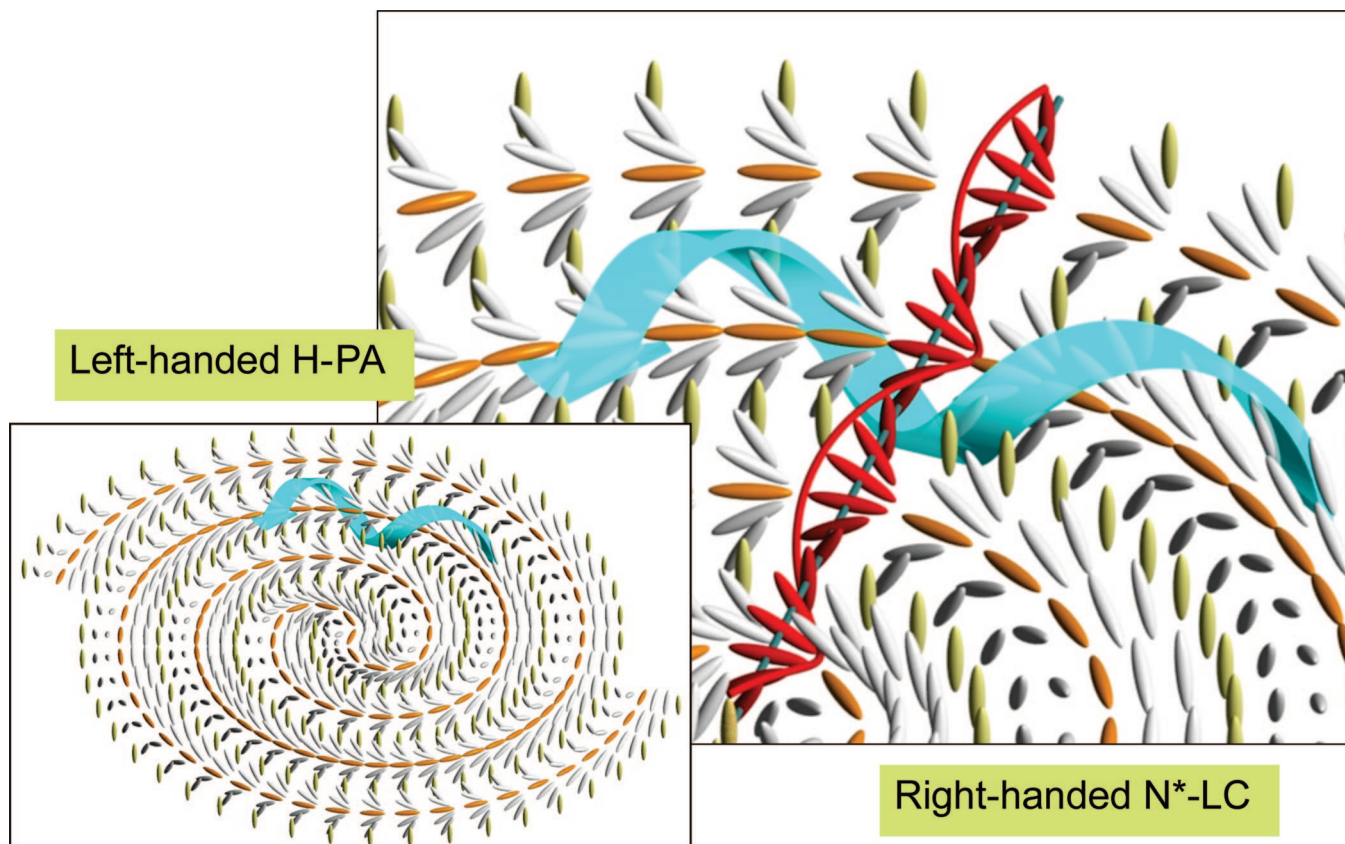


Figure 8. Schematic representation of mechanism for acetylene polymerization in the N*-LC. The H-PA with left-handed screw direction grows starting from the catalytic species in the right-handed N*-LC.

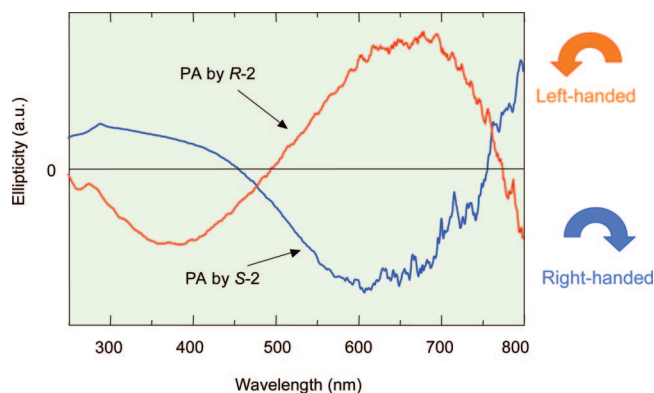


Figure 9. CD spectra of H-PA films. The PA films synthesized in the ((*R*)-2)- and ((*S*)-2)-N*-LCs including (*R*)- and (*S*)-6,6'-PCH506-2,2'-Et-Binol are designated as "PA by (*R*)-2" and "PA by (*S*)-2", respectively.

In circular dichroism (CD) spectra of the PA thin films synthesized under the ((*R*)-2)- and ((*S*)-2)-N*-LCs, positive and negative Cotton effects are observed respectively in the region from 450 to 800 nm corresponding to $\pi \rightarrow \pi^*$ transition of PA chain (Figure 9), despite the absence of a chiroptical substituent in side chains. This indicates that the PA chain itself is helically screwed. It is evident that the above Cotton effect is not due to the chiral dopant [(*R*)- or (*S*)-6,6'-PCH506-2,2'-Et-Binol] because the Cotton effect of the chiral dopant is observed only at shorter wavelengths such as 240–340 nm.

From the results mentioned above, it can be stated that left-handed and right-handed H-PA chains are formed in (*R*)- and (*S*)-N*-LCs, respectively, and that these helical chains are bundled through van der Waals interactions to form

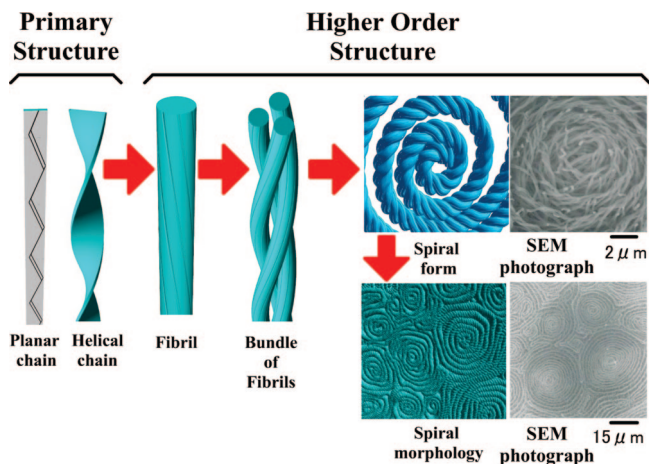


Figure 10. Hierarchical helical structures from primary to higher order in H-PA.

helical fibrils with screw directions opposite to those of the N*-LCs. The bundles of fibrils further form the spiral morphology with various sizes of domains (Figure 10).

The dihedral angle between neighboring unit cells, ($-\text{CH}=\text{CH}-$), of the H-PA was estimated to be from 0.02° to 0.23° . Although such a very small dihedral angle may allow us to regard the present PA as an approximately planar structure, the polymer is rigorously screwed by a one-handed direction with the nonzero dihedral angle. The present H-PA films have high trans contents of 90% and become highly conductive upon iodine doping. In fact, the electrical conductivities of the doped films are $1.5\text{--}1.8 \times 10^3 \text{ S/cm}$ at room temperature, which are comparable to those of metals. The iodine-doped PA showed the same Cotton effect as that

of nondoped PA, although the CD peak was slightly shifted to shorter wavelengths. This indicates that the helical structure is preserved even after iodine doping. Furthermore, CD and X-ray diffraction measurements showed that the helical structure was also preserved after heating up to 150 °C (which corresponds to the isomerization temperature from cis to trans form). The most stable structure of PA is the planar one. However, since the PA is actually insoluble and infusible, the helical structure formed during the polymerization can be preserved even if it is washed by toluene or thermally heated below the isomerization temperature. In other words, the insolubility and infusibility of PA are indispensable for preserving the metastable helical structure.

Here, it is worthwhile to emphasize the following experimental results. First, acetylene polymerization was carried out under a N*-LC environment using the equal weighted mixture of PCH302 and PCH304, but without the chiral dopant. The PA film showed neither helical morphology in the SEM photograph nor Cotton effect in the CD spectrum: The morphology observed was composed of fibrils that were locally aligned because of the spontaneous orientation of the LC solvent. This has also been confirmed in previous works.¹² Second, acetylene polymerization was performed in toluene and a small amount (less than 10%) of the chiral dopant. The PA synthesized showed usually encountered a randomly oriented fibrillar morphology, but not a helical one. At the same time, the PA showed no Cotton effect in the CD spectrum, although the characteristic very broad absorption band due to the $\pi \rightarrow \pi^*$ transitions in the conjugated polyene chain was observed in the region from 450 to 800 nm. Third, the acetylene polymerization at 35–40 °C, where the LC mixture including the chiral dopant was isotropic, produced the PA with no helical morphology. These results demonstrate that the N*-LC environment is essential for producing H-PA.

In summary, H-PA with a superhierarchical structure was synthesized in an asymmetric reaction field consisting of N*-LC. The N*-LC was prepared by adding a chiroptical binaphthyl derivative as a chiral dopant to a mixture of two N-LCs. Acetylene polymerizations were carried out using the catalyst of $\text{Ti}(\text{O}-n\text{-Bu})_4\text{-AlEt}_3$ dissolved in the N*-LC solvent. The PA film consisted of a right- or left-handed helical structure of fibrils, as seen in the SEM. The Cotton effect was observed in the region of $\pi \rightarrow \pi^*$ transition of the PA chain in the circular dichroism spectrum. The high electrical conductivities of $1.5\text{--}1.8 \times 10^3$ S/cm after iodine doping and the chiral helicity of the present films should be available for novel electromagnetic properties such as an induced solenoid magnetism. Macroscopic alignment of H-PA has also been successfully carried out to prepare the samples available for examinations of electromagnetic and optical properties. It is worth noting that by using the N*-LC as an asymmetric polymerization solvent, the helix formation is possible not only for PA but also for π -conjugated polymers without chiroptical substituents in side chains. In fact, very recently, other kinds of spiral morphology containing conjugated polymers such as polybithiophene, polyethylenedioxythiophene derivatives, and phenylene-thiophene copolymers^{78–80} were synthesized through chemical or electrochemical polymerization in the N*-LC.^{81–83}

3. Advances in N*-LC Reaction Field

3.1. Liquid-Crystalline Binaphthyl Derivatives

Chiral nematic liquid crystals (N*-LCs) have been drawing substantial interest for their potential applications in circularly polarized light,^{79,84} reflectable polarizer,^{85–88} liquid-crystal laser,^{89–92} asymmetric synthesis,^{93–97} and chirality induction for conducting polymers.^{10,98–101} There are many kinds of chiral liquid crystals in terms of chiral LC phase, i.e., cholesteric or N*, blue phases,^{102,103} and twist grain boundary phases.^{104,105} Especially, the N*-LC can be easily induced by adding a small amount of chiral compounds as a chiral dopant into nematic liquid crystal (N-LC). The helical pitch of the N*-LC can be easily adjusted by changing the concentration of chiral dopant or by modifying the helical twisting power (HTP) of the chiral dopant itself.⁷⁰ Most chiral dopants have no liquid crystallinity and relatively large molecular weights. It follows that an addition of a large amount of the chiral dopant to the host N-LC causes a lowering of phase transition temperature from an isotropic to a nematic phase and an increase in viscosity of the liquid crystal, and also an occurrence of crystallization.^{71–74} The chiral dopant with large HTP can prevent the degradation of the N*-LC because the desired helical pitch can be obtained by adding a relatively small amount of chiral dopant to the host N-LC. Thus, it may be more preferable for induction of a highly twisted N*-LC to change the HTP of the chiral dopant rather than the concentration of the chiral dopant.¹⁰⁶

It is known that the binaphthyl derivatives have large twisting powers. This property comes from large steric repulsions between hydrogen atoms at the 8,8'-positions of the naphthyl rings.¹⁰⁷ Many types of binaphthyl derivatives with different substituents in the 2,2'-positions,^{108–115} 2,2',6,6'-positions,^{75,116,117} or 2,2',5,5',6,6'-positions¹¹⁸ have been examined for usages of chiral dopants to induce N*-LC. Particularly, the binaphthyl derivatives, substituted with liquid-crystalline groups at the 2,2',6,6'-positions of binaphthyl rings, have a good miscibility toward the host N-LC because of their liquid crystallinities, and also they have high HTPs based on axial chirality. However, in spite of usage of the binaphthyl derivatives with high HTPs, it was difficult to induce the N*-LCs with nano-ordered helical pitches. Thus, both the miscibility and the high HTP are required for the effective transfer of the axial chirality of the binaphthyl derivatives to the host N-LCs.

It has been reported that the rigid aromatic substituents generate large HTPs in $\alpha,\alpha,\alpha',\alpha'$ -tetra-aryl-1,3-dioxolan-4,5-dimethanol derivatives, and that the HTPs increase with the rigidity of substituents.^{119–122} Here, to investigate an amplification of HTPs in the axially chiral binaphthyl derivatives, several rigid substituents were introduced into the 2,2',6,6'-positions of the binaphthyl rings. Among them, the tetra-substituted binaphthyl derivative, **D-8**, which has the direct linkage between the *para*-hexaoxybiphenyl moieties and the 6,6'-positions of the binaphthyl rings, showed an extremely high HTP of $757 \mu\text{m}^{-1}$. The roles of HTP and liquid crystallinity of the chiral dopant in induction of highly twisted N*-LC were elucidated.

N-LCs of phenylcyclohexane derivatives, 4-(*trans*-4-*n*-propylcyclohexyl)ethoxybenzene (PCH302) and 4-(*trans*-4-*n*-propylcyclohexyl)butoxybenzene (PCH304), and also disubstituted binaphthyl derivatives [(*R*)-, (*S*)-2,2'-PCH506-1,1'-binaphthyl, abbreviated as (*R*)-, (*S*)-**D-1**] (shown in Table

1), were synthesized according to a previous report.¹⁰ The tetrasubstituted binaphthyl derivatives, **D-2** to **D-8**, were synthesized by substituting aromatic moieties into the 6,6'-positions of the binaphthyl rings without methylene spacers. The chiral binaphthyl derivative of **D-9** was synthesized by means of a previously reported procedure.^{75,123} It should be mentioned that to improve the miscibility of a chiral dopant to the host N-LCs, PCH moieties are introduced into the 2,2'-positions of binaphthyl rings (**D-1**) or into the 2,2',6,6'-positions of the binaphthyl rings (**D-2**, **D-3**, and **D-9**).

3.1.1. Mesomorphic Properties of Chiral Dopants

Mesomorphic properties of the binaphthyl derivatives were investigated with DSC, POM, and X-ray diffraction (XRD). Among the chiral dopants synthesized here, **D-3** and **D-9** showed liquid crystallinity. On one hand, the phase transition temperatures of **D-3** were as follows: G \rightarrow 79 °C \rightarrow S_x \rightarrow 99 °C \rightarrow I and G \leftarrow 52 °C \leftarrow S_x \leftarrow 63 °C \leftarrow I in the heating and cooling processes, respectively (Figure 11). Note that G, S, and I denote glassy, smectic, and isotropic phases, respectively. The POM of **D-3** showed a focal conic texture characteristic of smectic (S_x) phase (Figure 12a). The XRD of **D-2** measured at 90 °C gave a sharp diffraction peak in the small angle region ($2\theta = 2.4^\circ$), corresponding to 36.8 Å, which is ascribed to the interlayer distance. The diffraction peak in the wide angle region ($2\theta = 18\text{--}22^\circ$) was assigned to the intermolecular distance of LCs (from 4.9 to 4.07 Å). From the POM and XRD results, the LC phase of **D-3** was assigned to the smectic one. On the other hand, the phase transition temperatures of **D-9** were as follows: G \rightarrow 79 °C \rightarrow S_A \rightarrow 99 °C \rightarrow I and G \leftarrow 52 °C \leftarrow S_A \leftarrow 63 °C \leftarrow I in the heating and cooling processes, respectively (Figure 11). POM of **D-9** showed a fan-shape texture characteristic of smectic A (S_A) phase (Figure 12b).

3.1.2. Amplification of HTP

The N*-LCs were prepared by adding a small amount of chiral dopant into an equimolar mixture of the N-LCs of PCH302 and PCH304. The molecular structures of PCH302 and PCH304 are shown in Figure 3 in section 2. It should be noted that although each component (PCH302 or PCH304) shows a LC phase, the LC temperature region is very narrow, i.e., less than 1–2 °C. This is not suitable for evaluating the properties of N*-LC because even a small change in temperature easily destroys the LC phase, changing into an isotropic one. Hence, a mixture is prepared by using two N-LCs with equimolar concentration. In the mixture, the nematic to isotropic temperature, T_{N-I} , and the crystalline to nematic temperature, T_{C-N} , might be raised and lowered, respectively. In fact, the mixture exhibited N-LC phase in the region from 0 to 30 °C.^{45,46}

The helical pitch of N*-LCs were precisely evaluated by measuring the distance between Cano lines appearing on the surface of a wedge-type cell under a POM microscope.^{124–127} Meanwhile, when the helical pitch was smaller than 1 μm, it was evaluated with the selective light reflection method. The helical pitch was evaluated according to the equation

$$p = \lambda_{\max}/n$$

where λ_{\max} is the wavelength for the reflected light and n is the mean refraction index of N*-LC ($n \cong 1.5$).¹²⁸

Subsequently, HTP (β_M) of the chiral dopant, i.e., an ability to convert N-LC into N*-LC, was evaluated using the

equation

$$\beta_M = [(1/p)/c]_{c \rightarrow 0}$$

where p is the helical pitch in μm and c is the mole fraction of the chiral dopant in the N*-LC.^{107,122,129} The inverse of pitch ($1/p$) is plotted as a function of the mole fraction of the chiral dopant, and obtained linear relationship between $1/p$ and c in the low-concentration regime.

The relationship between the number of substituents and HTP was investigated. **D-1** and **D-9** have the PCH substituents at the 2,2'-positions of the binaphthyl rings but the latter (**D-9**) has furthermore the same PCH moieties at the 6,6'-positions of the binaphthyl rings. Therefore, there is a difference between the HTPs of **D-1** (171 μm⁻¹) and **D-9** (200 μm⁻¹) (see Table 1). Besides, all the HTPs of the tetrasubstituted chiral dopants (**D-2** to **D-9**) are larger than that of **D-1**. This may be rationalized with a difference in the number of substituents. Namely, the axially twisting torque of the tetrasubstituted chiral dopants are more effectively transferred to the environmental N-LC molecules, by virtue of intermolecular interactions between four PCH substituents and the host N-LC molecules, rather than in the case of **D-1** bearing two PCH substituents.

Interestingly, **D-3** showed a high HTP of 449 μm⁻¹, which is about 2.2 times larger than that of **D-9** (200 μm⁻¹). The PCH moieties of **D-3** and **D-9** are linked directly and indirectly to the 6,6'-positions of the binaphthyl rings, respectively. To elucidate the relationship between the molecular structure and HTP, it is helpful to show equilibrium geometries of **D-3** and **D-9**. It can be understood that absence of the hexamethylene spacer, [-(CH₂)₆-], in **D-3** leads to a large rigidity in the linkage between the PCH moieties and the binaphthyl rings.

When the substituent group changes from PCH moiety (**D-3**) to phenyl (**D-5**), *p*-hexaoxy-phenyl (**D-7**), and *p*-hexaoxy-biphenyl one (**D-8**), the HTPs of these binaphthyl derivatives changed from 449 to 183, 192, and 757 μm⁻¹, respectively. Interestingly, a close relationship between the length of aromatic group and the HTP was observed (see Table 1). The molecular extension increased as follows: *para*-hexaoxy-biphenyl > PCH > *para*-hexaoxy-phenyl > phenyl. The HTPs increased in proportion to the molecular extension. As a result, one obtained the HTP of 757 μm⁻¹ in **D-8**, which is about 4 times larger than that (183 μm⁻¹) of **D-5**.

D-3 has a rigid linkage between the 6,6'-positions of the binaphthyl rings and the PCH moieties, similar to that of **D-2**. Thus, it has a large HTP (449 μm⁻¹), although the value is slightly smaller than that (510 μm⁻¹) of **D-2**. The difference is due to an increase in the length of methylene spacer between the 2,2'-positions of the binaphthyl rings and the PCH moieties. The dodecamethylene spacer [-(CH₂)₁₂-] in **D-3** makes the PCH fragments at the 2,2'-positions of the binaphthyl rings more flexible than the case of **D-2**. This results in a slightly smaller twisting power than **D-2**.

3.1.3. Role of Liquid Crystallinity of Chiral Dopant in Induction of N*-LC

Since the helical pitch of the N*-LC is a primarily important index for practical use, we examined the role of the HTP and the miscibility of chiral dopant to the host N-LC in induction of N*-LC. It is useful to focus on the helical pitch of the N*-LC as a function of mole percentage {mole of chiral dopant/(mole of PCH302 + mole of PCH304)} of

Table 1. Comparison of Rigidity, Helical Twisting Power (HTP, β_M), and Liquid Crystallinity between Several Types of Tetrasubstituted Binaphthyl Derivatives ((*R*)-Configuration)

	Rigidity ^a	HTP, β_M (μm^{-1})	Liquid crystallinity ^b	Molecular structure
D-1	low	171	—	
D-2	high	510	—	
D-3	high	449	S _X	
D-4	high	226	—	
D-5	high	183	—	
D-6	high	234	—	
D-7	high	192	—	
D-8	high	757	—	
D-9	low	200	S _A	

^a Rigidity in terms of linkages between the 6,6'-positions of the binaphthyl rings and the PCH moieties. ^b Liquid crystallinity of the chiral dopant itself.

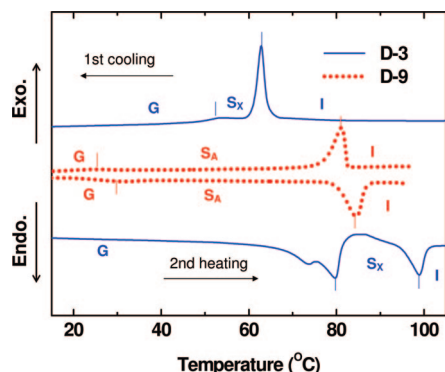


Figure 11. Differential scanning calorimetry thermographs of tetrasubstituted binaphthyl derivatives, **D-3** and **D-9**.

the chiral dopant. Higher concentration and high HTP of the chiral dopants make the helical pitches smaller. However, the N*-LC becomes a solid state through the phase separation over an upper limit of concentration of the chiral dopant. In spite of high HTP of **D-2**, its miscibility to the host N-LC is low due to the rigidity, depressing the maximum concentration to 0.25 mol %. However, because of the increase in the flexibility, **D-3** has liquid crystallinity itself. Then the liquid crystallinity raises the miscibility of **D-3** to the host N-LC, giving a maximum concentration of 1.5 mol %. Consequently, both the high HTP and the high miscibility of **D-3** allowed us to prepare highly twisted N*-LC whose helical pitch is nano-order, i.e., 270 nm.

Figure 13 shows POMs of the N*-LCs, which are induced by 0.05, 0.125, and 1.5 mol % of chiral dopant (*R*)-**D-3**, respectively. Figure 13a,b gave a fingerprint texture with striae. The distance between the striae corresponds to a half of the helical pitch in N*-LC. Meanwhile, the POM of Figure 13c gave a fan-shaped texture, but no striae were observed. This is due to the fact that the distance between the striae formed in N*-LC including 1.5 mol % of chiral dopant (*R*)-**D-3** is too small to be detected in the POM microscope with a resolution limit of ca. 1 μm . It should be emphasized here that although the liquid crystallinity of the chiral dopant has no direct influence on the HTP, it plays the important role of increasing the miscibility of the chiral dopant, leading to an increase of the upper limit concentration usable for the chiral dopant to the host N-LC.

The phase transition temperature (clearing temperature) from N*-LC to isotropic phase depends on the molecular structure and the mole concentration of the chiral dopant, and also the intermolecular interactions between the chiral dopant and the N-LCs.^{130–132} The N*-LC-isotropic phase transition temperatures of the mixed systems as a function of mole concentration of the chiral dopant is examined. Since the chiral dopants of **D-3** and **D-9** have liquid crystallinity themselves, the intermolecular interactions between the chiral dopants and the N-LCs should be larger than those in the case of **D-1** and **D-7** having no liquid crystallinity. Thus, the increases in mole concentration of **D-3** and **D-9** raise the clearing point.¹³³ This suggests a thermal stability of the N*-LC phase including **D-3** or **D-9**. However, the N*-LC including **D-1** or **D-7** showed a reverse trend, i.e., a lowering of the clearing temperature with increasing mole concentration. It is also found that the N*-LCs induced by **D-3** showed selective light reflections in the visible region. The reflection color depends on the helical pitch of the N*-LC. Because of a high upper limit (1.5 mol %) in mole concentration, it is possible to adjust the helical pitches of N*-LCs. The N*-

LCs with blue, green, and red colors in the selective light reflection were prepared by using the chiral dopant **D-3** of 0.75, 1, and 1.5 mol %, respectively.

The helical sense of the N*-LCs was examined through the miscibility test. The mixing area between the N*-LC and a standard LC was observed under the POM. When the screw direction of the N*-LC is the same as that of the standard LC, the mixing area should be continuous. However, there should appear a discontinuous boundary (a Schlieren texture characteristic of N-LC) between the N*-LC and the standard LC when they have opposite screwed directions. The cholesteryl oleyl carbonate was used as the standard LC for the miscibility test. There appeared a discontinuous or continuous area between the N*-LC with (*R*)- or (*S*)-**D-3** and the standard LC, respectively. Because the screw direction of the standard LC is known to be left-handed, the screw directions of the N*-LCs induced by (*R*)- and (*S*)-**D-3** can be deduced to be opposite to and the same as that of the standard LC, i.e., right- and left-handed, respectively.

In summary, axially chiral binaphthyl derivatives with highly twisting powers were synthesized by substituting PCH mesogenic moieties into 2,2'-positions or 2,2',6,6'-positions of binaphthyl rings. The di- and tetrasubstituted binaphthyl derivatives were adopted as chiral dopants to induce chiral nematic liquid crystals (N*-LCs). The helical twisting power (β_M) of tetrasubstituted binaphthyl derivative, **D-3**, having direct linkages between the PCH moieties and the binaphthyl rings at the 6,6'-positions, was 449 μm^{-1} . This is ca. 2.6 times larger than that (171 μm^{-1}) of the disubstituted one, **D-1**. Interestingly, **D-3** and **D-9** showed liquid crystallinity. Although the liquid crystallinity of the chiral dopant has no direct influence on the helical twisting power of the N*-LC, it plays the role of increasing the miscibility of the chiral dopant to host N-LC, leading to an increase of the upper limit concentration of the chiral dopant. Consequently, both the highly helical twisting power and the high miscibility of **D-3** allowed us to prepare highly twisted N*-LC, whose helical pitch is nano-order, i.e., 270 nm.

Part 2. Control of the Morphology

4. Control of the Fibril Morphology

4.1. Bundle-Free Fibril Morphology of H-PA

There has been increasing interest in chiral conducting polymers because of their potential application for nanowires,^{55,56,134–136} electrodevices,^{137,138} and biological technologies.^{139–141} Since H-PA characterized by a hierarchical spiral morphology was synthesized in a chiral nematic liquid crystal (N*-LC), the N*-LC has been currently focused on an asymmetric reaction field to produce chiral conducting polymers. It has been found that the chirality of the H-PA is controllable by selecting the chirality of the chiral dopant to be added to the nematic LC (N-LC). H-PA is anticipated to be a prototype of a molecular solenoid owing to its helical structure and high electrical conductivity. It is therefore desirable to synthesize a highly screwed H-PA for inducing the solenoidal magnetism. To this end, it is essentially important to construct a more highly twisted LC reaction field. However, from a nanoscience point of view, it is very intriguing to elucidate the physical properties of the single helical fibril. The H-PA chains are self-assembled owing to van der Waals interactions forming a helical fibril, which is

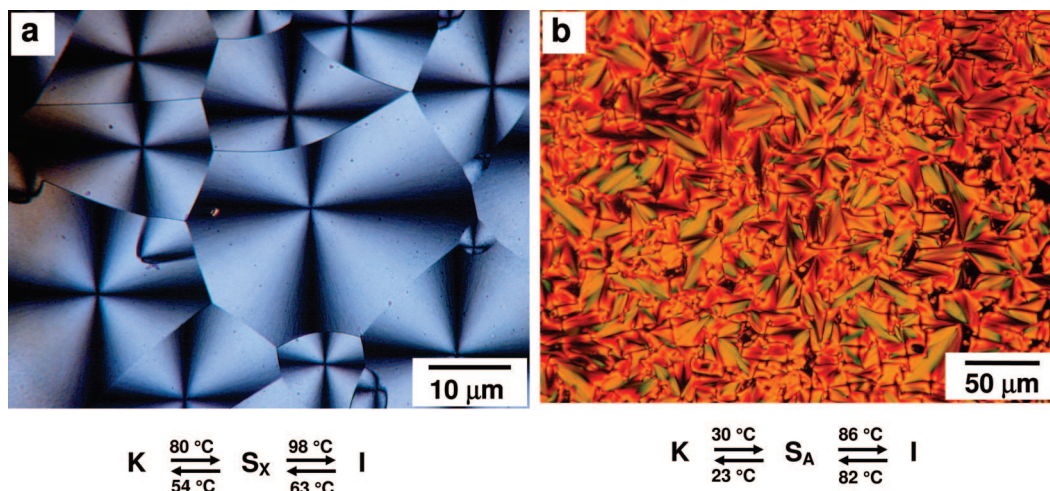


Figure 12. Polarizing optical micrographs of D-3 at 62 °C in the cooling process (a) and D-9 at 83 °C in the heating process (b).

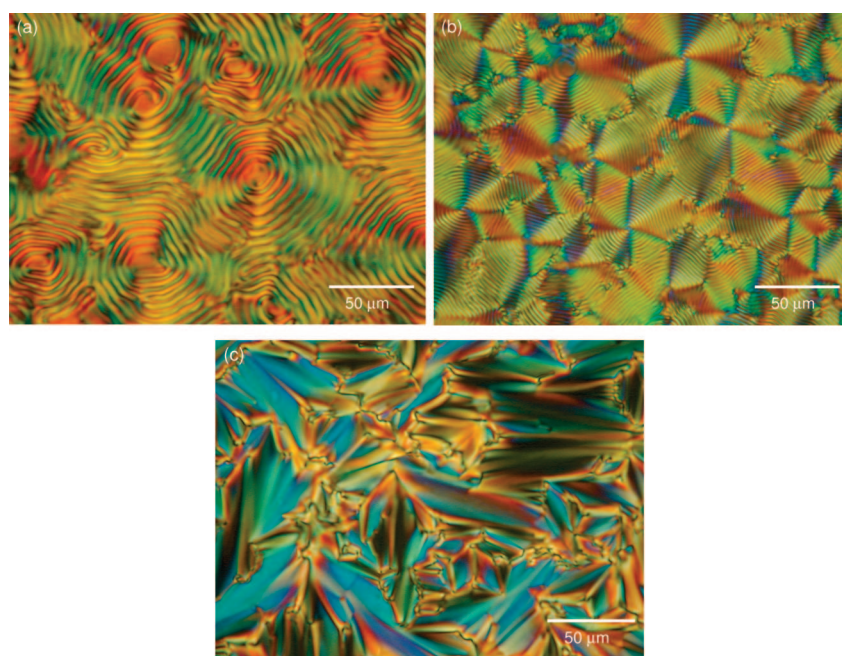


Figure 13. Polarizing optical micrographs of N*-LCs at 27 °C. The helical pitches of N*-LC are 5.3 (a), 2.3 (b), and 0.27 μm (c), respectively. The N*-LCs of (a), (b), and (c) contain 0.05, 0.125, and 1.5 mol % of chiral dopant (*R*)-D-3, respectively.

a bundle of polymer chains. In addition, the helical fibrils are gathered to form a bundle of fibrils. The bundles of fibrils give a spiral morphology in a domain, resulting in a multidomain of helical structure. However, the insolubility and infusibility of PA make it difficult to separate the bundle of fibrils into single fibrils. This situation is similar to the case of carbon nanotubes; because of substantial van der Waals attractive interactions, carbon nanotubes tend to form aggregates that can hardly be separated into single tubes.^{142,143}

The only way to obtain a single fibril that has been recently put forward is to soak a piece of PA film in *N,N*-dimethylformamide solution, including a surfactant such as hexaethylene glycol monododecyl ether, and then to ultrasonicate it for dispersion.^{55,56,133,134} However, this procedure might lead to cleavage and/or damage of the fibrils during ultrasonication. This would prevent us from evaluating the intrinsic electromagnetic properties of the single fibril of H-PA. Here it is found that the H-PA film, which consists of only single fibrils but not the bundle of fibrils, can be synthesized by using a highly twisted N*-LC reaction field.

The helical pitch of the N*-LC can be adjusted by changing the concentration of the chiral dopant or by changing the helical twisting power of the chiral dopant itself.⁷⁰ However, the mesophase temperature region of the N*-LC is also affected by the concentration of the chiral dopant. Namely, it becomes narrow as the concentration of the chiral dopant increases, and finally the mesophase will be destroyed when the concentration is close to a critical value.^{144–147} Therefore, the latter approach of utilizing chiral dopants with various helical twisting powers might be preferable. It has been elucidated so far that the binaphthyl derivatives have not only good miscibility toward the N-LC by virtue of their LC moieties but also a higher helical twisting power than asymmetric center-containing chiral compounds due to axial chirality.^{107–111,148–151} However, even when a binaphthyl derivative with a high twisting power was used, the helical pitch of the induced N*-LC was not in the nano-order range, but nearly equal to or larger than 1 μm. Thus, to affect the axial chirality more effectively to the environmental LC molecules, a high miscibility, reinforced

by the liquid crystallinity of the chiral dopant itself, and a high helical twisting power were required.

This section focuses on novel di- and tetrasubstituted binaphthyl derivatives, where the phenylcyclohexyl (PCH) moieties are substituted at the 2,2'- or 2,2',6,6'-positions of the binaphthyl rings. Among them, the tetrasubstituted binaphthyl derivative (**D-2**), having a direct linkage between the PCH moieties and the binaphthyl rings at the 6- and 6'-positions, gave nano-order (270 nm) helical pitches when added as a chiral dopant into the N-LC.¹⁵² Thus, the prepared N*-LC enabled us to synthesize a highly twisted nano-single fibril of H-PA.

4.1.1. Highly Twisted Chiral Dopants and N*-LCs

The tetrasubstituted binaphthyl derivatives [(*R*)-, (*S*)-2,2'-PCH5012-6,6'-PCH5-1,1'-binaphthyl, abbreviated as (*R*)-, (*S*)-**D-2**] were synthesized by substituting the PCH moieties without methylene spacers into the 6,6'-positions of the binaphthyl ring. As reference compounds to the **D-2**, [(*R*)-2,2',6,6'-PCH506-1,1'-binaphthyl, abbreviated as **RC-1**] and [(*R*)-2,2'-PCH506-6,6'-PCH5-1,1'-binaphthyl, abbreviated as **RC-2**] were synthesized by means of the previously reported procedure¹¹⁷ and a synthetic method similar to that used for **D-2**, respectively.

The mesomorphic properties of the binaphthyl derivatives were investigated with a DSC, POM, and XRD measurements. Although the disubstituted binaphthyl (**D-1**) and tetrasubstituted (**RC-2**) derivatives showed no mesophase, the tetrasubstituted derivatives (**D-2** and **RC-1**) showed liquid crystallinity. The phase transition temperatures of **D-2** were as follows: $G \rightarrow 79\text{ }^\circ\text{C} \rightarrow S_x \rightarrow 99\text{ }^\circ\text{C} \rightarrow I$ and $G \leftarrow 52\text{ }^\circ\text{C} \leftarrow S_x \leftarrow 63\text{ }^\circ\text{C} \leftarrow I$ in the heating and cooling processes, respectively. Note that G, S, and I denote glassy, smectic, and isotropic phases, respectively. The POM of **D-2** showed a focal conic texture characteristic of a smectic (S_x) phase. The XRD of **D-2** measured at 90 °C showed the sharp diffraction peak in the small-angle region, $2\theta = 2.4^\circ$, corresponding to 36.8 Å, which is ascribed to the interlayer distance. The diffraction peak in the wide-angle region ($2\theta = 18^\circ\text{--}22^\circ$) was assigned to the intermolecular distance of LCs (from 4.9 to 4.07 Å). From the POM and XRD results, the LC phase of **D-2** was assigned to the smectic phase.

The N*-LC was prepared by adding a small amount of chiral dopant into an equimolar mixture of the N-LCs of PCH302 and PCH304. It should be noted that although each component (PCH302 or PCH304) shows an LC phase, the LC temperature region is very narrow, i.e., less than 1–2 °C. This is not suitable for acetylene polymerization irrespective of the N-LC or N*-LC reaction field because the exothermal heat evoked during the acetylene polymerization would raise the temperature inside a Schlenk flask and easily destroy the LC phase, becoming an isotropic one. Hence, a LC mixture was prepared by mixing the two equimolar nematic LCs. In the N-LC mixture, the nematic to isotropic temperature, T_{N-I} , and the crystalline to nematic temperature, T_{C-N} , might be raised and lowered, respectively. In fact, the mixture exhibited the LC phase in the region from 20 to 35 °C. The change of T_{N-I} upon the addition of $\text{Ti}(\text{O}-n\text{-Bu})_4\text{-AlEt}_3$ catalyst was examined through DSC measurements. Taking into account the effect of supercooling LCs, the catalyst solution consisting of the LC mixture and the chiral dopant was found available for room-temperature polymerization ranging from 5 to 25 °C. This sufficiently

wide temperature region enabled us to perform the acetylene polymerization in the N*-LC phase.

The molecular fragments in both the nematic liquid crystals and the chiral dopants (binaphthyl derivatives) are composed of only phenyl, cyclohexyl, and alky moieties and also ether-type oxygen. These molecular fragments are chemically stable toward not only extremely reactive Ziegler–Natta catalysts, such as triethylaluminum and tetrabutoxytitanium, but also other kinds of transition-metal (Ni, Pd, Pt) compounds. This means that the present chiral nematic liquid crystal is available as an asymmetric reaction solvent for other kinds of polymerizations, and even for chemical reactions of chiral compounds. The potential versatility as an asymmetric reaction solvent in the present chiral nematic liquid crystal is worth emphasizing from the viewpoint of further application.

The helical pitch of N*-LCs were precisely evaluated by measuring the distance between Cano lines appearing on the surface of a wedge-type cell under the POM microscope.^{124–127} Meanwhile, when the helical pitch was smaller than 1 μm, it was evaluated with the selective light reflection method. The helical pitch was evaluated according to the equation

$$p = \lambda_{\text{max}}/n$$

where λ_{max} is the center wavelength for the maximally reflected light and n is the mean refraction index of the N*-LC ($n \approx 1.5$).^{128,153}

Subsequently, the helical twisting powers (β_M) of the chiral dopant, i.e., the ability to convert the N-LC into the N*-LC, was evaluated using the equation

$$\beta_M = [(1/p)/c]_{c \rightarrow 0}$$

where p is the helical pitch in micrometers and c is the mole fraction of the chiral dopant in the N*-LC.^{107,122} The inverse pitch ($1/p$) was plotted as a function of the mole fraction of the chiral dopant, and a linear relationship between $1/p$ and c in the low-concentration regime was obtained. The helical twisting powers of **D-1** and **D-2** were 171 and 449 μm⁻¹, respectively. It is clear that the helical twisting power of the chiral dopant **D-2** is ca. 2.6 times larger than that of **D-1**. This may be rationalized with a difference in the number of substituents. Namely, the axially twisting torque of **D-2** is more effectively transferred to environmental nematic LC molecules by virtue of intermolecular interactions between the four PCH substituents of **D-2** and the PCH moieties of the LC molecules, rather than in the case of **D-1** bearing two PCH substituents. Note that although the chiral dopant of the (*S*)-configuration should have the same helical twisting power as that of the (*R*)-configuration, the former gave a smaller value in the helical twisting power than the latter, irrespective of the di- or tetrasubstituted binaphthyl derivatives. This is due to the fact that the (*S*)-binaphthol used as a starting compound has lower optical purity than (*R*)-binaphthol, although both binaphthols are commercially available.

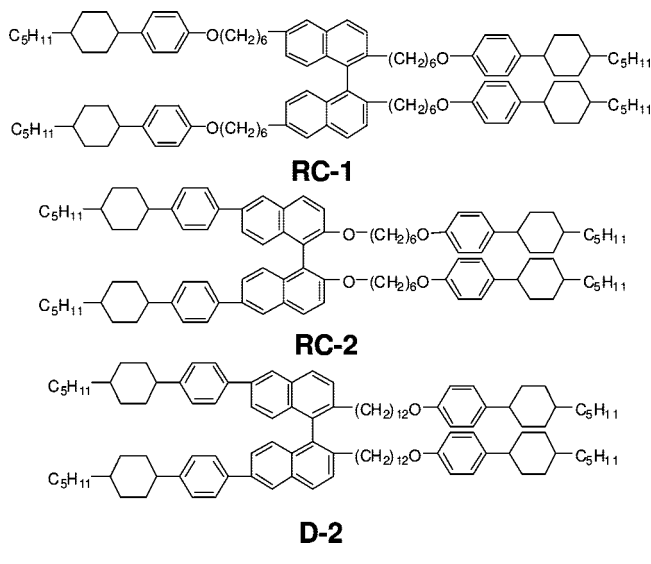
4.1.2. Contribution of the HTP and Miscibility of a Chiral Dopant in the Helical Pitch of the N*-LC

Since the helical pitch of the N*-LC might be essential to control the morphology of H-PA, it is worthwhile to examine in more detail how the helical twisting power (β_M) and the miscibility of the chiral dopant affect the helical pitch of

Table 2. Comparison between Several Types of Tetrasubstituted Axially Chiral Binaphthyl Derivatives (R-Configuration)

	RC-1	RC-2	D-2
rigidity ^a	low	high	high
helical twisting power (β_M)	200 μm^{-1}	510 μm^{-1}	449 μm^{-1}
liquid crystallinity ^b	yes	no	yes
maximum mol % ^c	1.5	0.25	1.5
helical pitch of induced N*-LC ^d	940 nm	1.3 μm	270 nm

^aRigidity in linkages between the 6- and 6'-positions of the binaphthyl rings and the PCH moieties. ^bLiquid crystallinity of chiral dopant itself. ^cMaximum mole percentage of chiral dopant, over which N*-LC changes into the solid state through phase separation. Mole percentage = mole of chiral dopant/(mole of PCH302 + mole of PCH304) \times 100. ^dHelical pitch of N*-LC induced by the chiral dopant of maximum mole percentage.



the N*-LC. Table 2 shows some properties of the tetrasubstituted binaphthyl derivatives.

The structural difference between **RC-1** and **RC-2** is that the PCH moieties are indirectly and directly linked with the 6,6'-positions of the binaphthyl rings, respectively. That is, the absence of the hexamethylene spacer, $[-(\text{CH}_2)_6-]$, leads to a rigidity in the linkage between the PCH moieties and the binaphthyl rings, resulting in a high helical twisting power of 510 μm^{-1} in **RC-2**, which is about 2.5 times higher than that of **RC-1** (200 μm^{-1}). However, **RC-2** has no liquid crystallinity owing to its rigidity, which depresses the miscibility of the chiral dopant to the parent N-LC. In fact, the maximum mole percentage (0.25 mol %) usable as the dopant was one-sixth that of **RC-1** (1.5 mol %) having liquid crystallinity. As a result, the N*-LC induced by the chiral dopant of **RC-2** has a longer helical pitch (1.3 μm) than that by the dopant of **RC-1** (910 nm), in spite of the larger helical twisting power of **RC-2** (510 μm^{-1}).

Meanwhile, **D-2** shows rigidity in the linkage between the 6,6'-positions of the binaphthyl rings and the PCH moieties, similar to that of **RC-2**. Thus, it has a higher helical twisting power (449 μm^{-1}), although the value is slightly smaller than that of **RC-2** (510 μm^{-1}). The difference is due to an increase in the length of the methylene spacer between the 2,2'-positions of the binaphthyl rings and the PCH moieties; the dodecamethylene spacer $[-(\text{CH}_2)_{12}-]$ in **D-2** makes the PCH fragments at the 2,2'-positions of the binaphthyl rings more flexible than in the case of **RC-2**. This results in a slightly smaller twisting power than that of **RC-2**. At the same time, however, owing to the increase of the flexibility, **D-2** has

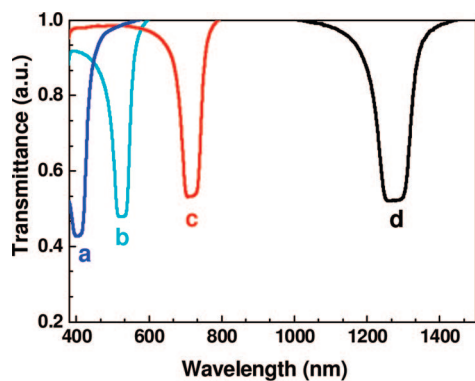
liquid crystallinity itself, similar to the case of **RC-1**. Actually, the liquid crystallinity increased the miscibility of **D-2** to the parent N-LC, yielding a maximum concentration of 1.5 mol %. As a consequence, both the high helical twisting power and the high miscibility of **D-2** allowed us to prepare a highly twisted N*-LC, whose helical pitch is nano-order, i.e., 270 nm. It should be emphasized here that although the liquid crystallinity of the chiral dopant has no direct influence on the helical twisting power of the N*-LC, it plays the role of increasing the miscibility of the chiral dopant, leading to an increase of the upper limit concentration usable for the chiral dopant to the parent N-LC.

4.1.3. Asymmetric Reaction Field Constructed with the N*-LC

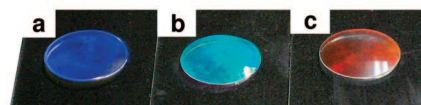
We examined the changes of helical pitches in N*-LCs as a function of mole percentage of the chiral dopants **D-1** and **D-2**. The PCH moieties substituted in the binaphthyl derivatives enhance the miscibility of the chiral dopants **D-1** and **D-2** in the nematic mixture of PCH302 and PCH304, even at a relatively high mole percentage (1.5 mol %) of the binaphthyl derivatives. The helical pitches of N*-LCs varied from 9.4 to 3.2 μm with a change in the mole percentage of **D-1** (from 0.25 to 1.5 mol %) and from 5.24 μm to 270 nm with **D-2** (from 0.05 to 1.5 mol %). This result shows that the chiral dopant **D-2** has a highly helical twisting power, enough to give the nano-order helical pitch in the N*-LC. It is also confirmed that the N*-LCs induced by **D-2** showed selective light reflections in the visible region, as shown in Figure 14. The color depends on the helical pitch of the N*-LC. The N*-LCs with blue, green, and red colors in the selective light reflection were prepared by using the chiral dopant **D-2** of 0.75, 1, and 1.5 mol %, respectively.

The phase transition temperature (clearing temperature) from chiral nematic to isotropic phase depends on the molecular structure and the mole percentage of the chiral dopant, and also the intermolecular interactions between the chiral dopant and the N-LCs.^{130–132} The N*-LC isotropic phase transition temperatures of the mixed systems as a function of mole percentage of the chiral dopant were examined. Since the chiral dopant of **D-2** has liquid crystallinity itself, the intermolecular interactions between **D-2** and the nematic molecules should be larger than those in the case of **D-1**. Thus, the increase in mole percentage of **D-2** raises the clearing point.¹³³ This suggests a thermal stability of the N*-LC phase including **D-2**. However, the N*-LC including **D-1** showed a reverse trend, i.e., a lowering of the clearing temperature with increasing mole percentage of **D-1**.

From the reaction field point of view, the stable and highly twisted N*-LC is preferred. The N*-LC including **D-2** of 1.5 mol % showed thermal stability and a small helical pitch of 270 nm. Meanwhile, the N*-LC including **D-1** of 1.5 mol % showed a relatively larger helical pitch of 3.2 μm and lower thermal stability than in the case of **D-2**. Hence, the N*-LCs including **D-1** of 1 mol % {PCH302/PCH304/**D-1** = 100:100:2 (mole ratio)} and **D-2** of 1.5 mol % {PCH302/PCH304/**D-2** = 100:100:3 (mole ratio)}, abbreviated as **System 1** and **System 2**, respectively, were prepared as the asymmetric reaction field for acetylene polymerization. The helical pitches of **System 1** and **System 2** were 5 μm and 270 nm, respectively. Figure 15 shows POMs of the N*-LCs, **System 1** and **System 2**. **System 1** gave a fingerprint texture with striae (Figure 15a). The distance between the striae (2.5 μm) corresponds to half of the helical pitch in



$$p = \lambda_{\max} / n, \text{ where } n \cong 1.5$$



	a	b	c	d
mol %	1.5	1.0	0.75	0.5
λ_{\max} (nm)	405	520	710	1270
p (nm)	270	350	470	850

Figure 14. Selective light reflection spectra of N*-LCs. The N*-LCs of curves (a), (b), (c), and (d) contain 1.5, 1.0, 0.75, and 0.5 mol % of chiral dopant (*R*)-**D-2**, respectively. Photographs of the selective light reflections, wavelengths of the selective light reflection, and helical pitches of N*-LCs are shown on the right side.

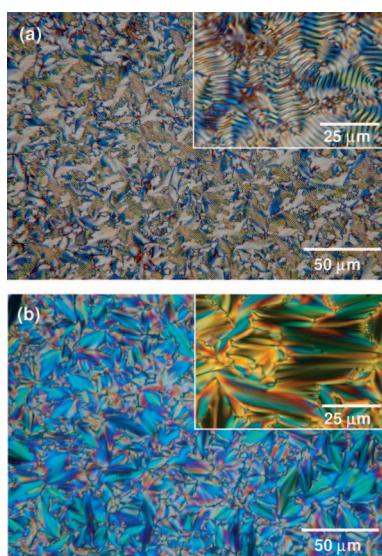


Figure 15. Polarizing optical micrographs of N*-LCs at 27 °C. The insets show the magnified photographs. (a) (*S*)-**System 1** containing 1.0 mol % of chiral dopant, (*S*)-**D-1**. (b) (*R*)-**System 2** containing 1.5 mol % of chiral dopant, (*R*)-**D-2**.

the N*-LC. Meanwhile, the POM of **System 2** gave a fan-shaped texture, but no striae were observed (Figure 15b). This is due to the fact that the distance between the striae formed in **System 2** is too small to be detected in the POM microscope with a resolution limit of ca. 1 μm.

The helical senses of the N*-LCs were examined through a miscibility test¹⁵⁴ and a selective light reflection in circular dichroism (CD) spectra.^{152,155,156} Whereas the miscibility test can be used regardless of the length in helical pitch, the selective light reflection method can be used only when the helical pitch is between the UV and near-infrared regions (from 250 nm to 1 μm). This is the reason why both methods are used to evaluate the helical sense for **System 1f** (helical pitch of 5 μm) and **System 2** (helical pitch of 270 nm). However, we will hereafter focus only on the results of the selective light reflection method. It is known that the cholesteryl oleyl carbonate is a left-handed cholesteric LC showing a selective light reflection in the visible region. Therefore, cholesteryl oleyl carbonate was used as a reference for determining the handedness of the N*-LC. As shown in

Figure 16, the N*-LC inducing (*R*)-**D-2** showed a negative sign, whereas the N*-LC including (*S*)-**D-2** and cholesteryl oleyl carbonate showed positive sign peaks in the CD spectra. These results indicate that the handed senses of the (*R*)- and (*S*)-N*-LCs are right- and left-handed, respectively.

4.1.4. Synthesis of HP with Bundle-Free Morphology

The N*-LCs of **System 1** and **System 2** can be regarded as weakly and highly twisted asymmetric reaction fields, respectively. Thus, two kinds of N*-LCs were prepared as solvents using a Ziegler–Natta catalyst consisting of Ti(*O-n*-Bu)₄ and AlEt₃. The concentration of Ti(*O-n*-Bu)₄ was 50 mM, and the mole ratio of the cocatalyst to catalyst, [AlEt₃]/[Ti(*O-n*-Bu)₄], was 4.0. The catalyst solution was aged for 30 min at room temperature. The polymerization temperature was kept constant at 20–21 °C to maintain the N*-LC phase. The initial pressure of acetylene gas was 140–150 Torr, and the polymerization time was 3–5 min. After polymerization, PA film was carefully stripped off from the container and washed with toluene several times and subsequently with a methanol solution of hydrochloric acid (1 N) under argon gas at room temperature. The film was dried with vacuum pumping on a Teflon sheet and was stored in a freezer at –20 °C.

Figure 17 shows SEM photographs of the H-PA films synthesized in right-handed N*-LC with a helical pitch of 5 μm [(*R*)-**System 1**] and left-handed N*-LC with a helical pitch of 270 nm [(*S*)-**System 2**], respectively. The hierarchical helical structures are observed in both H-PA films. It is confirmed that the screw directions of the fibril and even the bundle of fibrils are opposite to the helical sense of the N*-LC. For instance, in the right-handed N*-LC of (*R*)-**System 1**, the fibrils are screwed left to form the bundle of fibrils. Similarly, in the left-handed N*-LC of (*S*)-**System 2**, the fibrils are screwed right, although no bundle is formed. The relationship between the screw direction of the fibril and the helical sense of the N*-LC has been partly rationalized.¹¹⁷ It is of particular interest that the highly twisted N*-LC (**System 2**) gave the fibrils but not the bundle of fibrils (Figure 17c). This is in contrast to the morphology of H-PA synthesized in the moderately twisted N*-LC (**System 1**). It is evident that the PA fibrils synthesized in (*S*)-**System 2** are more highly twisted than those in (*R*)-**System 1**.

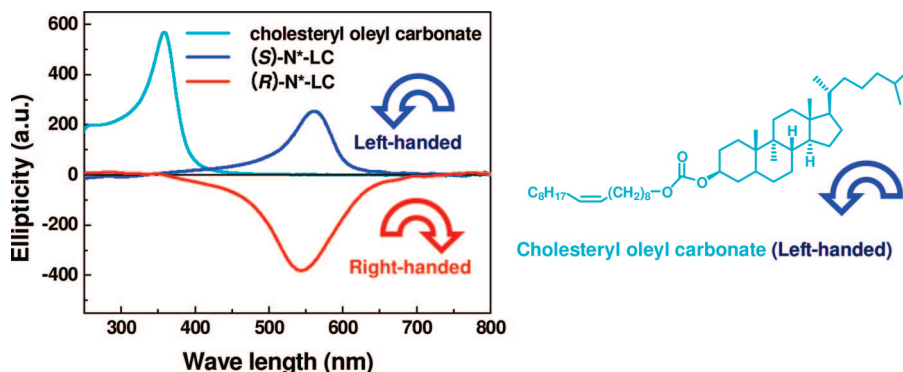


Figure 16. Reflection CD spectra of the cholesteryl oleyl carbonate and the N*-LCs induced by (*R*)-**D-2** and (*S*)-**D-2**. (*R*)-N*-LC, PCH302:PCH304:(*R*)-**D-2** = 100:100:2 (mole ratio). (*S*)-N*-LC, PCH302:PCH304:(*S*)-**D-2** = 100:100:2 (mole ratio).

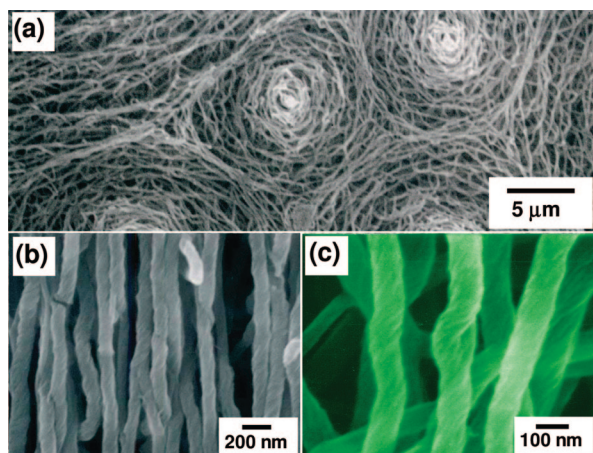


Figure 17. SEM micrographs of H-PA film synthesized in the left-handed (*S*)-**System 2** {PCH302:PCH304:(*S*)-**D-2** = 100:100:3 (mole ratio)} with a helical pitch of 270 nm. The photographs of (b) and (c) show the magnified one of (a).

To elucidate the relationship between the degree of helical pitch of the N*-LC and the morphology of H-PA, various N*-LCs with helical pitches (2.3 μm , 850 nm, and 470 nm) between 5 μm and 270 nm were prepared by changing the mole percentage of the chiral dopant of **D-2**. A series of SEM photographs of H-PA films synthesized in the above-mentioned N*-LCs were examined. The N*-LC with a helical pitch of 2.3 μm gave the bundle of fibrils in the morphology of H-PA. In the case of the N*-LC with a helical pitch of 850 nm, bundles consisting of several fibrils were observed. The interdistance between the bundles was less than 550 nm. When the N*-LC of a helical pitch of 470 nm was used, almost single fibrils were observed, but part of the fibrils overlapped. These results indicate that the morphology of H-PA is dominated by the degree of helical pitch of the N*-LC but not by the species of the chiral dopant.

Figure 18 shows a schematic representation of the relationship between the twisting degree of the N*-LC and the hierarchical morphology of H-PA. In the weakly twisted N*-LC, PA fibrils (whose diameters are from 70 to 120 nm) are gathered to form the bundle of fibrils (whose diameters are up to 1 μm). Interestingly, the interdistance between the bundles of fibrils is close to half of the helical pitch. The bundle of fibrils can be formed in the N*-LC whose helical pitches are up to 1 μm . However, in the highly twisted N*-LC (whose helical pitch is narrower than 1 μm), PA has highly screwed fibrils, but not the bundle of fibrils. Therein, the diameters of the fibrils are in the range from 70 to 120 nm. This may be due to the fact that the helical pitch of 270

nm in the strongly twisted N*-LC is smaller than the diameter (ca. 1 μm) of the bundle of fibrils. This situation might prevent the formation of the bundle of fibrils. The morphology free from the bundle of fibrils should make it much easier to evaluate the electromagnetic properties of the screwed fibril.

The H-PA films with morphology free from the bundle of fibrils have high trans contents of 90%. This is mainly due to polymerization temperatures such as 20–21 $^{\circ}\text{C}$. It is known that the cis form of the PA segment is a kinetically favorable product because of the so-called cis opening mechanism of acetylene polymerization, whereas the trans form is a thermodynamically stable product.¹¹ The cis form is actually transformed to the trans form, depending on the degree of the exothermal heat during the acetylene polymerization. Since exothermal heat evolves in the polymerization at 20 $^{\circ}\text{C}$, the cis–trans isomerization is enhanced to give high trans content in the present H-PA. H-PA showed high electrical conductivities such as ca. 1.8×10^3 to 2.0×10^3 S/cm at room temperature after iodine doping. Meanwhile, the PA films synthesized in **System 1** and **System 2** have bulk densities of ca. 0.5 and 0.96 g/cm², respectively. This indicates that the single fibrils give a more closely packed morphology than the bundle of fibrils.

In summary, the N*-LC induced by the novel tetrasubstituted binaphthyl derivative (**D-2**) used as a chiral dopant gave rise to helical pitches of 270–850 nm, depending on the concentration of the chiral dopant. By virtue of the high helical twisting power and liquid crystallinity of **D-2**, the N*-LC with a nano-order helical pitch can be prepared by adding a high mole percentage of the chiral dopant to the nematic LC without destruction of the liquid-crystalline phase. The helical pitches (270–850 nm) are smaller than the radius (1 μm) of the bundle of fibrils of PA. Especially, the highly screwed chiral nematic liquid crystal with a helical pitch of 270 nm depresses the formation of the bundle of fibrils, resulting in a bundle-free fibril morphology consisting of single fibrils. Thus, it is found that the degree of screwing in the chiral nematic reaction field is a key factor to control the bundle formation and/or depression in the fibril morphology of PA. It is expected that the highly twisted H-PA without the bundle of fibrils might be feasible for the evaluation of unprecedented electromagnetic properties of a single fibril of conducting polymer.

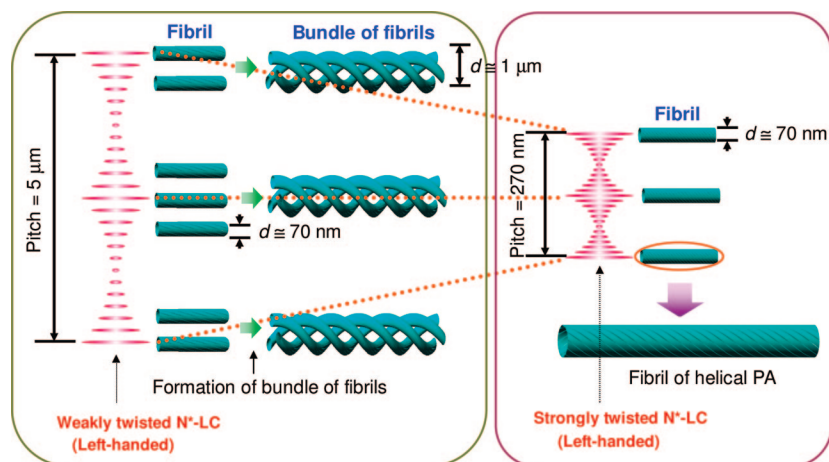


Figure 18. Relationship between the twisting degree of N^* -LC and the morphology of H-PA.

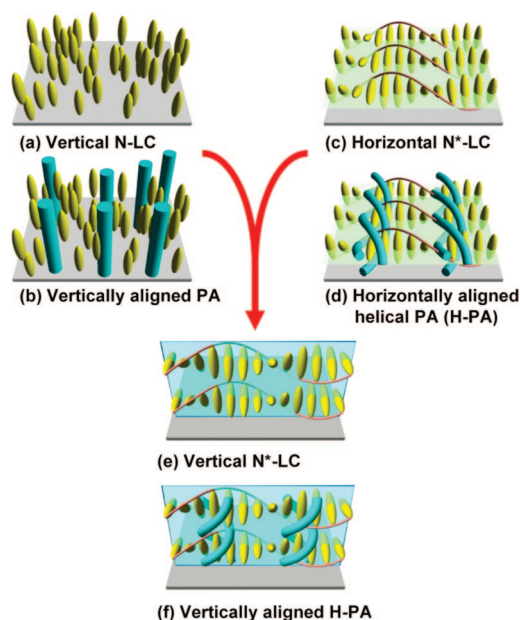


Figure 19. Schematic representations of vertical N-LC (a), vertically aligned PA (b), horizontal N^* -LC (c), horizontally aligned H-PA (d), vertical N^* -LC (e), and vertically aligned H-PA (f).

5. Orientation-Controllable N^* -LC Field

5.1. Aligned H-PA Synthesized in N^* -LC Using Orientation Dopant

The fibrils of the H-PAs synthesized hitherto are horizontally aligned because the N^* -LC used for acetylene polymerization has a horizontal alignment (see Figure 19d). However, the vertically aligned fibril morphologies of H-PA are not comprehensively exploited. It is therefore desired to develop the vertical N^* -LC useful for the synthesis of vertically aligned H-PA. Previously, it was found that the vertically aligned PA is synthesized in the N-LC including a *vertical orientation inducer* which has two PCH mesogenic moieties linked with a flexible methylene chain.^{157,158} The preliminary study indicated that the vertically aligned H-PA can also be synthesized in the vertical N^* -LC, when it is prepared by adding both the chiral dopant and the vertical orientation inducer into the parent N-LC. However, through the above preliminary study, one encountered several subjects to be solved for the construction of the orientation-controlled asymmetric reaction field: (i) No chemically graspable description of the vertical N^* -LC is given, as a guideline,

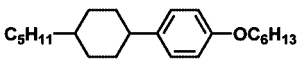
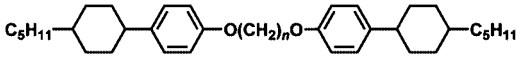
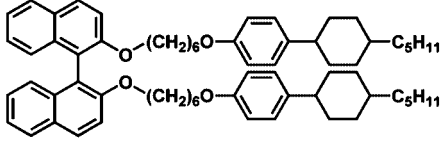
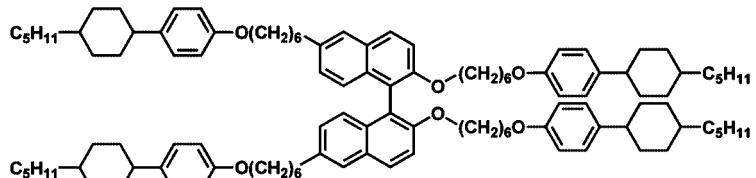
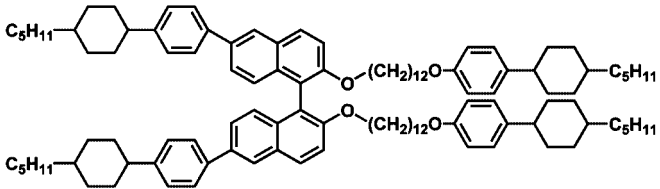
making it difficult to disclose the synthetic conditions for the vertically aligned H-PA. (ii) The helical twisting power of the axially chiral disubstituted binaphthyl derivative, used as a chiral dopant, is not strong enough for giving sufficiently screwed fibrils of H-PA in the existence of the vertical orientation inducer. (iii) The formation of the vertical N^* -LC is less reproducible because it sensitively depends on the relative concentration of the vertical orientation inducer and the chiral dopant in the N^* -LC. Here, the systematic studies of the N^* -LCs and the resultant H-PAs are presented, by focusing on the relative concentrations of the vertical orientation inducer and the chiral dopants in N^* -LCs.^{159,160}

5.1.1. Comprehensive Description of N^* -LC Fields and Resultant Products

The comprehensive description of the N^* -LC fields and the polymerization products are shown in Figure 19. Parts (a) and (b) of Figure 19 show the vertical (homeotropic) N-LC and the vertically aligned PA, respectively. The vertical N-LC can be prepared by adding the vertical orientation inducer into the horizontal (homogeneous) N-LC used as a parent N-LC. Parts (c) and (d) of Figure 19 show the horizontal N^* -LC and the H-PA (H-PA), respectively. The horizontal N^* -LC can be prepared by adding the chiral dopant into the horizontal N-LC. The H-PA is lying on the substrate; namely, the helical axis of the H-PA is parallel to the surface of the substrate. It should be emphasized that the H-PA grows along the direction orthogonal to the helical axis of the N^* -LC and that the helical sense of the H-PA and that of the N^* -LC are opposite each other. Parts (e) and (f) of Figure 19 show the vertical N^* -LC and the vertically aligned H-PA, respectively. The vertical N^* -LC can be prepared by adding both the chiral dopant and the vertical orientation inducer into the parent N-LC under appropriate mole ratios for them. The helical axis of the vertically aligned H-PA is also orthogonal to that of the vertical N^* -LC. It is of importance that the “orthogonal” relationship in the helical axis between the H-PA and N^* -LC holds, irrespective of the alignment of the N^* -LCs.

Table 3 shows the molecular structure of the N-LC, the vertical orientation inducers, and the chiral dopants. The vertical orientation inducers with hexa- and octamethylene chains, (PCH50)₂6 and (PCH50)₂8, were synthesized using the methods similar to that for PCH506. Axially chiral binaphthyl derivatives, bearing LC substituents at the 2,2'-positions of the binaphthyl rings, (*R*)- or (*S*)-2,2'-PCH506-

Table 3. Molecular Structures of Parent Liquid Crystal, Vertical Orientation Inducers, and Chiral Dopants

Parent liquid crystal	 PCH506
Vertical orientation inducers	 (PCH50) _{2n} , (n = 6, 8)
Chiral dopants	 (<i>R</i>)- or (<i>S</i>)-D1
	 (<i>R</i>)- or (<i>S</i>)-D2
	 (<i>R</i>)- or (<i>S</i>)-D3

1,1'-binaphthyl [abbreviated as (*R*)- or (*S*)-**D-1**], and LC substituents at the 2,2'- and 6,6'-positions of the binaphthyl ones, (*R*)- or (*S*)-2,2'-6,6'-PCH506-1,1'-binaphthyl [abbreviated as (*R*)- or (*S*)-**D-2**], and (*R*)- or (*S*)-2,2'-PCH5012-6,6'-PCH5-1,1'-binaphthyl [abbreviated as (*R*)- or (*S*)-**D-3**], were synthesized along the previously reported procedure.^{75,152}

The concentration ratios and the helical pitches of the N*-LCs are examined. The N*-LCs of **System 1** and **System 2** were respectively prepared by adding 3 mol % of the vertical orientation inducers, (PCH50)₂₆ and (PCH50)₂₈, and 1–2 mol % of the chiral dopant, **D-1**, into the parent LC, PCH506. The N*-LCs of **System 3** to **System 7** were prepared by adding 3–10 mol % of (PCH50)₂₆ or (PCH50)₂₈ and 0.5–1 mol % of **D-2** into PCH506. The N*-LC of **System 8** was prepared by adding 10 mol % of (PCH50)₂₆ and 0.5 mol % of **D-3** into PCH506.

The helical pitches of N*-LCs were evaluated with Cano's wedge method, which was based on the observation of discontinuity lines that appeared when an N*-LC was inserted into a cell with a gradient thickness.^{124–127} Meanwhile, when the helical pitch was smaller than 1 μm, it was evaluated with the selective light reflection method.^{128,153} The helical pitch was evaluated according to the equation $p = \lambda_{\max}/n$, where λ_{\max} is the center wavelength for the maximally reflected light and n is the mean refraction index of N*-LC ($n = 1.5$). The absolute value of HTP (β_M), defined as $\beta_M =$

$(pc)^{-1}$, was evaluated as the reciprocal of the product between the helical pitch (p) and the mole fraction of the chiral dopant (c).¹²²

Characterization of N*-LCs. The screw directions of the N*-LCs were determined through the miscibility test (contact method).^{126,161} The miscibility test is based on the observation of the mixing area between the N*-LC and the standard LC in POM. Cholesteryl oleyl carbonate is known to be a left-handed N*-LC (cholesteric LC), and therefore it is useful for the standard LC for the miscibility test. If the screw direction of the N*-LC is the same as that of the standard LC, the mixing area will be continuous. Otherwise, it will be discontinuous (shown as a Schlieren texture of the N-LC). The miscibility test indicated that the N*-LCs induced by (*R*)-chiral dopants (**D-1** to **D-3**) have right-handed screw structures and those by (*S*)-chiral dopants have left-handed ones.

Table 4 summarizes the phase transition temperatures of the N*-LCs. **System 1** to **System 7** showed N* and smectic (S) phases in a cooling process, but only the N* phase in the heating process. **System 8** showed N* and S phases in both cooling and heating processes. The temperature region of the N* phase becomes narrow as the concentration of the chiral dopant increases. For instance, **System 2-1** [PCH506:(PCH50)₂₈:(*R*)-**D-1** = 100:3:1] showed the N* phase in the region of 37–47 °C in the heating process. However, **System**

Table 4. Phase Transition Temperatures of N*-LCs

System	Mole ratios between components of N*-LCs	Phase transition temperature (°C) ^{a, b}			
		0	20	40	60
1	PCH506 : (PCH50) ₂ 6 : (R)-D1 = 100 : 3 : 2	32	50		
		19	30	45	
2-1	PCH506 : (PCH50) ₂ 8 : (R)-D1 = 100 : 3 : 1	37	47		
		15	32	47	
2-2	ibid. = 100 : 3 : 2	35	42		
		15	28	42	
3-1	PCH506 : (PCH50) ₂ 6 : (R)-D2 = 100 : 5 : 0.5	32	54		
		15	30	54	
3-2	ibid. = 100 : 5 : 1	31	52		
		9	30	51	
4	PCH506 : (PCH50) ₂ 6 : (R)-D2 = 100 : 10 : 1	28	62		
		8	29	61	
5-1	PCH506 : (PCH50) ₂ 8 : (R)-D2 = 100 : 3 : 0.5	33	49		
		4	34	49	
5-2	ibid. = 100 : 3 : 1	30	50		
		0	34	50	
6-1	PCH506 : (PCH50) ₂ 8 : (R)-D2 = 100 : 5 : 0.5	30	51		
		4	34	52	
6-2	ibid. = 100 : 5 : 1	31	52		
		0	33	52	
7-1	PCH506 : (PCH50) ₂ 8 : (R)-D2 = 100 : 10 : 0.5	31	55		
		3	30	57	
7-2	ibid. = 100 : 10 : 1	30	55		
		0	30	55	
8	PCH506 : (PCH50) ₂ 6 : (R)-D3 = 100 : 10 : 0.5	26	35	50	
		15	35	51	

^a C: crystal, S: smectic, N*: chiral nematic, I: isotropic.

^b Upper and lower bar graphs indicate the heating and cooling processes, respectively.

2-2 [PCH506:(PCH50)₂8:(R)-D-1 = 100:3:2] showed the N* phase in the region of 35–42 °C in the heating process. This is because the miscibility of the chiral dopant itself to the parent N-LC decreases.

On one hand, the helical pitches of **System 1** to **System 7** (including **D-1** and **D-2**) were evaluated with Cano's wedge method. This method was based on the observation of the distance between discontinuity lines that appeared when the N*-LC was inserted into a cell with a gradient thickness. The helical pitches of N*-LCs varied from 5.6 to 3.0 μm with a change of the mole percentage of **D-1** (from 1.0 to 2.0 mol %) and from 2.4 to 1.1 μm with **D-2** (from 0.5 to 1.0 mol %). On the other hand, the helical pitch of **System 8** (including **D-3**) was evaluated with the selective light reflection method because the helical pitch of **System 8** is too short to be observed in the Cano's wedge method. The center wavelength for the maximally reflected light (λ_{\max}) was 1380 nm. Thus, the helical pitch of **System 8** was evaluated to be 920 nm by using the equation $p = \lambda_{\max}/n$ ($n = 1.5$). The HTPs (β_M) of **D-1** and **D-2** were 18 and 90 μm⁻¹, respectively. It is clear that the HTP of the chiral dopant **D-2** is 5 times larger than that of **D-1**. This may be

rationalized with a difference in the number of substituents. Namely, the axially twisting torque of **D-2** is more effectively transferred to environmental N-LC molecules, by virtue of intermolecular interactions between four PCH substituents of **D-2** and the PCH moieties of LC molecules, rather than in the case of **D-1** bearing two PCH substituents. Besides, the HTP of **D-3** was evaluated to be 240 μm⁻¹, which is ca. 2.7 times larger than that (90 μm⁻¹) of **D-2**. The structural difference between **D-2** and **D-3** is that the PCH moieties are indirectly and directly linked with the 6,6'-positions of the binaphthyl rings, respectively. That is, the absence of the hexamethylene spacer, [-(CH₂)₆-] leads to a rigidity in the linkage between the PCH moieties and the binaphthyl rings of **D-3**, resulting in a larger HTP of **D-3** than that of **D-2**.

Liquid Crystallinity of the Chiral Dopant. Here it is important to emphasize the liquid crystallinity of the chiral dopant itself. The helical pitches of the N*-LCs induced by **D-2** and **D-3** (**System 3** to **System 8**) were shorter than those by **D-1**. This is partly because **D-2** and **D-3** have larger HTPs than **D-1**, and partly because they have a higher miscibility to the parent N-LC than **D-1**. The latter is due to the fact

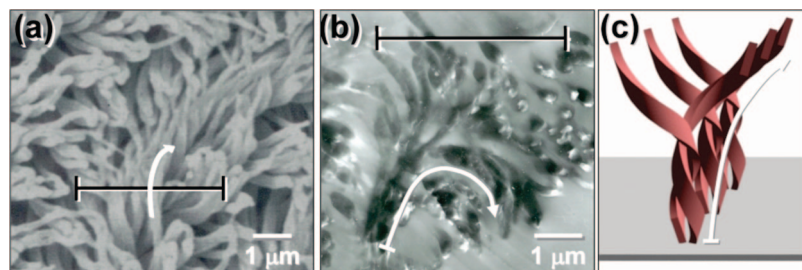


Figure 20. (a) SEM image of the surface of the vertically aligned H-PA. (b) TEM image of the cross section of the vertically aligned H-PA. The H-PA film was synthesized in the N*-LC, **System 1** [PCH506:(PCH50)₂:6:(R)-**D-1** = 100:3:2]. (c) Schematic representation of vertically aligned H-PA fibrils with left-handed screw direction.

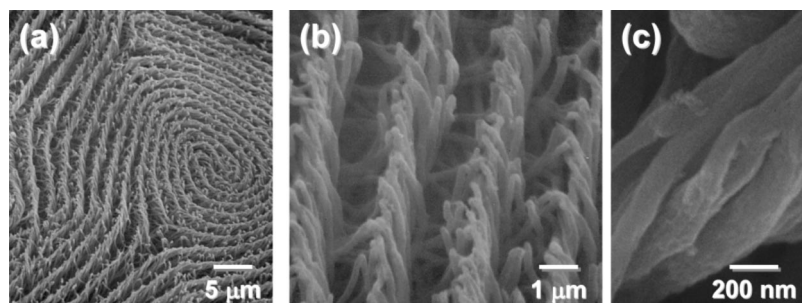


Figure 21. SEM images showing hierarchical spiral morphology of vertically aligned H-PAs synthesized in the N*-LC including (R)-**D-2**, **System 5-1**, [PCH506:(PCH50)₂:8:(R)-**D-2** = 100:3:0.5].

that **D-2** and **D-3** have liquid crystallinity. The high miscibility of the chiral dopant allows the concentration of the chiral dopant to be increased for preparation of highly twisted N*-LC and also the temperature region of the N* phase to be enlarged. The wide range of temperature for the N*-LC is favorable for the acetylene polymerization because the exothermal heat inevitably produced in the acetylene polymerization might raise the temperature inside a Schlenk flask and easily destroy the LC phase, becoming an isotropic one (Table 4). Therefore, the high miscibility based on the liquid crystallinity of the chiral dopants, and also the high HTPs, are important factors in preparing highly twisted N*-LCs, irrespective of a horizontally or vertically oriented reaction field.

Morphologies of H-PAs. Figure 20 shows a SEM image of the H-PA synthesized in **System 1** [PCH506 + (PCH50)₂:6 + (R)-**D-1**]. The fibrils of the H-PA are vertically aligned and screwed with left-handed direction. The helical axis of the fibril bundle is perpendicular to the film surface. This is in contrast to the case of the horizontally aligned H-PA, where the helical axis is parallel to the film surface. As found in Figure 20, the fibrils of the H-PA grow perpendicular to the helical axis of the N*-LC in which the screw direction of the fibril bundle is opposite that of the N*-LC. This is in accordance with the mechanistic picture of Figure 19f. The height of the vertically aligned fibril is estimated to be about 2 μm on the basis of the TEM image of Figure 20b.

We examined the SEM images of the H-PA films synthesized in **System 2** [PCH506 + (PCH50)₂:8 + (R)-**D-1**]. The fibrils are vertically aligned but loosely screwed, forming a swirl of the fibril bundle. When the concentration of the chiral dopant increases, the fibrils are highly screwed and grow rather parallel to the surface of the film. It may be argued that **System 1**, using (PCH50)₂:6 as the vertical orientation inducer, is more favorable than **System 2**, using (PCH50)₂:8, so far as the formation of the vertically aligned and twisted fibril morphology is concerned.

Figures 21 and 22 show SEM images of the H-PA films synthesized in **System 5-1** [PCH506 + (PCH50)₂:8 + (R)-

D-2]. The bundle of fibrils of the H-PA are vertically aligned and highly twisted in the left-handed direction. The hierarchy in the helical structure is observed in the vertically aligned H-PA. Namely, the H-PA has a spiral morphology (Figure 21a), and each spiral is composed of bundles of vertically aligned fibrils with one-handed screwed direction (Figure 21b), and furthermore the fibril itself is screwed with the same direction of the bundles (Figure 21c). It is confirmed that the screw directions of the fibril and the bundle are opposite to the helical sense (right-handed screw direction) of the N*-LC. As clearly seen in Figure 22, even the left- and right-handed screw directions of the vertically aligned fibrils are controllable by the chiral dopants with (R)- and (S)-configurations, respectively.

5.1.2. Horizontal and Vertical Alignments of N*-LC and H-PA

The interdistances ($d = 0.6\text{--}1.2\ \mu\text{m}$) between the fibril bundles and the helical pitches ($p = 1.1\text{--}2.4\ \mu\text{m}$) of the fibrils of the H-PAs synthesized in **System 3** to **System 7** are shorter than those ($d = 1.7\ \mu\text{m}$, $p = 3.6\ \mu\text{m}$) in **System 1** or those ($d = 1.5\text{--}2.8\ \mu\text{m}$, $p = 3.1\text{--}5.8\ \mu\text{m}$) in **System 2**. This is because **System 3** to **System 7** have the chiral dopant of **D-2** whose HTP ($\beta_M = 90\ \mu\text{m}^{-1}$) is much larger than that of **D-1** ($\beta_M = 18\ \mu\text{m}^{-1}$) used in **System 1** or **System 2**, and therefore, they serve for highly twisted N*-LCs. However, it should be emphasized that the synthesis of the vertically aligned H-PA is not always guaranteed even if the chiral dopant with large HTP, such as **D-2**, is used to prepare the N*-LC. For instance, the SEM image of the H-PA synthesized in **System 5-2** [PCH506:(PCH50)₂:8:(R)-**D-2** = 100:3:1] shows that the helical pitch is 1.2 μm. Although the H-PA has a spiral morphology consisting of helical fibrils, the fibrils are not vertically aligned, but horizontally aligned, i.e., lying on the surface. This may be due to the fact that the nature of the horizontal N*-LC became too strong due to the relatively high concentration of the chiral dopant with large HTP and that the concentration of the vertical orienta-

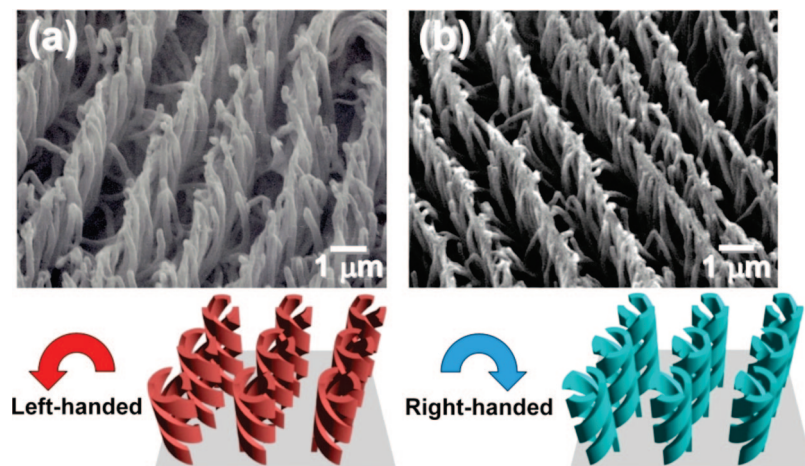


Figure 22. SEM images of the vertically aligned H-PAs synthesized in the N*-LCs with opposite screwed structures. (a) **System 5-1** [PCH506:(PCH50)₂8:(R)-D-2 = 100:3:0.5]; (b) **System 5-1** [PCH506:(PCH50)₂8:(S)-D-2 = 100:3:0.5].

tion inducer [(PCH50)₂8] is too low to change the horizontal N*-LC into the vertical one.

Let us see the SEM images of the H-PAs synthesized in **System 6-1** [PCH506:(PCH50)₂8:(R)-D-2 = 100:5:0.5] and **System 6-2** [PCH506:(PCH50)₂8:(R)-D-2 = 100:5:1]. It is evident that the combination of the orientation inducer (PCH50)₂8 and the chiral dopant **D-2** enabled us to control not only the vertical orientation but also the horizontal one, even in the N*-LC, and therefore those of the H-PAs. At the same time, it was found that the vertical and horizontal orientations in the present systems sensitively depend on the relative concentration of the orientation inducer and the chiral dopant. For instance, in a concentration where the nature of the orientation inducer (PCH50)₂8 becomes stronger than that of the chiral dopant **D-2**, the LC shows a vertical orientation of helically twisted structure. However, in another concentration where the nature of the former becomes weaker than that of the latter, the LC shows a horizontal orientation of helically twisted structure. The chiral dopants (**D-1** and **D-2**) have a tendency to align the parent LC horizontally as well as a tendency to twist it in a one-handed direction. Therefore, a certain amount of the vertical orientation inducer, (PCH50)₂6 or (PCH50)₂8, is required to prepare the vertically aligned and helically twisted N*-LC.

Let us examine the SEM images of the H-PA films synthesized in **System 4** [PCH506:(PCH50)₂6:(R)-D-2 = 100:10:1] and **System 7-2** [PCH506:(PCH50)₂8:(R)-D-2 = 100:10:1]. Although both systems have the same components and concentrations except the vertical orientation inducer, **System 4** and **System 7-2** gave the vertically aligned and horizontally aligned H-PAs, respectively. As far as the synthesis of vertically aligned H-PA is concerned, the former (**System 4**) is more preferable than the latter (**System 7-2**).

In the vertical but nonhelically twisted orientation of N-LC, (PCH50)₂8 shows a stronger ability to align the parent LC molecules [PCH506] than (PCH50)₂6. In contrast, (PCH50)₂8 shows less ability as a vertical orientation inducer than (PCH50)₂6 in the case of the vertical and helically twisted orientation, as clarified here. This indicates that the ability of the vertical orientation inducer depends on the matching in molecular structure between the chiral dopant and the parent LC in a nonhelical or helical LC environment.

We are concerned with the helical pitches of N*-LCs (**System 1** to **System 7**) and the structural parameters, such as the interdistances between the fibril bundles, the diameters

of the fibril bundle and those of the fibrils, and the directions of fibril alignment of the H-PAs. It is confirmed through the table that the interdistance (d) between the fibril bundles almost equals half of the helical pitches (p), $d = p/2$, and that this relationship holds irrespective of the direction of the fibril alignment.

Besides, it is worth noting that although the fibril bundles decrease in diameter with decreasing helical pitch (i.e., with increasing helical twist) of the N*-LC, the fibril remains unchanged, keeping the diameter in the range of 150–250 nm. This suggests that when acetylene polymerization is carried out in the highly twisted N*-LC, the resultant H-PA may not form the bundle of the fibrils, but give bundle-free fibrils, as currently found in the ordinary (horizontally aligned) H-PA. This motivates us to use the chiral dopant with much larger HTP, as will be discussed below.

The SEM image of the H-PA film synthesized in **System 8** [PCH506:(PCH50)₂6:(S)-D-3 = 100:5:0.5] was examined. **System 8** is a highly twisted N*-LC having a helical pitch of 920 nm because it includes the tetrasubstituted binaphthyl derivative (**D-3**) as a chiral dopant, whose HTP ($240 \mu\text{m}^{-1}$) is ca. 2.7 times larger than that ($90 \mu\text{m}^{-1}$) of **D-2**, as mentioned before. The H-PA has right-handed and vertically aligned fibrils, but it has no bundle of the fibrils. This is in quite contrast to the morphology of other H-PAs synthesized in **System 1** to **System 7**. Such a difference in morphology may be explained as follows.

In the weakly twisted N*-LCs (**System 1** to **System 7**) whose helical pitches are larger than $1 \mu\text{m}$, the fibrils of the resultant H-PA are gathered, owing to van der Waals interactions, to form the bundle of fibrils. Therein, the diameters of the fibril and the bundle are 150–250 nm and about $1 \mu\text{m}$, respectively. On the other hand, in the strongly twisted N*-LC (**System 8**) whose helical pitch is smaller than $1 \mu\text{m}$, the resultant H-PA has highly screwed fibrils but not the bundle of fibrils. This is because the helical pitch of 920 nm of **System 8** is too small to form the bundle of fibrils. The morphology free from the bundle of fibrils might be useful in evaluating electromagnetic properties of the vertically aligned and screwed fibril.

In summary, macroscopically aligned H-PAs are synthesized in the orientation-controlled N*-LCs. The N*-LCs are prepared by adding the vertical orientation inducer [(PCH50)₂6 or (PCH50)₂8] and the chiral dopant (the binaphthyl derivatives such as **D-1**, **D-2**, or **D-3**) into the parent N-LC [PCH506]. It is found that the horizontal or

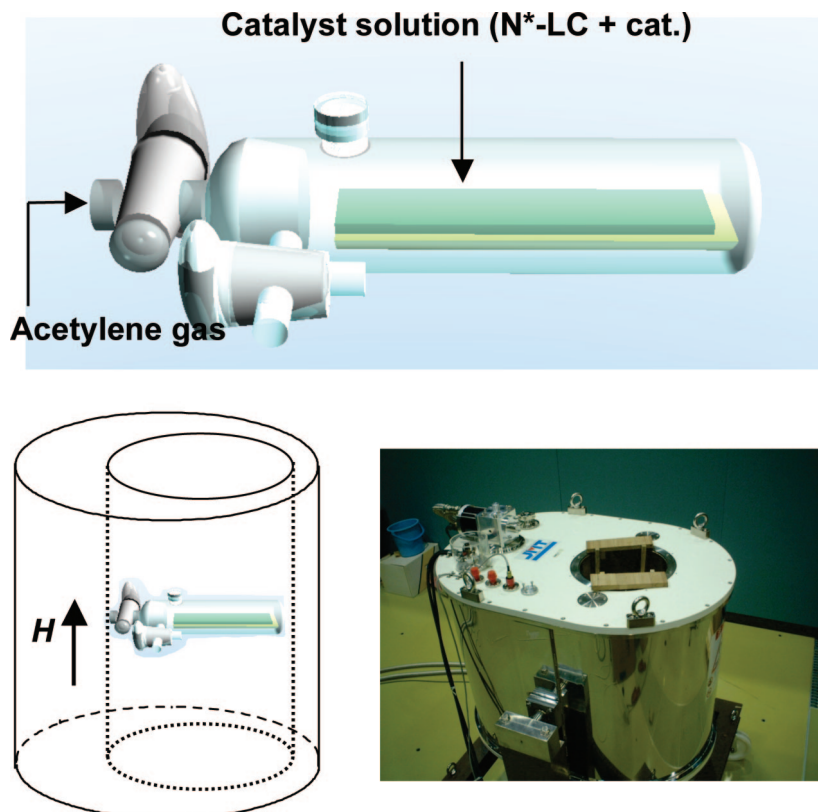


Figure 23. Apparatus for acetylene polymerization in N- and N*-LC solvents under a vertically applied magnetic field.

vertical orientation of the N*-LC crucially depends on (i) the relative concentrations of the vertical orientation inducer and the chiral dopant, (ii) the miscibility of the vertical orientation inducer to the parent N-LC, and (iii) the helical twisting power of the chiral dopant. In other words, the balance in effectiveness of the roles between the vertical orientation inducer and the chiral dopant dominates the macroscopic orientation of the N*-LC and hence the morphological alignment resultant of the H-PA. The present orientation controllable N*-LCs are useful for the synthesis of macroscopically aligned conjugated polymers, allowing morphological control without any external force or oriented substrate.

5.2. Aligned H-PA Synthesized in a N*-LC under a Magnetic Field

The morphology of PA film is determined during the polymerization owing to its insolubility and infusibility. Now we aim to prepare a macroscopically aligned H-PA film to draw on the intrinsic electromagnetic properties such as induced solenoid magnetism. Note that although there is a choice for synthesizing horizontally^{44,46} or vertically^{162,163} aligned PA film, only the latter is focused on in this section.

Previously, the vertically aligned PA film was synthesized in a homeotropic LC.¹⁵⁸ The homeotropic LC was prepared by adding a so-called orientation dopant into the nematic LC, where the orientation dopant is composed of two mesogenic cores linked with a hexamethylene spacer. Although the orientation dopant technique gave us a very convenient and easy way to achieve the homeotropic alignment of the LC, it prevented us from obtaining highly homogeneous vertically aligned fibrils. This is because the effect of the orientation dopant in the N-LC is sensitively

affected by changes of temperature and pressure during acetylene polymerization.

Therefore, it is desirable to employ an alternative method for the construction of the homeotropic LC phase. In this study, a magnetic field of 5 T was applied as an external perturbation⁴⁶ to the vertical direction of the PA film (parallel to film thickness), as shown in Figure 23. Under such an external force field, the N-LC and N*-LC were vertically aligned. These reaction fields were used to synthesize macroscopically vertically aligned PA and H-PA films, respectively.¹⁶⁴

N*-LCs were prepared by adding a small amount of chiral dopant (0.5–1 mol %) into an equimolar mixture of two kinds of N-LCs, 4-(*trans*-4-*n*-propylcyclohexyl)ethoxybenzene [PCH302] and 4-(*trans*-4-*n*-propylcyclohexyl)butoxybenzene [PCH304]. The binaphthyl derivatives, (*R*)- or (*S*)-(PCH506)_{*n*}-Binol (*n* = 2, 4), were used as chiral dopants, where the binaphthyl rings have substitutions of PCH moieties at the 2,2'-positions (*n* = 2) and 2,2'- and 6,6'-positions (*n* = 4), respectively.

These di- and tetrasubstituted binaphthyl derivatives were miscible in the N-LC of PCH320 and PCH304 and exhibited large twisting powers owing to their axial chirality. The helical pitches of N*-LCs were measured using the Cano-Grandjean method.¹²⁶ The N*-LCs including the di- and tetrasubstituted binaphthyl derivatives showed helical pitches of 5 μm (1 mol %) and 1.5 μm (0.5 mol %), respectively. This indicates that the tetrasubstituted binaphthyl derivative has a larger twisting power than the disubstituted one.

Figure 24a shows SEM photographs of PA films synthesized in a homeotropic N-LC under a vertically applied magnetic field of 5 T. It is clearly observed that the fibrils are vertically aligned. This implies that the nematic LCs are aligned parallel to the magnetic field, giving rise to the

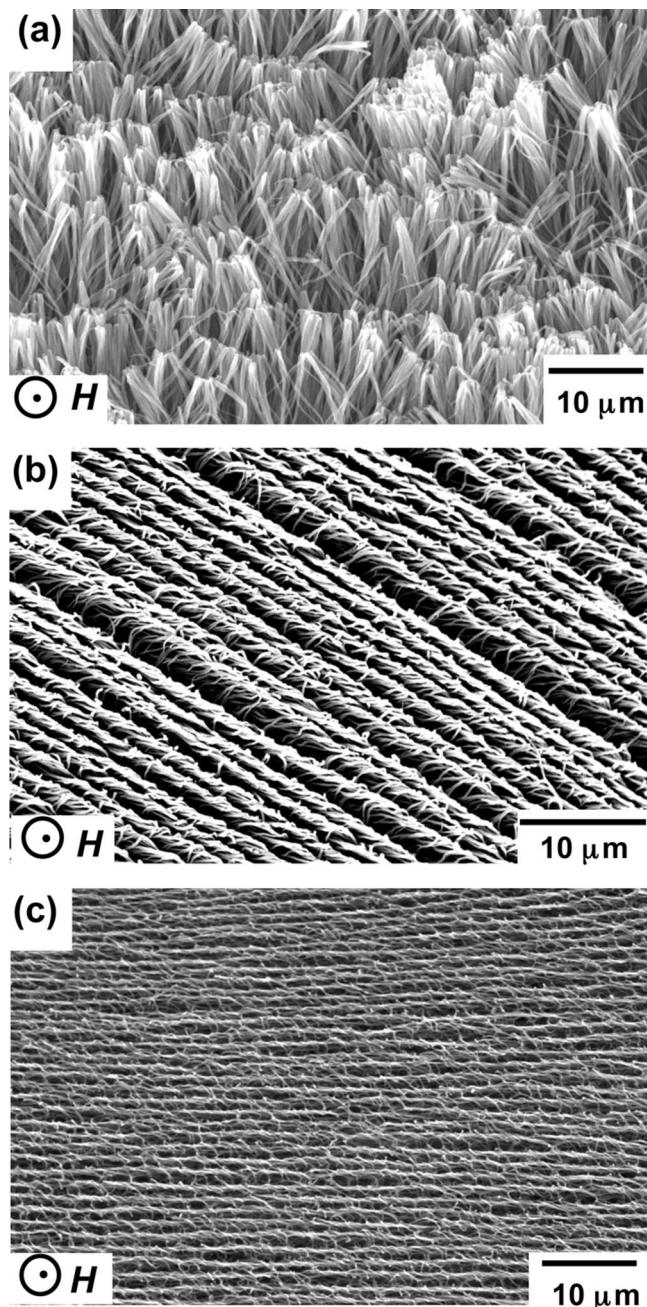
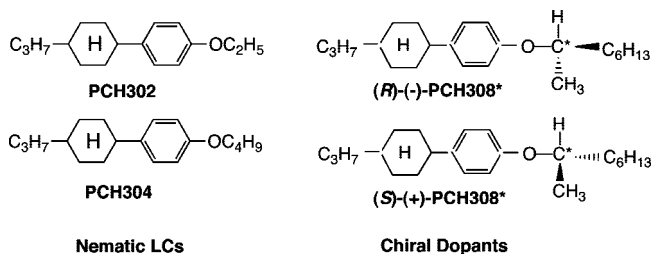


Figure 24. SEM photographs of PA film synthesized under a magnetic field. (a) Vertically aligned PA film in N-LC; (b) H-PA film in N*-LC including disubstituted binaphthyl derivative, (R)-(PCH506)₂-Binol; (c) H-PA film in N*-LC including tetrasubstituted binaphthyl derivative, (S)-(PCH506)₄-Binol.

monodomain structure of homeotropic alignment. The fibril length was in the range of 5–15 μm, depending on the polymerization time, acetylene gas pressure, and catalyst concentration.

Parts (b) and (c) of Figure 24 show SEM photographs of H-PA films synthesized in N*-LCs including the di- and tetrasubstituted binaphthyl derivatives, respectively, under a vertically applied magnetic field of 5 T. It is seen from Figure 24b that the fibrils form twisted bundles of fibrils with a counterclockwise screw direction. The bundles are aligned horizontally (perpendicular to the magnetic field), and at the same time the fibrils grow vertically toward the inside of the film (parallel to the magnetic field). In the case of a highly twisted N*-LC (Figure 24c), however, the vertically aligned fibril morphology is not observed, although

Scheme 3. Chiral Nematic LCs Including the Parent LCs and Asymmetric Center-Containing Chiral Compounds



the twisted bundles of fibrils with clockwise screw direction are aligned horizontally. The results suggest that the magnetic field of 5 T is not enough for the complete alignment of the N*-LC, especially in the case of a highly twisted N*-LC. Sophisticated control of the alignment in the region of the free surface of the N*-LC is also required.

It is interesting to find the relationship between the orientation of N*-LCs and H-PAs under a vertically applied magnetic field. It is helpful to keep in mind that the helical axes of N*-LCs are aligned perpendicular to the direction of the magnetic field, when the magnetic field is applied. This explains the fibril morphology formed in the N*-LC under a vertically applied magnetic field. The homeotropic N-LC of monodomain structure was constructed with a vertically applied magnetic field. The macroscopically vertically aligned PA film was synthesized using this homeotropic N-LC as a solvent. Next, H-PA films were synthesized in a N*-LC under a vertically applied magnetic field. The magnetic field of 5 T is sufficient for the alignment of the N*-LC including the disubstituted binaphthyl derivative, but not so for the complete alignment of a more highly twisted N*-LC including the tetrasubstituted binaphthyl derivative.

In summary, PA films with vertically aligned fibril morphology were synthesized in homeotropic N-LC solvent by using a magnetic field of 5 T as an external perturbation. Next, H-PA films with vertically aligned and screwed fibril morphology were synthesized in a macroscopically aligned N*-LC under a magnetic field. A scanning electron micrograph indicated that the lengths of the fibrils from the substrate were 5–20 μm, depending on the polymerization time, acetylene pressure, and catalyst concentration.

6. Extension in the N*-LC Reaction Field

6.1. Polymerization in a N*-LC Including an Asymmetric Center-Type Chiral Dopant

This section aims to elucidate the fact that the N*-LC available for synthesis of H-PA can also be prepared with other types of chiral dopants, except for the axially chiral binaphthyl derivatives. Here, the asymmetric center, including the phenylcyclohexyl derivatives, designated as (R)- and (S)-PCH308*, are subjected (Scheme 3).¹⁶⁵ Through characterizations of catalyst dissolved in N*-LC solvent and PA films, the feasibility of the PCH308* as the chiral dopant was examined.

The coupling reaction between *para*-(*trans*-4-propylcyclohexyl)phenol (PCH300) and (S)-(+)-2-octanol or (R)-(-)-2-octanol was carried out according to the Mitsunobu reaction with diethyl azodicarboxylate and triphenylphosphine, producing a chiral phenylcyclohexyl derivative, (R)-(-)- or (S)-(+)-2-(4-(*trans*-4-*n*-propylcyclohexyl)phenoxy)-octane. For simplicity, they are abbreviated as (R)-PCH308*

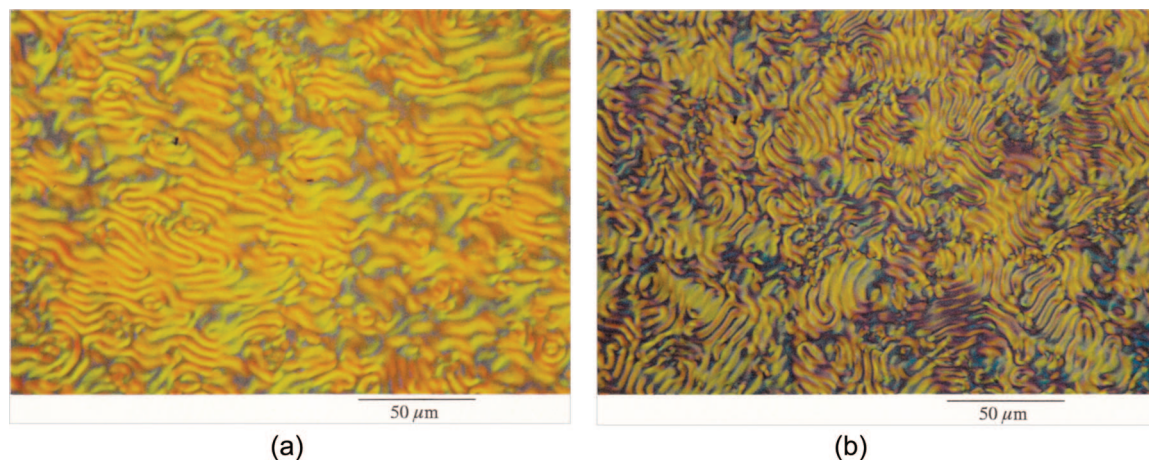


Figure 25. Polarizing optical micrographs of N*-LCs with $\text{Ti}(\text{O}-n\text{-Bu})_4\text{-AlEt}_3$ catalyst including (*R*)-PCH308* (a) and (*S*)-PCH308* (b).

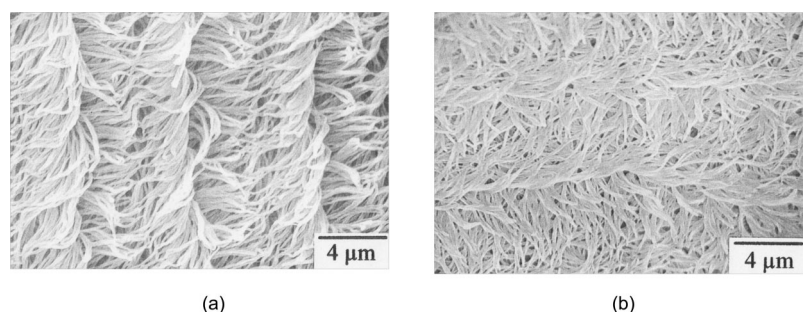


Figure 26. Scanning electron micrographs photographs of H-PAs films synthesized in N*-LCs including (*R*)-PCH308* (a) and (*S*)-PCH308* (b).

and (*S*)-PCH308*, respectively. Note that this kind of coupling reaction is of the $\text{S}_{\text{N}}2$ type, and the steric configuration is inverted.

The CD spectra of (*R*)- and (*S*)-PCH308* showed negative and positive Cotton effects, respectively. The specific rotatory powers, $[\alpha]_{\text{D}}$, for (*R*)- and (*S*)-PCH308* were respectively -9.2° and $+9.2^\circ$ ($c = 1$, THF). It should be noted that although the absolute values of the specific rotatory powers are substantially smaller than those of chiral binaphthol derivatives ($[\alpha]_{\text{D}} = +24.0^\circ$), the chiral PCH308* derivatives were confirmed to be feasible for the chiral dopant to the nematic LC, as will be shown below.

Next, the chiral nematic LC was prepared by adding 5 wt % of the (*R*)- or (*S*)-PCH308* into the equiweighted mixture of nematic LCs, PCH302 and PCH304. To elucidate the screw direction of the N*-LC, the miscibility test was carried out using cholesteryl chloride, which is a representative cholesteric (N*) LC with a right-handed screw direction. The mixture of the (*R*)-N*-LC and cholesteryl chloride showed no change in optical texture, keeping a chiral nematic phase. In contrast, the mixture of the (*S*)-N*-LC and cholesteryl chloride lost the striae characteristic of a chiral nematic phase in the optical microscope, yielding instead a feature corresponding to an ordinary nematic phase. The results demonstrate that the screw directions of the (*R*)- and (*S*)-N*-LCs are the same as and opposite to that of cholesteryl chloride, respectively. Namely, the (*R*)- and (*S*)-N*-LCs are screwed clockwise and counterclockwise, respectively.

The (*R*)- and (*S*)-N*-LCs were used as solvents for a Ziegler–Natta catalyst consisting of $\text{Ti}(\text{O}-n\text{-Bu})_4$ and AlEt_3 . The concentration of $\text{Ti}(\text{O}-n\text{-Bu})_4$ was 20 mmol/L, and the mole ratio of the cocatalyst-to-catalyst, $[\text{AlEt}_3]/[\text{Ti}(\text{O}-n\text{-Bu})_4]$, was 4.0. Figure 25 shows polarizing optical micrographs of

(*R*)- and (*S*)-N*-LC systems including the $\text{Ti}(\text{O}-n\text{-Bu})_4\text{-AlEt}_3$ catalyst. In both cases striated Schlieren textures characteristic of chiral nematic phases were observed. The catalyst solution was aged for 0.5 h at room temperature and was moved, using a syringe, into the flat-bottom container inside a Schlenk flask.

The polymerization was carried out by introducing acetylene gas into the catalyst solution. The polymerization temperature was kept at 18°C to maintain the chiral nematic phase. The initial acetylene pressure was 130 Torr, and the polymerization time was 5–8 min. After polymerization, the PA film was carefully stripped off from the container and washed with toluene and subsequently with a 1 N HCl–methanol mixture under argon gas. The film was dried through vacuum pumping on a Teflon sheet and stored in a freezer at -20°C .

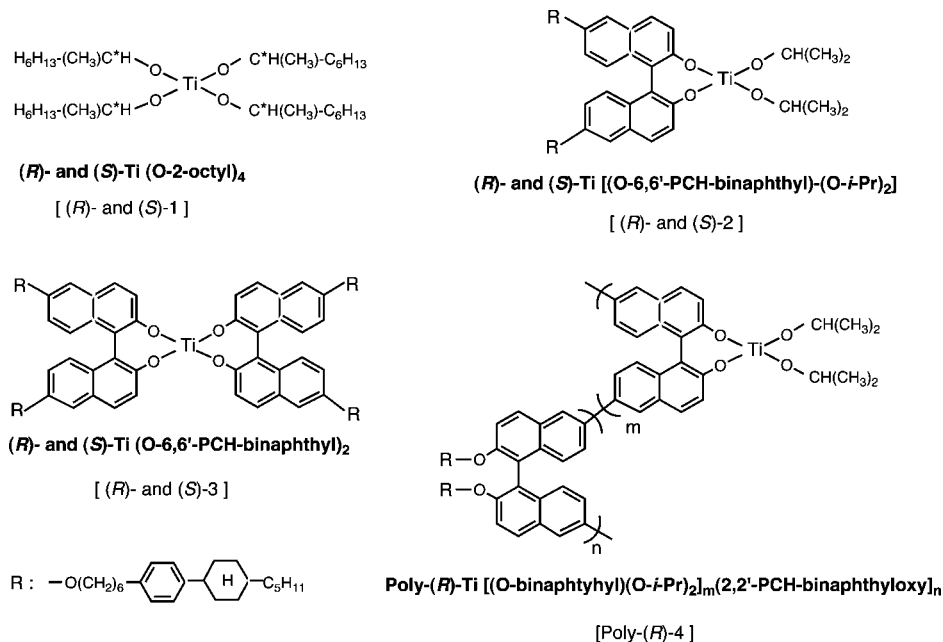
Figure 26 shows scanning electron micrographs of PA films. The bundles of PA fibrils synthesized under the (*R*)- and (*S*)-N*-LCs are screwed clockwise and counterclockwise, respectively. In addition, the screw directions of the bundles of the fibrils coincide with those of the N*-LCs used as polymerization solvents. The locally aligned fibril morphology is due to spontaneous orientation within the LC domain.

The (*R*) and (*S*)-PA films showed negative and positive Cotton effects, respectively, in the region from 400 to 800 nm corresponding to the $\pi \rightarrow \pi^*$ transition of the PA chain. This indicates that the PA chain itself is also helically screwed. The right-handed direction of the (*R*)-PA is determined by the (*R*)-N*-LC, similar to the left-handed direction of the (*S*)-PA by the (*S*)-N*-LC.

It is worth noting that the present PA film showed high electrical conductivities of $1.5\text{--}4.0 \times 10^3$ S/cm after iodine doping. The high conductivity and the helical structure may

Table 5. Helical Pitches of N*-LCs

N*-LCs	(<i>R</i>)-1 system	(<i>S</i>)-1 system	(<i>R</i>)-2 system	(<i>S</i>)-2 system	(<i>R</i>)-3 system	(<i>S</i>)-3 system	Poly-(<i>R</i>)-4 system
helical pitch (μm)	8.4	10.0	5.2	7.7	2.4	2.8	4.7

Scheme 4. Chiral Titanium Complexes with Chiral Center-Containing Groups [(*R*)-, (*S*)-1] and Axially Chiral 1,1'-Binaphthyl Derivatives [(*R*)-, (*S*)-2; (*R*)-, (*S*)-3; Poly-(*R*)-4]

allow us to expect that the present PA could be available for molecular solenoid in which an induced magnetic field is generated by virtue of the solenoidal current at the molecular level. As another application, the H-PA is anticipated to be a second-order nonlinear optical material, and also a third-order nonlinear one.

In summary, H-PAs were synthesized under an asymmetric and anisotropic reaction field constructed with the chiral nematic LC. It is expected that the present polymerization method using the chiral nematic LC might be applicable even for the synthesis of other kinds of helical π -conjugated polymers without chiral substituents.

6.2. Chiral Titanium Catalysts

The N*-LC used in the asymmetric polymerization, however, requires at least the following four components: nematic liquid crystal, chiral dopant, catalyst, and cocatalyst. This made the polymerization conditions difficult to optimize. The current aim is to develop a new compound that can be used for both the chiral dopant and catalyst. Chiral titanium complexes are suitable for this aim because of their well-confirmed catalytic activity for acetylene polymerization. Such titanium complexes could not only make it much easier to optimize the polymerization conditions, owing to a substantial decrease of parameters, but also should be helpful in understanding a mechanism for the formation of the helical structure in a chiral mesophase.¹⁶⁶ At the present stage, it seems undeniable that the reaction field available for the synthesis of H-PA requires the following four components: nematic LC, chiral dopant, catalyst, and cocatalyst. However, if there existed a compound that could be used as both the chiral dopant and the catalyst, it could become much easier to optimize the polymerization conditions owing to a substantial decrease of the parameters. Such a compound would be helpful in understanding a mechanism for the

formation of the helical structure. This is because there are at least two factors to be elucidated, such as local asymmetry on the catalytically active species, and a helical environment affecting the propagation processes of polymer chains and fibrils. Thus, the preparation of a compound satisfying the above-mentioned requirement is desirable. The most convincing approach should be to synthesize chiral dopants with catalytic activity by introducing chiral ligands into titanium complexes.

We synthesized a series of chiral titanium complexes with chiral center-containing groups [(*R*)-, (*S*)-1] and axially chiral 1,1'-binaphthyl ones [(*R*)-, (*S*)-2; (*R*)-, (*S*)-3; Poly-(*R*)-4] as coordination ligands to develop catalytically active chiral dopants feasible for the synthesis of H-PA. As shown in Table 5, the chiral titanium complexes with axially chiral 1,1'-binaphthyl groups, (*R*)-2, (*S*)-2, (*R*)-3, (*S*)-3, and Poly-(*R*)-4 systems, have shorter helical pitches than those with a chiral center [(*R*)-, (*S*)-1 system]. This indicates that the former has a larger helical twisting power than the latter. Such a difference in the catalyst solutions should influence the formation of the helical structure of PA.

Here we focus on novel chiral titanium complexes, **1** and **2**, as shown in Scheme 4. Chiral center-containing (*R*)- and (*S*)-2-octanol and axially chiral binaphthyl derivatives, (*R*)- and (*S*)-6,6'-di-[4-(*trans*-4-*n*-pentylcyclohexyl)phenoxy-1-hexyl]-2,2'-dihydroxy-1,1'-binaphthyl, were adopted as coordination ligands of titanium complexes to yield novel titanium complexes, (*R*)- and (*S*)-Ti(O-2-octyl)₄ [(*R*)-, (*S*)-1] and (*R*)- and (*S*)-Ti(O-6,6'-PCH506-Binaphthyl)₂ [(*R*)-, (*S*)-2]. It was found that these complexes exhibit not only the N* phase when dissolved in a mixture of nematic LCs of phenylcyclohexane derivatives, 4-(*trans*-4-*n*-propylcyclohexyl)ethoxybenzene (PCH302) and 4-(*trans*-4-*n*-propylcyclohexyl)butoxybenzene (PCH304), but also the catalytic activity for acetylene polymerization.

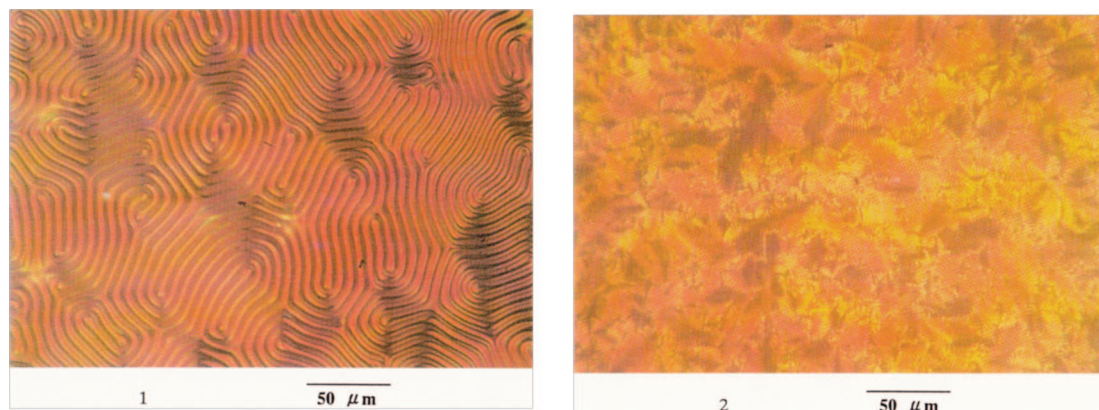


Figure 27. POMs of N*-LCs including (S)-1 and (S)-3. (1) PCH302:PCH304:(S)-1 = 100:100:10 (weight ratio), [Al]/[Ti] = 4, at 4 °C; (2) PCH302:PCH304:(S)-3 = 100:100:15 (weight ratio), [Al]/[Ti] = 4, at 18 °C.

The enantiotropic N*-LCs were prepared by adding a small amount (10–20 wt %) of chiral titanium complex **1** or **2** as a dopant into an equiweighted mixture of two kinds of nematic LCs of PCH302 and PCH304. The N*-LCs were used as an asymmetric reaction field including polymerization solvent and catalytic species. The concentrations of chiral titanium complexes **1** and **2** used as catalysts were 35–77 mmol/L, whereas the concentration ratio of cocatalyst-to-catalyst, [AlEt₃]/[Ti], was kept at 4. The catalyst solution was aged for 0.5–1.0 h at room temperature. Even after aging, the N* phase remained unchanged in the temperature range from –5 to 34 °C.

The polymerization temperature was controlled between 0 and 20 °C to maintain the N* phase. The initial acetylene pressure was 15–50 Torr and the polymerization time was 1–20 min. After polymerization, the PA films were carefully stripped off from the container and washed with toluene several times, and subsequently with methanol solution of hydrochloric acid (1 mol/L) under argon gas at room temperature. The film was dried through vacuum pumping on a Teflon sheet and stored in a freezer at –20 °C.

Figure 27 shows a polarizing optical micrograph of the N*-LC including (S)-1 and (S)-2. Fingerprinted textures observed for the catalyst solutions are characteristic of the N*-LC phase. The distance between the striae in the texture corresponds to a helical half pitch, and thus (S)-1 has a longer helical pitch than that of (S)-2. In other words, the degree of helicity in the former [(S)-1] is less than that of the latter [(S)-specific rotatory **2**]. This is well rationalized with the powers of (S)-1 and (S)-2, where $[\alpha]_D$ are +17.9° and +25.0°, respectively. To elucidate the screw directions of the present N*-LCs, miscibility tests were carried out using cholesteryl chloride, which is a clockwise cholesteric LC. The mixture of the N*-LC including (R)-Ti complex [(R)-1 or (R)-2] and cholesteryl chloride lost the striae characteristic of the N* phase in the polarizing optical microscope, yielding a texture of an ordinary nematic phase. In contrast, the mixture of the N*-LC including (S)-Ti complex [(S)-1 or (S)-2] and cholesteryl chloride showed no change in optical texture, keeping the N* phase. The results indicate that the screw directions of the (R)- and (S)-N*-LCs are opposite to and the same as that of cholesteryl chloride, respectively. Namely, they are counterclockwise and clockwise, respectively. The SEM photograph of H-PA film synthesized under the N*-LC including (S)-2 shows that the fibrils, bundles of PA chains, are further gathered to each other to form helical fibrils with clockwise direction, although the formation of the helical fibrils remains intermediate. Nevertheless, it is

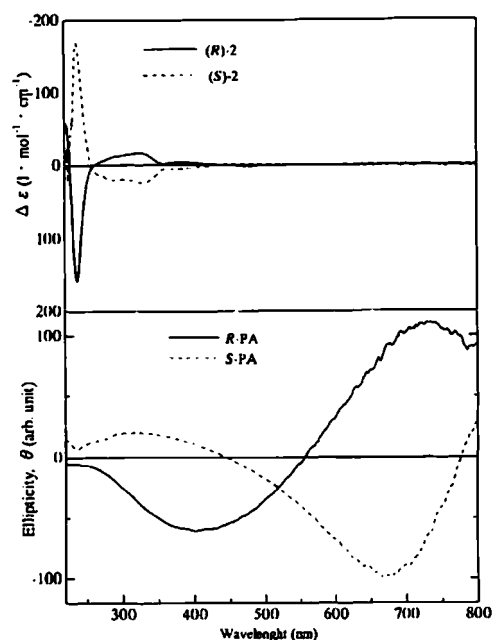


Figure 28. CD spectra of the chiral titanium complexes **3** in THF (upper) and H-PA films synthesized under the N*-LC including **3** (lower).

worth noting that the screw direction of the fibril is the same as that of the (S)-N*-LC.

Figure 28 shows the CD spectra of the chiral titanium complexes [(R)-, (S)-2] and the H-PA films [(R)-PA, (S)-PA] synthesized under the N*-LCs including the (R)-2 and (S)-2. The (R)-PA and (S)-PA exhibit positive and negative Cotton effects, respectively, in the region of 450–800 nm corresponding to the $\pi \rightarrow \pi^*$ transition of the PA chain. The signs of these Cotton effects are coincident with those of the chiral titanium complexes, (R)-2 and (S)-2. Thus, it is evident that the PA chain itself is helically screwed with the same direction as that of the N*-LC. Furthermore, it may be argued that the helical chains are bundled through van der Waals interaction to form helical fibrils. It should be noted that the substituent group such as 4-(*trans*-4-*n*-pentylcyclohexyl)phenoxy-1-hexyl (PCH506) in the chiral titanium complexes enhances the miscibility between the nematic LCs. In fact, usages of other chiral titanium complexes such as (R)-Ti(O-binaphthyl)₂ and (R)-(O-binaphthyl)(O-*i*-Pr)₂ gave insufficient miscibility, yielding no N* phase. This resulted in PA with no helical morphology. Meanwhile, acetylene polymerization in isotropic solution,

such as toluene, including the chiral titanium complex produced no helical structure.

In addition, it is worthwhile to reintroduce the previous experimental results: acetylene polymerization was carried out by using a $\text{Ti}(\text{O}-n\text{-Bu})_4\text{-AlEt}_3$ catalyst in a nematic LC solvent consisting of an equally weighted mixture of PCH302 and PCH304, but without a chiral dopant. The resultant PA film showed neither helical morphology in SEM micrographs nor a Cotton effect in the CD spectrum. The observed morphology was composed of fibrils that were locally aligned owing to the spontaneous orientation of the LC solvent. These results indicate that the N^* -LC environment is essential for the formation of the H-PA. It has been confirmed from the present study that the chiral titanium complexes, **1** and **2**, not only serve as chiral dopants to nematic LCs giving an induced N^* phase but also play the role of catalysts for acetylene polymerization. The H-PA film showed high electrical conductivities of $2.0 \times 10^3 \text{ S/cm}$ after iodine doping.

In summary, a series of chiral titanium complexes with chiral center-containing groups or axially chiral 1,1'-binaphthyl groups as coordination ligands were synthesized to develop catalytically active chiral dopants feasible for the asymmetric polymerization of acetylene. It has been found that these chiral titanium complexes not only serve as chiral dopants to nematic LCs giving an induced N^* phase but also play the role as catalysts for acetylene polymerization. The synthesized H-PA films showed spiral fibril morphologies and high electrical conductivities of $2.0 \times 10^3 \text{ S}\cdot\text{cm}^{-1}$ after iodine doping.

Part 3. Control of Helicity

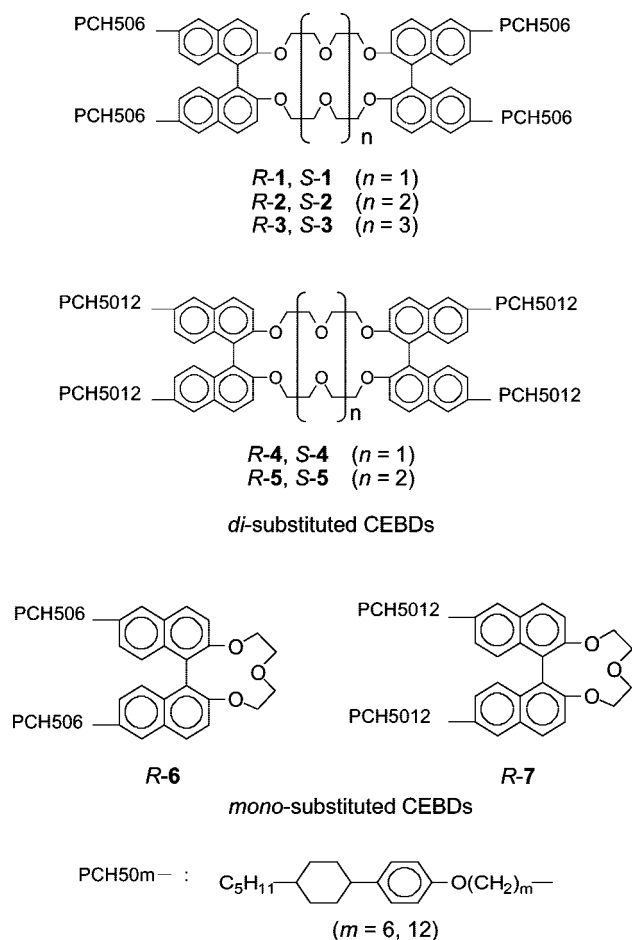
7. Control of the Helical Twisting Power

7.1. Chiral Dopants of Crown Ether-Type Binaphthyl Derivatives

H-PA films consist of a clockwise or counterclockwise helical structure of fibrils, which are the bundles of polyene chains. H-PA is anticipated to show novel electromagnetic and optical properties, and these properties are considered to depend on the screw degree of the fibrils. The morphology and the screw degree of the fibrils of H-PA are determined by the helical pitch of the N^* -LC. An N^* -LC is prepared by adding a small amount of chiral dopant into a nematic LC. The helical pitch (p) of the N^* -LC can be adjusted by two methods: changing the twisting power or changing the concentration of the chiral dopant.⁷⁰ However, the mesophase temperature region of the N^* -LC may also be affected by changing the concentration of the chiral dopant, which often becomes narrow as the concentration increases. Finally, the mesophase will be destroyed when the concentration is close to a critical value.^{71–74}

Addressing the limitation of the concentration method, this section focuses on an approach of utilizing chiral dopants with large twisting power for H-PA synthesis. Axially chiral binaphthyl derivatives have been reported to possess larger twisting powers than the compounds having asymmetric carbon atoms. Meanwhile, crown ethers are well-known to have the ability of forming complexes with alkali, alkaline earth, or a primary ammonium cations.¹⁶⁷ This interaction between the crown ether and cation is named a host–guest effect.¹⁶⁸ Here, a series of crown ether-type binaphthyl

Scheme 5. Crown Ether-Type Binaphthyl Derivatives (CEBDs)



derivatives (CEBDs) were synthesized in which one or two binaphthyl moieties were linked to a crown ether, with LC substituents being introduced to the 6,6'-positions of the binaphthyl moiety.

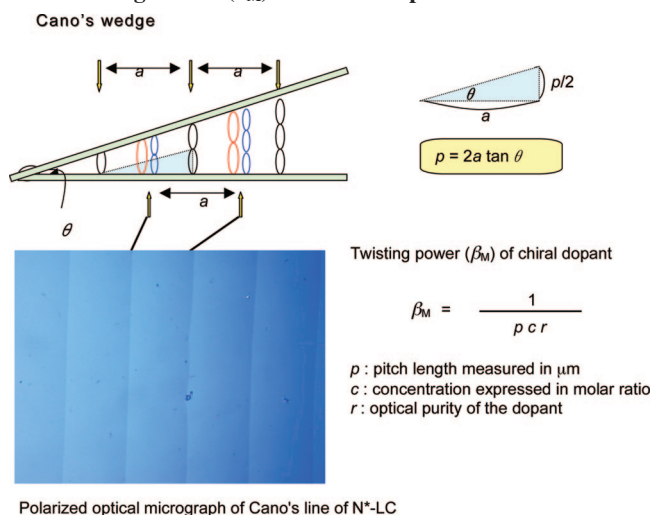
The aim is to control the twisting power of the CEBDs for the nematic LC, by optimizing the ring size of the crown ether. Additionally, the twisting powers of the CEBDs might be controlled through the host–guest interaction between the crown ether and cation. The target of this research is to control the helical pitch of N^* -LCs by changing the twisting power of the CEBDs, through which the morphology of H-PA can be controlled.

7.1.1. Synthesis of CEBDs

Two types of CEBDs, mono- and disubstituted CEBDs, were synthesized in which one and two binaphthyl moieties were linked to a crown ether, respectively. Their molecular structures are shown in Scheme 5. To improve their miscibility with the PCH-derived nematic LCs used for acetylene polymerization, LC substituents having a PCH mesogen core were introduced to the 6,6'-positions of the binaphthyl group. For the investigation of the effect of the methylene spacer length in the LC substituents on the twisting powers of the CEBDs, two kinds of methylene spacers ($m = 6, 12$) were designed.

The helical pitch of the N^* -LC was evaluated with Cano's wedge method,^{124,125} using a polarized optical microscope under temperature control (heating and cooling rate of $10 \text{ }^\circ\text{C/min}$). The Cano's wedge method is schematically de-

Scheme 6. Cano's Wedge Method for the Helical Pitch (p) and Twisting Power (β_M) of Chiral Dopant in N*-LC



scribed in Scheme 6. When the N*-LC sample was inserted into a wedge-type cell with gradient thickness, the discontinuity lines named Cano lines appeared on the surface of the cell under crossed nicols.^{154,169,170} The helical pitch (p) was evaluated by measuring the distance (a) between the Cano lines as follows:

$$p = 2a \tan \theta$$

where θ is the angle of wedge of the cell. The twisting power (β_M) of the chiral dopant was evaluated with the following equation:^{124,125,127}

$$\beta_M = 1/(pcr)$$

where c is the molar concentration of the chiral dopant and r is the enantiometric purity of the chiral dopant, and where r is assumed to be 1. The concentration of the chiral dopant was 5 mmol %, where the concentrations of PCH302 and PCH304 and the chiral dopant were 100:100:1 in molar ratio.

7.1.2. Twisting Power and Specific Rotation of the CEBDs

The twisting powers (β_M) of the CEBDs were evaluated with Cano's wedge method, which was based on the observation of the appearance of discontinuity lines when a N*-LC was inserted into a cell with gradient thickness. Table 6 shows the variation of twisting powers of the CEBDs having (R)-configuration with their structures.

As shown in Table 6, the twisting power (β) increased with the decrease of ring size of the crown ether for disubstituted CEBDs ((R)-1, (R)-2, and (R)-3). The ring size of the crown ether is expressed with the number of oxidimethylene repeat units (n) in the crown ether. Disubstituted CEBD ((R)-1, (R)-4) showed a larger twisting power than the monosubstituted one having the same substituent ((R)-6, ((R)-7). For both mono- and disubstituted CEBDs, the shorter the methylene spacer (m) in the LC substituents, the larger the twisting power ((R)-1 and (R)-4, (R)-2 and (R)-5, (R)-6 and (R)-7).

Besides the twisting power, the specific rotation ($[\alpha]_D^{23}$) can also be used to characterize the optical activity of a chiral compound.¹⁶⁹ To investigate the relationship between the twisting power and specific rotation, it is useful to measure

the specific rotation for the CEBDs at 23 °C. The results are shown in the fourth column of Table 6. For disubstituted CEBDs, the specific rotation increased with decreasing crown ether ring size. It also tends to increase with shortening of the methylene spacer (m) in the LC substitution of the biphenyl moiety. A similar tendency seems to be seen in the cases of monosubstituted CEBDs. Note that although the twisting power of monosubstituted CEBD (R)-7 is about one-third of that of disubstituted CEBD (R)-4, the specific rotation of (R)-7 is comparable to that of (R)-4 in absolute value. A similar situation can be seen between monosubstituted CEBD (R)-6 and disubstituted CEBD (R)-1. This implies that the twisting powers of the CEBDs have no direct relationship with their specific rotations.^{154,170} Nevertheless, one may remark that the relatively small size of the CEBD is suitable for generating a large specific rotation and/or twisting power.

It is interesting to note that the monosubstituted and disubstituted CEBDs having the same (R)-configuration show different symbols in specific rotation, the former a negative value and the latter a positive value. This implies that these two kinds of CEBDs have different screw directions. In fact, it is confirmed by the miscibility test that the N*-LCs induced by the mono- and disubstituted CEBDs exhibit different screw directions, i.e., left-handed and right-handed ones, respectively, as shown in Table 6. Before the above result is discussed, it is helpful to note that (R)-(+)-1,1'-bi-2-naphthol and (R)-(-)-1,1'-binaphthyl-2,2'-diyl-hydrogen-phosphate are dextro-rotatory (+) and levo-rotatory (-), respectively, in spite of the same (R)-configuration.¹⁷¹ The latter has a bridged structure linking two oxygen atoms at the 2,2'-positions of the binaphthyl rings via a -P(O)(OH)- moiety (see Scheme 7).

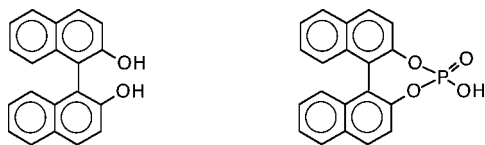
This implies that the axial chirality of the binaphthyl derivative sensitively depends on the local structure around the 2,2'-positions of the binaphthyl rings, and also on the change of the dihedral angle defined by two binaphthyl rings. This situation is similar to the present case where the mono- and disubstituted CEBDs with the same (R)-configuration give an opposite sign in specific rotation. It is expected that the larger crown ether-type cyclic ring of the disubstituted CEBD, compared with the monosubstituted CEBD, might lead to more flexibility in the dihedral angle. Although the specific rotation (specific rotatory power) is determined by the scalar product of the transition electric dipole moment and magnetic dipole moment, it is difficult here to argue how both the bridged structure and the change of the dihedral angle affect the sign of the specific rotation since this requires rigorous theoretical calculations.

The twisting power of the CEBDs may also be affected by temperature, and the affecting degree depends on the ring size of the crown ether. On one hand, the twisting power of (R)-1, which has the smallest ring size of any crown ether studied here ($n = 1$), decreased from 78 to 63 μm^{-1} when the temperature increased from 10 to 32 °C. On the other hand, the twisting powers of (R)-2 and (R)-3, which have larger crown ether ring sizes ($n = 2$ and 3), almost did not change with temperature. Because the helical pitch of a N*-LC is inversely proportional to the twisting power of a chiral dopant,⁷⁰ it can be deduced that the helical pitch of the N*-LC induced by (R)-1 will be shortened with a temperature decrease. That is to say, the acetylene polymerization temperature needs to be set at the lower side of the mesophase temperature region for the N*-LC to improve the screw degree of the PA fibrils. But, for the N*-LCs induced

Table 6. Twisting Power (β_M), Specific Rotation ($[\alpha]_D^{23}$) of CEBDs with (*R*)-Configuration, Helical Pitch, and Screw Direction of the Corresponding N*-LCs

type	n^a	CEBDs with (<i>R</i>)-configuration			N*-LCs ^c		
		CEBD (methylene spacer)	$[\alpha]_D^{23}$	β_M (μm^{-1}) ^b	helical pitch (μm) ^b	screw direction ^d	
disubstituted CEBDs	1	(<i>R</i>)-1 ($m = 6$)	+48.7	64.3	3.1	right-handed	
	2	(<i>R</i>)-2 ($m = 6$)	+24.5	51.3	4.2	right-handed	
	3	(<i>R</i>)-3 ($m = 6$)	+15.3	15.4	13.0	right-handed	
	1	(<i>R</i>)-4 ($m = 12$)	+22.8	53.2	3.8	right-handed	
	2	(<i>R</i>)-5 ($m = 12$)	+7.5	35.0	5.7	right-handed	
monosubstituted CEBDs	1	(<i>R</i>)-6 ($m = 6$)	-39.1	20.6	9.7	left-handed	
	1	(<i>R</i>)-7 ($m = 12$)	-25.0	16.1	12.4	left-handed	

^a n is the number of oxidimethylene repeat units in crown ether. ^b Measured with Cano's wedge method at room temperature (see Scheme 6). ^c Composed of PCH302, PCH304, and chiral dopant with the mole ratio of 100:100:1. ^d Determined with miscibility test in which cholesteryl oleyl carbonate is being used as standard N*-LC.

Scheme 7. (*R*)-(+)-1,1'-Bi-2-naphthol (Left) and (*R*)-(–)-1,1'-Binaphthyl-2,2'-diyl Hydrogen Phosphate (Right)

by (*R*)-2 and (*R*)-3, the polymerization temperature can be set at any point in the mesophase temperature region because the helical pitch will almost not change with temperature.

It is well-known that the conformation of the crown ether can be changed by adding a cation of a suitable size (e.g., K^+ , Cu^{2+}) into solution. The twisting power of the CEBDs may be controlled through this conformational change of the crown ether. Here it is desirable to examine the host–guest reactivity of CuCl_2 with the CEBDs. When CuCl_2 was added into the CHCl_3 solution of the CEBDs, the color of the solution changed from colorless to red. The DSC results showed that the original peaks of the CEBDs disappeared, whereas new peaks appeared with the addition of CuCl_2 . Meanwhile, the ^1H NMR spectra showed that the peaks derived from the chemical shifts of protons in the crown ether broadened with the addition of CuCl_2 . These results implied the formation of a host–guest complex between the crown ether and Cu^{2+} . The twisting powers of the disubstituted CEBDs decreased slightly by 4–6 μm^{-1} after complex formation with CuCl_2 . It is likely that the degree of decrease in the twisting power is larger in the CEBD with a smaller crown ether ring size. This suggests that complex formation tends to weaken the axial chirality of the CEBD by depressing the twisting of the binaphthyl dihedral angle, and that this is more effective in the CEBD with a smaller crown ether ring size. One may remark that the twisting power of the CEBDs can be adjusted to some extent through the host–guest interaction between the crown ether and the cation.

7.1.3. Spiral Morphologies of N*-LCs and H-PAs

As shown in Table 6, the helical pitch of N*-LCs induced by CEBDs varied from 3.0 to 13.1 μm upon changing the ring size of the crown ether, methylene spacer, and the number of binaphthyl moieties. The helical pitch of the N*-LC induced by (*R*)-1, which is the shortest one studied here, further decreased from 3.2 to 2.6 μm when the temperature decreased from 32 to 10 $^\circ\text{C}$. In this way, the N*-LC with the shortest helical pitch could be obtained.

The screw direction of the N*-LCs induced by the CEBDs were determined through the miscibility test method.¹⁷² This

method is based on the observation of the mixing area between a N*-LC and a standard LC through a POM in which the screw direction of the standard LC is known. If the screw direction of the N*-LC is the same as that of the standard LC, the mixing area will be continuous. Otherwise, it will be discontinuous (shown as Schlieren texture of the nematic LC). The POM image of the mixture of the N*-LC induced by (*R*)-2 and a standard LC of cholesteryl oleyl carbonate (left-handed) shows that there appeared a discontinuous area between the N*-LC and the standard LC. Because the screw direction of the standard LC is known to be left-handed, the screw direction of the N*-LC induced by (*R*)-2 can thus be deduced to be opposite to that of the standard LC, i.e., right-handed.

The screw direction of the N*-LCs induced by disubstituted and monosubstituted CEBDs are listed in the last column of Table 6. The N*-LCs induced by disubstituted CEBDs having (*R*)-configuration all showed a right-handed helical structure, but those induced by monosubstituted CEBDs having the same (*R*)-configuration showed a left-handed helical structure. These results coincide with the opposite symbols in specific rotation of these two kinds of CEBDs (the fourth row in Table 6). Using the disubstituted CEBDs of (*R*)-1, (*R*)-2, and (*R*)-3 for the induction of N*-LCs, and the thus obtained N*-LCs as the reaction field for acetylene polymerization, PA films with helical morphology were synthesized. Note that there were not enough amounts of (*R*)-4 to (*R*)-7 to carry out the polymerization reaction, owing to their low reaction yields. Figure 29 shows SEM photographs of PA film synthesized under a N*-LC induced by (*R*)-2. As shown in this figure, there existed many spiral domains in the film, and the fibrils screwed in a counterclockwise direction to form a bundle, which then screwed in the same direction to form the spiral domain.

It is interesting to investigate the parameters (such as the interdistance between the fibril bundles and diameter of a fibril bundle and that of a fibril) of these H-PAs through magnified SEM images. The parameters of the H-PAs synthesized in the N*-LCs induced by (*R*)-1, (*R*)-2, and (*R*)-3 are summarized in Table 7. The interdistance between the fibril bundles of H-PA decreased with an increase in the twisting power of the CEBDs (decrease of the helical pitch of the N*-LC), and equaled about half the helical pitch of the corresponding N*-LCs. Although the diameter of the fibril bundles decreased with increasing twisting power of the CEBDs, that of a fibril did not change, being in the range of 120–130 nm.

For H-PAs synthesized in the N*-LCs induced by disubstituted CEBDs having (*R*)-configuration, (*R*)-1 to (*R*)-3, the fibrils screwed in a counterclockwise direction (left-handed).

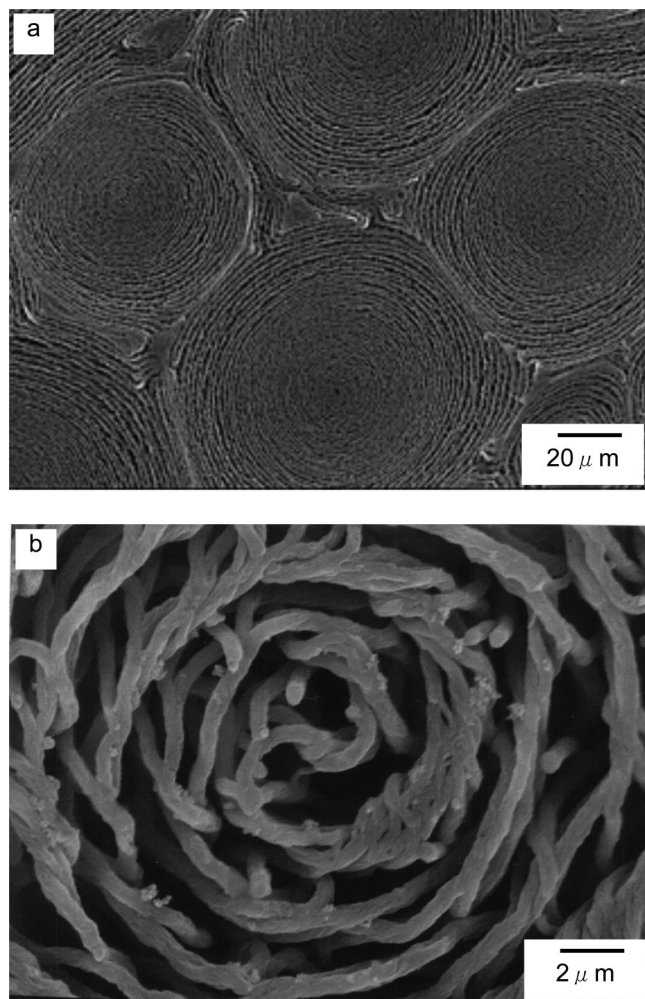


Figure 29. SEM images of the H-PA synthesized in N*-LC induced by (*R*)-2. (b) is the magnified image of (a).

However, the miscibility test showed that the N*-LCs induced by these CEBDs had a right-handed helical structure (the last column of Table 7), from which one can deduce that the screw direction of the fibrils of H-PA is opposite to that of the N*-LC used as the polymerization solvent. This is an unexpected and even surprising result, requiring a sound interpretation. It has been elucidated so far that the PA chains propagate along the director (an average direction for LC molecules within a domain) of the N*-LC. Since the helical axis of PA is parallel to the PA chain, and the director of the N*-LC is perpendicular to the helical axis of the N*-LC, the helical axis of PA is perpendicular to that of the N*-LC. Taking into account these aspects, a plausible mechanism for interfacial acetylene polymerization in the N*-LC can be drawn (see Figure 8 in section 2). In the case of a right-handed N*-LC, for instance, the PA chain would propagate in a left-handed manner, starting from the catalytic species, but not with a right-handed one. This is because PA chains with the opposite screw direction to that of the N*-LC could propagate along the LC molecules, but those with the same direction as that of the N*-LC would encounter LC molecules, making the propagation stereospecifically impossible.

Based on the results above, it is possible to derive the relationship between the morphology of H-PA and the helical structure of the N*-LC used as the polymerization solvent; i.e., the interdistance between the fibril bundles of H-PA is equal to about half of the helical pitch of the N*-LC, and

the screw direction of the PA fibrils is opposite to that of the N*-LC. These results are very important hints for clarifying the formation mechanism of H-PA in the asymmetric reaction field of the N*-LC.

H-PA films synthesized in this research were trans-rich polymers because a relatively high polymerization temperature of 16–18 °C was adopted to maintain the N* phase. The electrical conductivities of the films were in the range of $1.5\text{--}2.0 \times 10^3$ S/cm after iodine doping. With such a high electrical conductivity, H-PA has become one of the most prospective electrical conductive polymers for application. Research on the helical structure control and application of H-PA are ongoing.

In summary, a series of crown ether-type binaphthyl derivatives were synthesized and used as chiral dopants to induce N*-LCs. The twisting powers of the CEBDs for phenylcyclohexane-derived nematic LC were evaluated. It was found that the twisting power of the CEBDs increased with decreasing crown ether ring size. With increasing twisting power of the CEBDs, the interdistance between the fibril bundles of H-PA decreased, and the diameter of a fibril bundle decreased, but the diameter of a fibril showed no change. The interdistance between fibril bundles of H-PA equaled about half of the helical pitch of the N*-LC, and the screw direction of the fibrils was opposite to that of the N*-LC. The CEBDs should be promising chiral dopants to precisely control the screwed structures of the conjugated polymers, by virtue of the ring size effect of the crown ether and the host–guest interaction.

8. Control of the Helical Sense

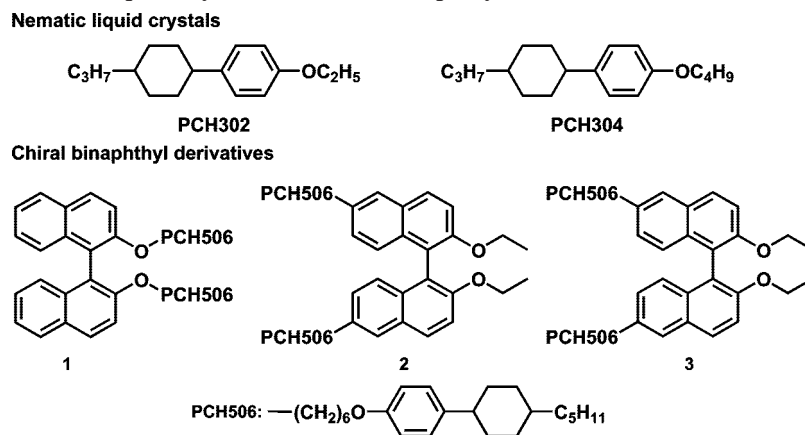
8.1. Chiral Dopants of Bridged- and Nonbridged-Type Binaphthyl Derivatives

One of the currently rejuvenated interests on the science of chirality is a chiral induction on a LC through chiral transcription from a chiral compound to an achiral nematic LC (N-LC). It has been elucidated that the chiral nematic LC (N*-LC) or cholesteric LC induced by the addition of the chiral compound, as a chiral dopant, into the N-LC is available for construction of the asymmetric reaction field, which enables us to synthesize helical conjugated polymers.¹⁷³ Chiral dopants are mainly employed as chiral center-containing compounds and axially chiral ones.^{148,174} The axially chiral binaphthyl derivatives are found to be feasible for the control of the helical sense and strength of the N*-LC, especially when they are chemically modified in molecular structure, such as by the introduction of long alkyl chains or mesogenic substituents into the binaphthyl rings. Besides, these chiral dopants play an essential role in determining the twisting direction of the helical conjugated polymer and even its spiral morphology synthesized in the N*-LC.¹⁵²

It is well-known that the chiral binaphthyl derivatives are atropisomers, and they are classified into (*R*) [*rectus*; right-handed or clockwise] and (*S*) [*sinister*; left-handed or counterclockwise] configurations, according to a difference in the twisting direction of the dihedral angle between the 1,1'-positions of the binaphthyl rings. It seems that the chirality is straightforwardly determined by the twisting direction of the dihedral angle. However, there is some experimental evidence to be taken into account when one judges the chirality. One example is that (*R*)-(+)-1,1'-bi-2-naphthol and (*R*)-(–)-1,1'-binaphthyl-2,2'-diyl-hydrogen-

Table 7. Parameters of Helical PAs Synthesized in N*-LCs Induced by Disubstituted CEEDs with (R)-Configuration

chiral dopant		N*-LC		helical PA	
CEED	twisting power (μm^{-1})	helical pitch (μm)	interdistance between fibril bundles ($\pm 0.2 \mu\text{m}$)	diameter of a fibril bundle ($\pm 0.2 \mu\text{m}$)	diameter of a fibril ($\pm 20 \text{ nm}$)
(R)-1	64.3	3.1	1.6	0.5	120
(R)-2	51.3	4.2	2.0	0.6	120
(R)-3	15.4	13.0	7.0	2.5	130

Scheme 8. Structures of Nematic Liquid Crystals and Chiral Binaphthyl Derivatives

phosphate are dextro-rotatory (+) and levo-rotatory (−), respectively, despite having the same (R)-configuration. The former has a nonbridged structure, and the latter has a bridged structure linking two oxygen atoms at the 2,2′-positions of the binaphthyl rings via a $-\text{P}(\text{O})(\text{OH})$ moiety.¹⁷¹ Another example is as follows: the mono- and disubstituted crown ether-type binaphthyl derivatives having the same (R)-configuration give rise to opposite signs in specific rotation (specific rotatory power), though both of them have bridged structures. These experimental facts suggest that the chirality (helicity) of the binaphthyl derivative sensitively depends on the local structure around the 2,2′-positions of the binaphthyl rings, such as bridged structure, and also on the twisting direction and degree of the dihedral angle defined by the binaphthyl rings. Namely, it remains unsolved how both the bridged structure and the change of the dihedral angle affect the helicity of the N*-LC.

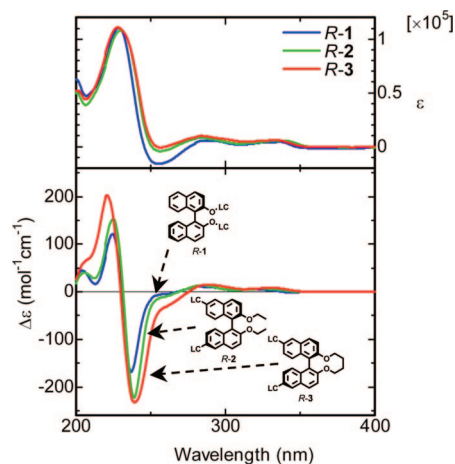
This section focuses on the nonbridged and bridged-type binaphthyl derivatives, where the latter has a linkage between the 2- and 2′-positions of the binaphthyl rings through a tetramethylene chain.¹⁷⁵ By focusing on these binaphthyl derivatives with the same configuration, one can rationalize why and how they give rise to N*-LCs with opposite helical twisting directions when used as chiral dopants to N-LCs. H-PA synthesized in N*-LCs thus prepared are examined in terms of the helical screw direction of the fibril bundles by means of SEM and CD measurements.

8.1.1. Synthesis and Characterization of Chiral Binaphthyl Derivatives

Scheme 8 shows the molecular structure of the binaphthyl derivatives. (R)- or (S)-1,1′-Binaphthyl-2,2′-bis-[para-(trans-4-n-pentylcyclohexyl)phenolxy-1-hexyl]ether (abbreviated as (R)-1 or (S)-1) and (R)- or (S)-6,6′-bis-[para-(trans-4-n-pentylcyclohexyl)phenolxy-1-hexyl]-2,2′-diethoxy-1,1′-binaphthyl ((R)-2 or (S)-2) were synthesized as the nonbridged binaphthyl derivatives. (R)- or (S)-6,6′-Bis-[para-(trans-4-n-pentylcyclohexyl)phenoxy-1-hexyl]-2,2′-butyl-bridged-1,1′-bi-2-naphthol ((R)-3 or (S)-3) was synthesized as the

bridged binaphthyl derivatives. Bromination of (R)-(-)-1,1′-bi-2-naphthol in CH_2Cl_2 gave (R)-(-)-6,6′-dibromo-1,1′-bi-2-naphthol ((R)-4) as a white solid.¹⁷⁶ Williamson etherification between (R)-4 and 1,4-dibromobutane gave compound (R)-5 as a white solid. A Grignard reaction between (R)-5 and 1-[para-(trans-4-n-pentylcyclohexyl)phenoxy]-6-bromohexane [PCH506Br] gave (R)-3 as a pale yellow solid. Figure 30 shows the UV-vis and CD spectra of the present nonbridged ((R)-1, (R)-2) and bridged ((R)-3) binaphthyl derivatives. The bands associated with the transitions of the binaphthyl rings are shown: the $^1\text{B}_b$ transition at 200–250 nm, the $^1\text{L}_a$ transition at 250–300 nm, and the $^1\text{L}_b$ transition at 300–350 nm. In the CD spectra, the nonbridged ((R)-1, (R)-2) and bridged ((R)-3) binaphthyl derivatives with an (R)-configuration show a negative Cotton effect for the $^1\text{B}_b$ transition and intense positive Cotton effects for the $^1\text{L}_a$ and $^1\text{L}_b$ transitions.

N*-LCs were prepared by adding 1.5 mol % of axially chiral binaphthyl derivatives ((R)-1, (R)-2, (R)-3; (S)-1, (S)-2, (S)-3) as chiral dopants to the equimolar mixture of N-LCs, 4-(trans-4-n-propylcyclohexyl)ethoxybenzene [PCH302] and

**Figure 30.** UV-vis and CD spectra of the nonbridged ((R)-1, (R)-2) and bridged ((R)-3) binaphthyl derivatives in *n*-heptane.

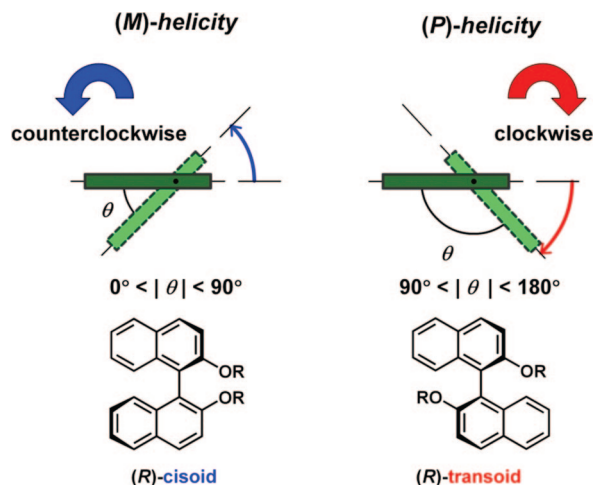


Figure 31. Structures of cisoid and transoid forms of the binaphthyl derivatives with an (*R*)-configuration.

4-(*trans*-4-*n*-propylcyclohexyl)butoxybenzene [PCH304]. The N*-LCs induced by (*R*)-1 and (*S*)-1, abbreviated as ((*R*)-1)-LC and ((*S*)-1)-LC, respectively, showed fingerprinted textures in the POM. Similar fingerprinted textures were also observed in the N*-LCs induced by (*R*)-2, (*R*)-3, (*S*)-2, and (*S*)-3. The temperature range of the N* phase was 14–32 °C in the heating process and –12 to 31 °C in the cooling process.

The binaphthyl derivative has restricted freedom in internal rotation along the carbon–carbon bond between the 1- and 1'-positions of the binaphthyl rings. The helicity of the binaphthyl derivative therefore depends on the dihedral angle (θ) between the two binaphthyl rings. For instance, the (*R*)-binaphthyl derivative of the cisoid conformation ($0^\circ < \theta < 90^\circ$) and that of the transoid one ($90^\circ < \theta < 180^\circ$) have (*M*)- and (*P*)-helicity, respectively, as described in Figure 31. It has been clarified so far that the binaphthyl derivatives of (*M*)- and (*P*)-helicity induce N*-LCs with counterclockwise and clockwise twisting directions, respectively, when they are added as chiral dopants into a N-LC.^{110,111,177–179}

The CD spectrum can be interpreted in terms of the exciton coupling theory.^{180–182} The sign and intensity of the CD couplet are related to the value of the dihedral angle (θ) between the two binaphthyl rings. The (*R*)-binaphthyl derivatives give a negative couplet for θ in the range from 0° to 110° and a positive couplet from 110° to 180° , with negative and positive maxima at 60° and 140° , respectively.^{183–188} The values of De at approximately 230 nm become larger in the order of the nonbridged (*R*)-1 and (*R*)-2 and the bridged (*R*)-3 binaphthyl derivatives, as shown in Figure 30. Thus, the dihedral angles become smaller in this order. The nonbridged ((*R*)-1, (*R*)-2) and bridged ((*R*)-3) binaphthyl derivatives show positive couplets around 230 nm, indicating (*M*)-helicity. It is therefore implied that (*R*)-1, (*R*)-2, and (*R*)-3 should form cisoid conformations in isotropic solvent like *n*-heptane. It is worth noting that this argument is supported by the results of the CD spectra of (*R*)-1, (*R*)-2, and (*R*)-3 in cyclohexane, one of the isotropic solvents. Positive couplets were also observed in these nonbridged binaphthyl derivatives, confirming the favorableness of the cisoid conformation in an isotropic solvent.

8.1.2. Characterization of the N*-LC

The helical pitch of the N*-LC was determined using the Cano method,¹⁸⁹ by means of POM under temperature

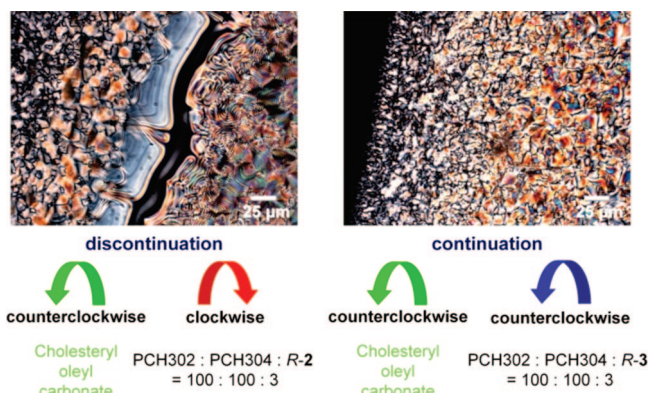


Figure 32. Contact method between the N*-LC induced by (*R*)-2 or (*R*)-3 and the standard LC, cholesteryl oleyl carbonate of the counterclockwise screw direction.

control. The Cano's wedge was warmed up in a hot stage to the preset temperature at the heating rate of 10 °C/min. After enough time passed and a heat equilibrium state was reached, the helical pitch of the N*-LC was measured by using the Cano method. The absolute value of the helical twisting power (HTP; β_M), defined as $\beta_M = (pc)^{-1}$, was calculated as the reciprocal of the product between the helical pitch (p) and the mole fraction of the chiral dopant (c). The concentration of the chiral dopant was 15 mmol %, where the concentrations of PCH302 and PCH304 and the chiral dopant were 100:100:3 in molar ratio, respectively.

We examined the temperature dependence of HTP (β_M) of (*R*)-1, (*R*)-2, and (*R*)-3. It is found that HTP depends on the dihedral angle between the two naphthyl moieties. The HTPs of the nonbridged binaphthyl derivatives ((*R*)-1, (*R*)-2) largely decrease with increasing temperature. Meanwhile, the HTP of the bridged binaphthyl derivative ((*R*)-3) slightly decreases with increasing temperature. This is due to the rigidity between the two naphthyl rings, where the 2- and 2'-positions of the binaphthyl rings are bridged with a tetramethylene chain.

Cholesteryl oleyl carbonate is known to be a counterclockwise N* (cholesteric) LC, and it is useful for the standard LC in the contact method to examine the helical sense of the N*-LC.¹²⁶ This method is based on the observation of the mixing area between the N*-LC and the standard LC using POM. When the screw direction of the N*-LC is the same as that of the standard LC, the mixing area will be continuous. Otherwise, it will be discontinuous. As shown in Figure 32, the mixture of ((*R*)-1)-LC or ((*R*)-2)-LC and cholesteryl oleyl carbonate gave the boundary of the Schlieren texture in POM. In contrast, the mixture of ((*R*)-3)-LC and cholesteryl oleyl carbonate showed no change in the optical texture. These results indicate that the screw direction of the ((*R*)-1)-LC or ((*R*)-2)-LC induced by the nonbridged binaphthyl derivative is opposite to that of cholesteryl oleyl carbonate. On the other hand, the screw direction of ((*R*)-3)-LC is the same as that of cholesteryl oleyl carbonate. That is, the screw directions of the ((*R*)-1)-LC and ((*R*)-2)-LC are clockwise and that of ((*R*)-3)-LC is counterclockwise. Thus, the N*-LC induced by (*R*)-1 or (*R*)-2 and that by (*R*)-3 have opposite screw directions from each other, though the nonbridged ((*R*)-1, (*R*)-2) and bridged ((*R*)-3) binaphthyl derivatives have the same configuration.

Figure 33 show UV–vis and CD spectra of the nonbridged ((*R*)-1, (*R*)-2) and bridged ((*R*)-3) binaphthyl derivatives in N-LC solvent. The nonbridged ((*R*)-1, (*R*)-2) binaphthyl

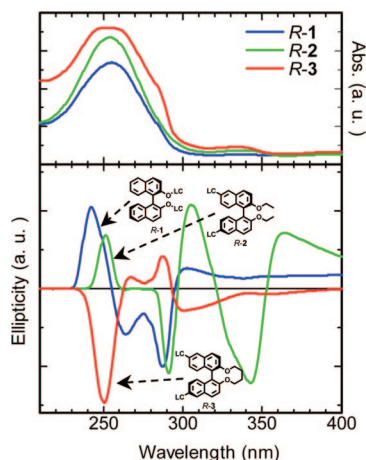


Figure 33. UV-vis and CD spectra of the nonbridged ((*R*)-1), (*R*)-2) and bridged ((*R*)-3) binaphthyl derivatives in LC (PCH302/PCH304 = 1:1) at room temperature.

derivatives showed positive Cotton effects in the region of 250 nm, and the bridged (*R*-3) derivative showed a negative Cotton effect. This result implies that the nonbridged ((*R*)-1, (*R*)-2) and bridged ((*R*)-3) binaphthyl derivatives have different conformations in LCs. Namely, the experimental facts that the nonbridged binaphthyl derivatives ((*R*)-1, (*R*)-2) showed positive Cotton effects and that they showed a clockwise screw direction in LC solvent indicate that they have (*P*)-helicity (transoid). On the other hand, the fact that the bridged binaphthyl derivative ((*R*)-3) showed a negative Cotton effect and a counterclockwise screw direction in LC solvent indicates that it has (*M*)-helicity (cisoid).

8.2. Helical Twisting Directions of N*-LCs and H-PAs

The stable conformations of the binaphthyl derivatives are examined by molecular mechanics (MM) calculations.¹⁹⁰ In the nonbridged binaphthyl derivative (*R*)-2, both the cisoid conformation ($\theta = 66^\circ$) and the transoid one ($\theta = 108^\circ$) have almost the same stability. In the bridged binaphthyl derivative (*R*)-3, the cisoid conformation ($\theta = 61^\circ$) is more stable by 21.3 kcal/mol than the *meta*-cisoid one ($\theta = 84^\circ$). The dihedral angle ($\theta = 66^\circ$) of the nonbridged binaphthyl derivative (*R*)-2 is larger than that ($\theta = 61^\circ$) of the bridged binaphthyl derivative (*R*)-3.

MM calculations indicated that, in the nonbridged binaphthyl derivative (*R*)-2, the stability of the cisoid and transoid conformations is almost equal. In the bridged binaphthyl derivative (*R*)-3, the cisoid conformation is the stable one.¹⁹¹ Such a difference between the nonbridged and bridged binaphthyl derivatives may cause opposite screw directions of the N*-LCs, though they have the same configuration. The nonbridged binaphthyl derivatives ((*R*)-1, (*R*)-2) showed negative Cotton effects in *n*-heptane, whereas they showed positive Cotton effects in the N-LC. This suggests that (*R*)-1 and (*R*)-2 have cisoid conformations ((*M*)-helicity) in *n*-heptane, but they have transoid ones ((*P*)-helicity) in the N-LC. It is shown that (*R*)-2 has two possible conformations, cisoid and transoid, where the former is slightly more stable by 2.4 kcal/mol than the latter. It is evident that the cisoid conformation is favorable in isotropic solvent such as *n*-heptane. Nevertheless, although it is not so clear at present, there is a possibility that (*R*)-2 takes the *meta*-stable transoid conformation in a specific environment like a LC. It is important to account for entropy effects in the molecular

interactions between the nonbridged binaphthyl derivatives of the transoid conformation and the surrounding self-assembled LC molecules.

On the other hand, the bridged binaphthyl derivative ((*R*)-3) has strictly restricted freedom in the internal rotation of the binaphthyl rings, giving a stable cisoid conformation, as found in Figure 35. Thus, (*R*)-3 shows (*M*)-helicity due to the cisoid conformation, resulting in a negative Cotton effect, irrespective of the isotropic (*n*-heptane) and anisotropic (N-LC) solvent.

As shown in Figure 34, PA films synthesized in ((*R*)-1)-, ((*R*)-2)-, and ((*R*)-3)-LCs showed helical fibrillar morphologies with counterclockwise and clockwise directions, respectively. Thus, the nonbridged ((*R*)-1, (*R*)-2) and bridged ((*R*)-3) binaphthyl derivatives give rise to H-PAs with opposite screw directions to each other, in spite of the fact that both of them have the same chirality. It should be noted here that the twisting direction of ((*R*)-1)-LC is clockwise, for instance, and the screw direction of the H-PA synthesized under ((*R*)-1)-LC is counterclockwise.

Figure 35 shows the CD spectra of H-PA films synthesized in N*-LCs including the nonbridged [(*R*)-2)-, (*S*)-2)-LCs] or bridged [(*R*)-3)-, (*S*)-3)-LCs] binaphthyl derivatives. It is evident that PA films have Cotton effects in the region from 450 to 800 nm, corresponding to a $\pi \rightarrow \pi^*$ transition of the conjugated PA chain, and that the signs of the Cotton effects are opposite to each other between the PA films synthesized in the N*-LCs, including the nonbridged and bridged binaphthyl derivatives. These results are consistent with those of the helical twisted directions of the PA fibrils observed in SEM photographs, as shown in Figure 34.

It is useful to summarize the signs of the Cotton effects and the screw directions of the binaphthyl derivatives, N*-LC and H-PAs. The chiral dopants, (*R*)-1 to (*R*)-3, showed a negative CD couplet (240 nm) in the CD spectra, as shown in Figure 30. This means that the nonbridged ((*R*)-1, (*R*)-2) and the bridged ((*R*)-3) binaphthyl derivatives have the same chirality. However, the N*-LCs induced by the nonbridged binaphthyl derivatives, ((*R*)-1) and ((*R*)-2)-LCs, showed clockwise screw directions, which are opposite to that of ((*R*)-3)-LC. As shown in Figure 33, ((*R*)-1)- and ((*R*)-2)-LCs showed positive Cotton effects around 250 nm, and ((*R*)-3)-LC showed a negative Cotton effect.

The CD spectra of H-PA films synthesized in ((*R*)-1)- or ((*R*)-2)-LCs showed positive Cotton effects in the region from 450 to 800 nm. On the other hand, the CD spectrum of a H-PA film synthesized in ((*R*)-3)-LC showed a negative Cotton effect. PA films synthesized in ((*R*)-1)-, ((*R*)-2)-, and ((*R*)-3)-LCs showed helical fibrillar morphologies with counterclockwise and clockwise directions, respectively. This can be understood by the fact that H-PA is formed by replicating the screwed structure of the N*-LC used as an asymmetric reaction field, and hence the screwed directions of the H-PA synthesized in the N*-LCs including the nonbridged ((*R*)-1, (*R*)-2) and bridged ((*R*)-3) binaphthyl derivatives are counterclockwise and clockwise, respectively. This also holds in the case of the chiral dopants of (*S*)-configuration, (*S*)-1 to (*S*)-3.

Figure 36 shows the structures of the nonbridged and bridged binaphthyl derivative with an (*R*)-configuration in the N*-LC and SEM images of the H-PA synthesized in the N*-LC induced by these binaphthyl derivatives. The nonbridged and bridged binaphthyl derivatives with (*R*)-configuration take the transoid conformation due to (*P*)-helicity

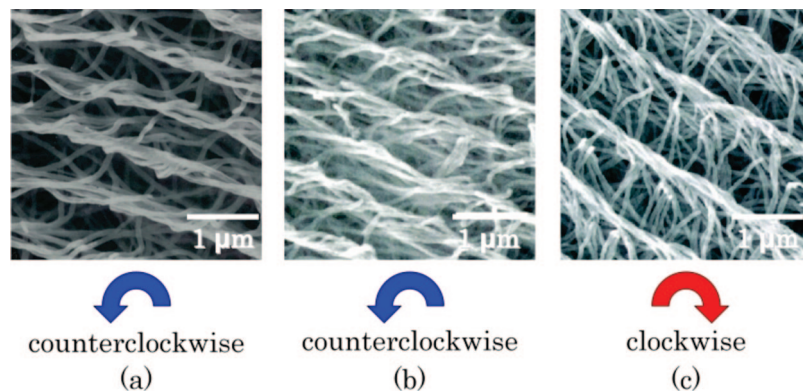


Figure 34. SEM photographs of H-PA synthesized in (a) ((*R*)-1)-LC, (b) ((*R*)-2)-LC, and (c) ((*R*)-3)-LC.

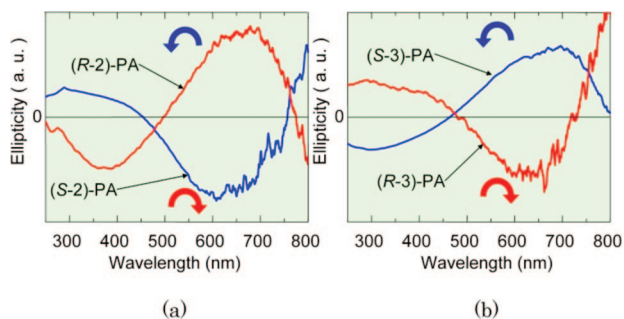


Figure 35. CD spectra of H-PA films synthesized in (a) ((*R*)-2)-LC and ((*S*)-2)-LC and (b) ((*R*)-3)-LC and ((*S*)-3)-LC.

and the cisoid conformation due to (*M*)-helicity in the N*-LC, respectively. Therefore, the N*-LCs induced by these types of binaphthyl derivatives show clockwise and counterclockwise screw directions. The screw directions of the N*-LC and H-PA fibril are opposite to each other, respectively. Namely, it follows that PA films synthesized in the N*-LC induced by the nonbridged and bridged binaphthyl derivative with an (*R*)-configuration have fibril morphologies with counterclockwise and clockwise screwed directions, respectively.

In summary, the nonbridged and bridged binaphthyl derivatives were synthesized and used as chiral dopants to N-LCs. The bridged structure has a linkage between the 2- and 2'-positions of the binaphthyl rings through a tetramethylene chain. It is found that the conformation of the nonbridged binaphthyl derivative changes between isotropic and N-LC solvents to give a different helicity, although its configuration remains unchanged. Namely, the nonbridged binaphthyl derivative exhibits cisoid (most stable) and transoid (metastable) conformations in isotropic and N-LC solvents, respectively. Meanwhile, the bridged derivative forms a cisoid conformation irrespective of solvent, as expected by the strictly restricted internal rotation of the binaphthyl rings. As a consequence, the nonbridged and bridged binaphthyl derivatives with an (*R*)-configuration take on (*P*)-helicity due to the transoid conformation and (*M*)-helicity due to the cisoid conformation in N-LCs, respectively. This leads to oppositely screwed N*-LCs when these binaphthyl derivatives are added as chiral dopants into N-LCs, though they have the same configuration. Concomitantly, H-PAs synthesized in the N*-LCs also have oppositely screwed structures in fibril bundles. The usage of the nonbridged and bridged binaphthyl derivatives, as chiral inducers having the same configuration but the opposite helical sense, affords a convenient way to construct the helicity-controlled LC reaction field.

9. Control of the Helical Twisting Power and Helical Sense

9.1. Chiral Dopants of Double Chirality-Based Binaphthyl Derivatives

Asymmetric polymerization in a chiral nematic liquid crystal (N*-LC), used as an asymmetric reaction field, has attracted current interest since it has been demonstrated to be promising for providing not only helical structure but also spiral morphology in rigid π -conjugated polymers composed of nonchiral repeating units. In fact, several types of helical conjugated homopolymers and copolymers have been successfully synthesized through chemical or electrochemical polymerization in a N*-LC. The N*-LC itself can be prepared by adding a small amount of chiral compound, as a chiral dopant or a chirality inducer, into a nematic liquid crystal (N-LC). It has been elucidated that the screw direction of the helical conjugated polymer is determined by the helical sense of the N*-LC, and that the helical sense itself is controllable by selecting the chirality of the chiral dopant.⁷⁰ However, the spiral morphology and even the screw direction of the helical conjugated polymer cannot be changed nor modified after polymerization because the conjugated polymer, if without side chains,^{18,30,31,38,192,193} is infusible and insoluble in organic solvent.¹⁵ This means that two kinds of N*-LCs with opposite helical sense might be required for synthesizing helical conjugated polymers with opposite screw directions such as right- and left-handed screw structures. It is therefore required to create an advanced chiral dopant that can afford both a helical sense and helical pitch-controllable N*-LC, so far as one tries to control the helical sense of the conjugated polymer by using only one kind of N*-LC.

The thermally induced chiral inversion reported so far can be classified into two categories. One is to mix two kinds of N*-LCs and another is to use one kind of N*-LC with a peculiar temperature dependence in the helical sense. The former is furthermore classified into three approaches: (i) two kinds of cholesterol derivatives with different helical twisting powers are added into the N-LC,^{150,170,195,196} (ii) two kinds of cholesteric LCs with opposite helical sense are mixed,¹⁹⁷ or (iii) two kinds of cholesteric LCs with the same helical sense are mixed.^{198,199} On the other hand, the latter is also classified into two approaches: (iv) a N*-LC composed of a double chiral center-containing compound with opposite helicity, different twisting power, and different temperature dependence is used^{200,201} or (v) a N*-LC composed of a single chiral center-containing compound is

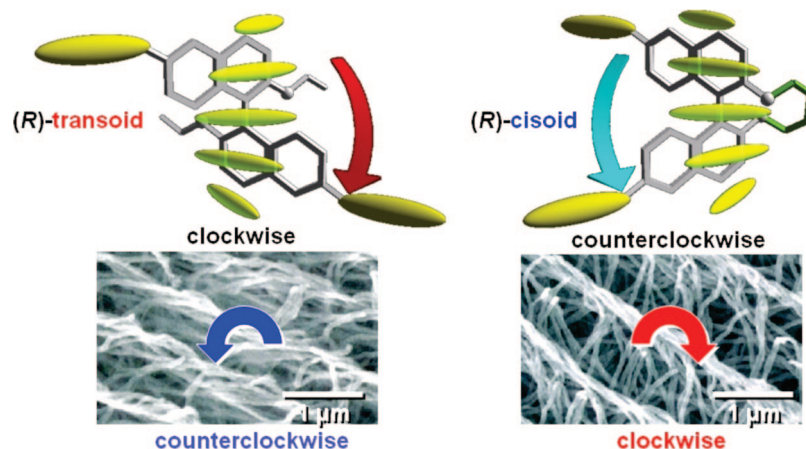


Figure 36. Model structures of the nonbridged (top left) and bridged (top right) binaphthyl derivative with an (*R*)-configuration in N^* -LC. The nonbridged and bridged binaphthyl derivatives take the transoid conformation due to (*P*)-helicity (clockwise) and the cisoid one due to (*M*)-helicity (counterclockwise) in N^* -LC. The SEM images of PA films synthesized in N^* -LC induced by the nonbridged (bottom left) and bridged (bottom right) binaphthyl derivative showed helical fibrillar morphologies with counterclockwise and clockwise directions, respectively.

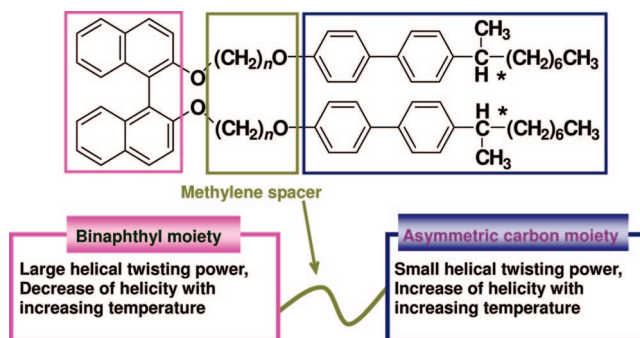
used.^{202–204} The mechanism for the helical inversion using one kind of N^* -LC still remains unclear.

The above-mentioned N^* -LC or cholesteric LC, however, would not be available for an asymmetric reaction field since the molecular species in the N^* -LCs include several kinds of functional groups such as ester, carbonyl, ene, yne, and chlorine atom. Namely, these functional groups should be reactive to catalyst and/or monomers, which might cause a subreaction and even the destruction of the LC reaction field. From the viewpoint of an asymmetric reaction field, where the helicity of the N^* -LC is replicated to the reaction product, it is essential to prepare a N^* -LC composed of chemically stable and nonreactive LC molecules and chiral compounds. It is also desirable for practical use that the N^* -LC is highly twisted, and that the temperature of the N^* -LC is close to room temperature for the sake of safety, especially in the case of acetylene polymerization.

This section focuses on an axially chiral binaphthyl derivative as well as an asymmetric center-containing chiral compound. The former (binaphthyl derivative) is known to possess a large twisting power and thermal stability.⁷⁵ These properties are attributed to large steric repulsions between hydrogens at the 2- and 2'-positions and those at the 8- and 8'-positions in the naphthyl rings.^{107,111,148} It is suggested that the twisting power of the binaphthyl derivative might be almost independent of temperature, owing to its large thermal stability. Meanwhile, the latter (the asymmetric center-containing chiral compound), such as **D-1**, is found to exhibit an opposite temperature dependence in helical twisting power,^{164,205,206} compared with that of the binaphthyl derivative. Hence, it might be possible to obtain a helical inversion-controllable N^* -LC by mixing both the binaphthyl compound and the asymmetric center-containing chiral one. Up to now, the helical inversion attributable to the binaphthyl derivatives by modifying the molecular structure has been reported.^{113,151} However, the helical inversion from the temperature dependence has not been reported.

To achieve the large temperature dependence in helical twisting power of the binaphthyl derivative, a novel chiral compound is designed where the binaphthyl moiety is linked with the asymmetric carbon moiety through flexible methylene chains in a molecule (Scheme 9).²⁰⁷ This is because the combination of the binaphthyl derivative with large temperature dependence and the asymmetric center-contain-

Scheme 9. Design of Double Chirality-Based Chiral Compound



ing compound should enable us to control the helical pitch of the N^* -LC and even to enable the helical inversion, by virtue of the different temperature dependence in twisting power between the two moieties. Scheme 9 describe novel N^* -LCs that exhibit not only an extraordinarily large temperature dependence in the helical pitch but also a temperature-dependent helical inversion.

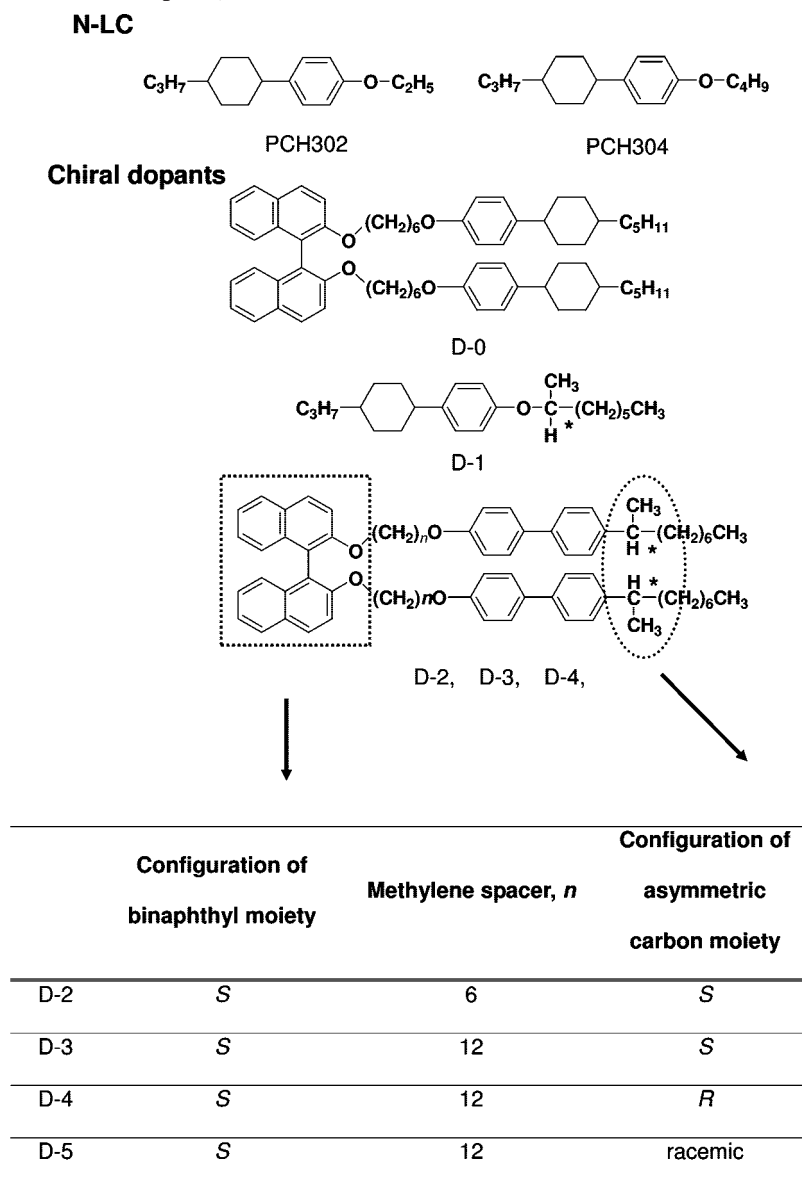
9.1.1. Synthesis of Double Chirality-Based Binaphthyl Derivatives

The asymmetric center-containing PCH derivative, 4-(*trans*-4-*n*-propylcyclohexyl)-[(*S*)-2-methyl]heptyloxybenzene, is abbreviated as **D-1**. The novel double chirality-based binaphthyl derivatives are abbreviated as **D-2** to **D-5**, where the biphenyl-type mesogenic moieties linked with chiral nonyl terminal group of (*S*)-, (*R*)-, or racemic configuration via a hexyl- or dodecylmethylene spacer are substituted at the 2,2'-positions of the binaphthyl ring, as shown in Scheme 10. For instance, **D-3** is a (*S*)-1,1'-binaphthyl-2,2'-bis[*para*-[4-(*S*)-2-methyl]-octyloxy]biphenyloxy-dodecyl}ether. It is also useful to abbreviate the name of the liquid crystals as PCH302 and PCH304, which stand for 4-(*trans*-4-*n*-propylcyclohexyl)ethoxybenzene and 4-(*trans*-4-*n*-propylcyclohexyl)butoxybenzene, respectively.

9.1.2. Preparation of the N^* -LC

The N^* -LCs were prepared by adding a small amount of chiral dopant into an equimolar mixture of two kinds of N -LCs of PCH302 and PCH304. It should be noted that

Scheme 10. Nematic LCs and Chiral Dopants, D-0 to D-5



although each compound (PCH302 or PCH304) shows a N-LC phase, the LC temperature region is very narrow, i.e., less than 1–2 °C. This is not suitable for acetylene polymerization in a nematic or chiral nematic LC reaction field because the exothermal heat evoked during the acetylene polymerization would increase the temperature inside the polymerization vessel and easily destroy the LC phase. Hence, the LC mixture was prepared by using two equimolar LCs. In the LC mixture, the nematic–isotropic temperature, T_{N-I} , and the crystalline–nematic temperature, T_{C-N} , were raised and lowered, respectively. Actually, the mixture exhibited the N-LC phase in the temperature region from 20 to 35 °C. Three kinds of N*-LCs were induced by adding a small amount of chiral dopants into the equimolar mixture of PCH nematic LC. Due to the effect of supercooling, the N*-LC phase consisting of the LC mixture and the chiral dopants were maintained in the temperature range from 0 to 30 °C. This sufficiently wide temperature region enabled us to examine the feasibility for the helical sense inversion in the present N*-LC system.

9.1.3. Temperature Dependence of N*-LCs

Figure 37 shows the temperature dependence of the helical pitch (p) and helical twisting power (β_M) of the N*-LC, which was induced by adding the axially chiral binaphthyl compound PCH506-Binol of (*R*)-configuration (abbreviated as **D-0**) into the equimolar mixture of PCH nematic LC. The PCH506-Binol was synthesized according to the previously reported procedure.^{10,75} It is clear that the binaphthyl derivative possesses a large twisting power and thermal stability. These properties are attributed to large steric repulsions between hydrogens at the 8- and 8'-positions in the naphthyl rings.^{107,111,148} It is also confirmed from this figure that the helical twisting power of the binaphthyl derivative slightly decreases with increasing temperature.

Next, the N*-LC including the asymmetric center-type chiral dopant was prepared by adding **D-1** to the equimolar mixture of PCH nematic LC (**System 1**). The N*-LC induced by the **D-1** of (*S*)-configuration was found to have a right-handed screw structure, and it showed a noteworthy temperature dependence in helical pitch.^{200,201} Namely, the helical pitch (twisting power) decreases (increases), with increasing

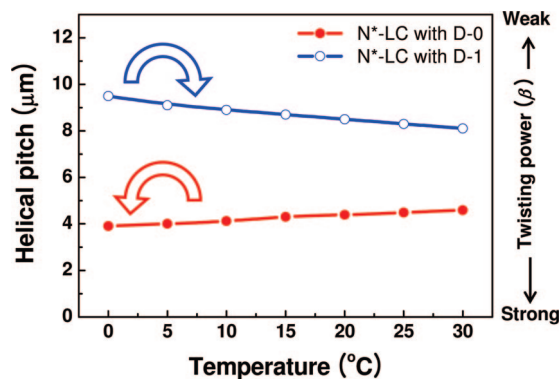


Figure 37. Temperature dependence of the helical pitch (p) and helical twisting power (β_M) of N*-LC induced by the axially chiral binaphthyl derivative, PCH-506-Binol of (*R*)-configuration (**D-0**) (PCH302:PCH304:**D-0** = 100:100:2 in mole ratio) and the asymmetric center-containing chiral compound, (**D-1**) (**System 1**). The helical pitch was determined by Cano's wedge cell method. The twisting power (β_M) was calculated as $\beta_M = (pcr)^{-1}$, where c is the molar concentration of the chiral dopant and r is the enantiomeric purity of the chiral dopant; here, r is assumed to be 1.

temperature, as also shown in Figure 37. This unusual temperature dependence of **D-1** is probably due to the fact that the miscibility of the chiral dopant (**D-1**) in the host nematic LC increased with increasing temperature. Better miscibility enables the chiral dopant to more effectively affect its helicity to the environmental host N-LC, which leads to an increasing twisting power (decreasing in helical pitch). It is noteworthy that the asymmetric center-containing chiral compound, such as **D-1**, has an opposite temperature dependence in helical twisting power (β_M), compared with the binaphthyl derivative, although the absolute value of β_M in the former is considerably smaller than that of the latter. Hence, if two kinds of chiral moieties with opposite temperature dependence and different twisting powers are linked by a flexible molecular chain, the resultant compound having a double chirality might exhibit novel temperature dependence.

Then the novel double chiral compounds **D-2** to **D-5** are designed and synthesized, where the axially chiral binaphthyl moiety is linked with the asymmetric carbon moiety through flexible methylene chains in a molecule (Scheme 9 and Scheme 10).

Four kinds of N*-LCs were prepared by adding the chiral dopants of double chirality-based binaphthyl derivatives (**D-2** to **D-5**) into the equimolar mixture of PCH nematic LC (PCH302:PCH304:(**D-2** to **D-5**) = 100:100:2 in mole ratio). It is known that the axially chiral binaphthyl derivatives of (*S*)-configuration and the asymmetric center moiety containing chiral dopants of (*S*)-configuration induce left- and right-handed N*-LCs, respectively, when each chiral dopant is added to the N-LC. Interestingly, the dopants **D-2** to **D-5**, bearing both the binaphthyl moiety and the asymmetric center-containing moiety, induced left-handed N*-LC. This result indicates that the helicity of the binaphthyl moiety is much larger than that of the asymmetric center-containing moiety, as also shown in Figure 9.2. Therefore, the chiral dopant of **D-3** induces a left-handed screw structure, even after a part cancellation of helicity between the two moieties. The temperature dependence in the helical pitch for the N*-LCs was investigated. In the Cano wedge-type cell, the helical pitch of the N*-LC with **D-3** (**System 2**) notably changed from 3.7 to 9.4 μm with increasing temperature from

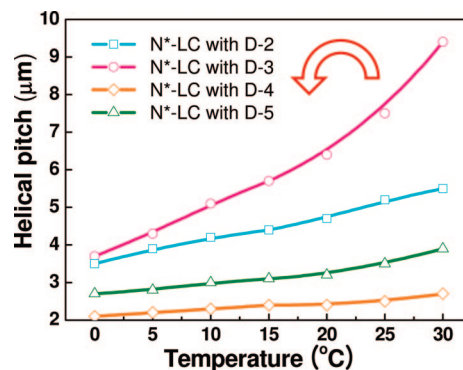


Figure 38. Temperature dependence of the helical pitch of the N*-LCs induced by the chiral dopant of **D-2** to **D-5** (PCH302:PCH304:chiral dopant = 100:100:2 in mole ratio).

0 to 30 $^{\circ}\text{C}$, whereas the left-handed screw structure remained unchanged through the whole range of temperature. It is useful to examine the effect of the spacer length (n) that links the binaphthyl moiety and the asymmetric center moiety. The methylene spacers of the chiral dopants **D-2** and **D-3** are 6 and 12, respectively. The longer spacer allows both chiral moieties to be less restricted in molecular motion, giving more free arrangement toward the environmental parent LCs. Taking into account that the binaphthyl and asymmetric center moieties with the same configurations give opposite helical twisting directions, the helical cancellation in **D-3** with the spacer length of 12 should be larger than that in **D-2** with the spacer length of 6. Namely, both the chiral moieties, especially the asymmetric center moiety, in **D-3** are more effectively enhanced in molecular motion with increasing temperature, leading to a larger helical cancellation and hence a more drastic increase in the helical pitch of the N*-LC than in the case of **D-2**. Moreover, since the binaphthyl moiety of (*S*)-configuration and the asymmetric moiety of (*R*)-configuration induced the same direction (left-handed) of the N*-LC, no cancellation occurred in the case of **D-4**. Thus, the temperature dependence of the N*-LC with **D-4** is the smallest one (Figure 38).

Figure 39 shows POMs of the N*-LC induced by **D-3** at 5 and 30 $^{\circ}\text{C}$ in the cooling process. The interdistance of the striae, which corresponds to a half helical pitch of the N*-LC, was 2.1 μm at 5 $^{\circ}\text{C}$. It increased to 4.6 μm with increasing temperature up to 30 $^{\circ}\text{C}$. We examined the temperature dependence of the N*-LC induced by the chiral dopant of **D-3** (**System 2**). The helicity of the binaphthyl moiety and that of the asymmetric moiety decreased and increased with increasing temperature, respectively. Although the sum of the helicity becomes smaller due to a part cancellation between the two moieties of opposite helical sense at each temperature, it exhibits an unprecedented temperature dependence in the helical twisting power of the N*-LC including **D-3**.

Figure 40 shows changes in the ratios of the helical pitches (P/P_0) as a function of temperature, where P and P_0 are the helical pitches of the N*-LC at an arbitrary temperature and at 0 $^{\circ}\text{C}$, respectively. It has been reported that the value (P/P_0) of the N*-LC induced by the binaphthyl derivative, bearing two LC moieties at the 2- and 2'-positions of the binaphthyl rings, is 1.2 (see Figure 37). Meanwhile, the value of the N*-LC induced by **D-3** (**System 2**) was over 2.5, indicating a large temperature dependence. It should be emphasized that the N*-LC with **D-1** (**System 1**) and those with **D-2** to **D-5** showed opposite temperature dependencies

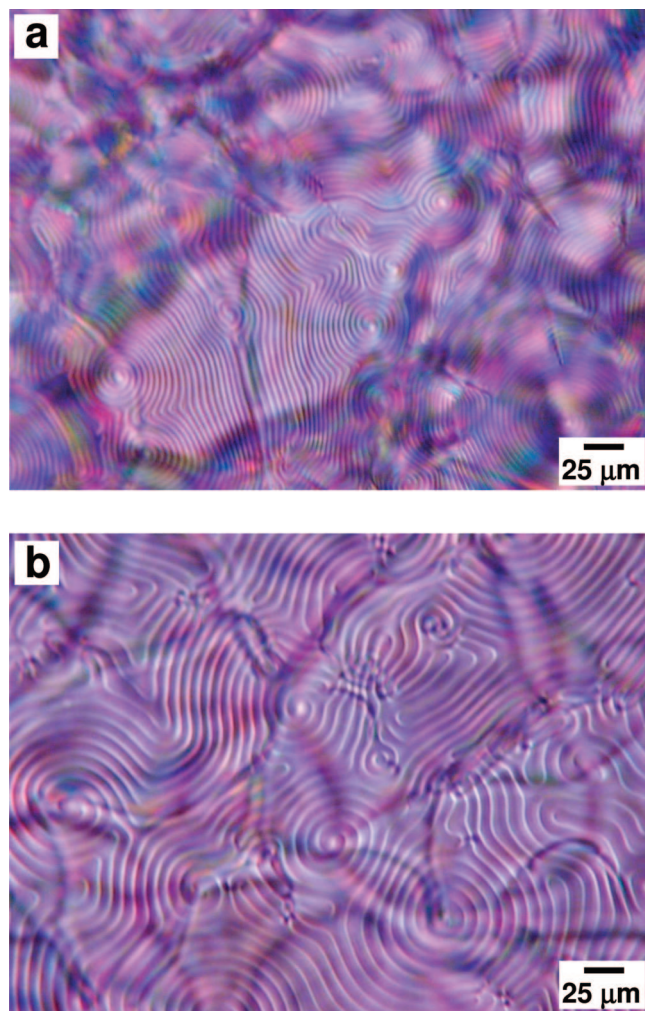


Figure 39. Fingerprint textures with striae observed in POM measurements for the N*-LC with **D-3** (**System 2**) at 5 °C (a) and at 30 °C (b).

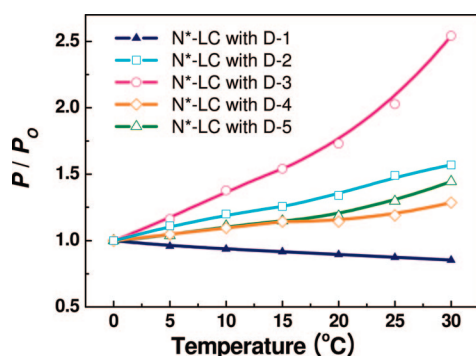


Figure 40. Changes of the variations in helical pitch defined as P/P_0 as a function of temperature. P and P_0 are the helical pitches of the N*-LCs at arbitrary temperature and 0 °C, respectively. The N*-LCs were prepared by **D-1** (**System 1**) or **D-2** to **D-5** (PCH302: PCH304:chiral dopant = 100:100:2 in mole ratio).

in the change of the helical pitch, and that the temperature dependence of the N*-LC with **D-3** (**System 2**) was much larger than those of the others. Thus, it is expected that the chiral dopants of **D-1** and **D-3** might be promising for realizing the helical inversion of the N*-LC when the two chiral dopants are mixed together.

9.2. H-PAAs in Helical Pitch and Helical Sense-Controllable N*-LCs

9.2.1. Helical Pitch-Controllable N*-LC

The helical pitch-controllable N*-LC (**System 2**) was actually used as a reaction field for acetylene polymerization. The acetylene polymerizations were carried out at 0, 10, and 20 °C, where the half helical pitches of the N*-LC were 1.9, 2.6, and 3.4 μm, respectively.

Figure 41 shows POMs of the N*-LCs (**System 2**) and SEM photographs of the H-PA films. The PA films exhibit spiral fibril morphologies, which are quite similar to those of the N*-LCs. It was confirmed that the fibrils screwed clockwise to form helical bundles of fibrils and that the bundles gave rise to the spiral morphology with one-handed screw direction.

It has been elucidated hitherto that the interdistance (a) between the fibril bundles of the H-PA is correlated with half of the helical pitch (p) of the N*-LC, i.e., $a = p/2$. This means that the interdistance of the fibril bundles can be an index to evaluate not only the degree of the twisting of the H-PA but also that of the N*-LC used as a solvent. The interdistances obtained for the present H-PAAs synthesized at 0, 10, and 20 °C were 2.1, 2.9, and 3.6 μm, respectively. They are very close to half of the helical pitches (1.9, 2.6, and 3.4 μm) of the N*-LC observed at 0, 10, and 20 °C, respectively (see Figure 41). This result demonstrates that the screw structure and the spiral morphology of the H-PA are well controlled by changing only the polymerization temperature, when the present helical pitch-controllable N*-LC is used as the asymmetric reaction field. Note that the slightly larger values of the interdistances for the H-PAAs, in comparison with the halves of the helical pitches of the N*-LCs, are probably due to the exothermic heat evolved during the acetylene polymerization. Namely, the exothermic heat might raise the polymerization temperature to increase the helical pitch of the N*-LC used as the polymerization solvent.

9.2.2. Helical Sense-Controllable N*-LCs

The curves of the helical pitches of the N*-LCs induced by **D-1** (**System 1**) and by **D-3** (**System 2**) are crossed at 26 °C, as shown in Figure 42. This suggests that the helical inversion might occur in the N*-LC including both **D-1** and **D-3** as chiral dopants. The N*-LC is prepared by adding these chiral dopants with appropriate ratios into the N-LCs.

The changes in the helical pitch of the N*-LC (**System 3**) as a function of temperature are shown in Figure 43. The polarized optical micrographs of **System 3** are shown in Figure 44. The helical pitch of 4.7 μm at 0 °C increased and became undetectable near 16 °C, as the temperature increased. On further heating, the fingerprint texture reappeared near 20 °C, and the helical pitch decreased to 15 μm at 25 °C. Above 25 °C, the N*-LC phase changed into an isotropic one. The N*-LC showed not only a fast response to temperature change but also good reversibility in the temperature range from 0 to 25 °C. The curves for the helical pitches of **System 1** and **System 2** are crossed at 26 °C, but the N-LC phase appeared from 16 to 19 °C, as seen in Figure 42. This temperature region can be regarded as the compensation point between the two kinds of chiral dopants with opposite helical sense (**D-1** and **D-3**) when dissolved in one N-LC.

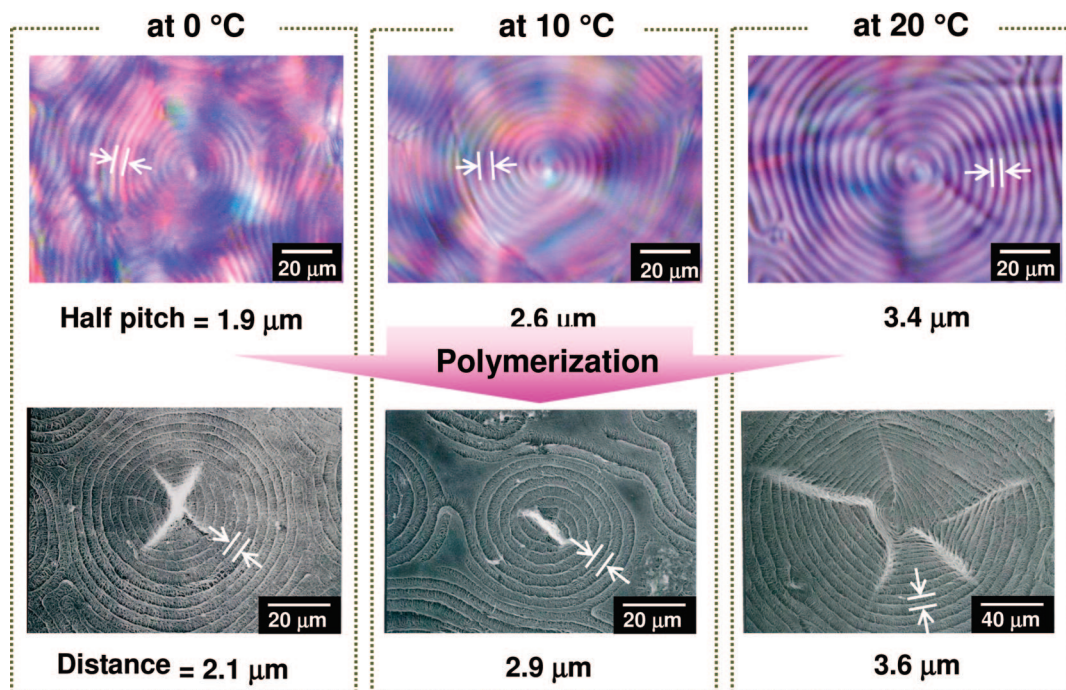


Figure 41. POM textures of N*-LC with D-3 (System 2) at 0 °C (left), 10 °C (middle), and 20 °C (right) and SEM photographs of H-PA synthesized in N*-LC with D-3 at 0 °C (left), 10 °C (middle), and 20 °C (right).

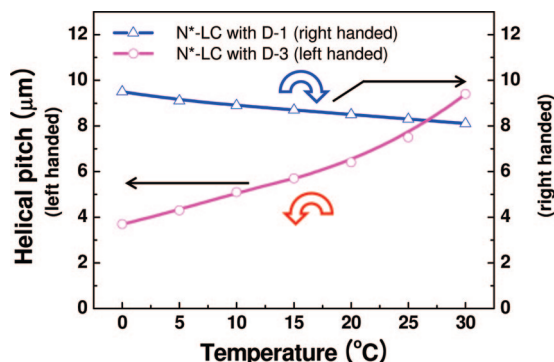


Figure 42. Temperature dependence of the helical pitches of the N*-LCs with D-1 (System 1) and D-3 (System 2).

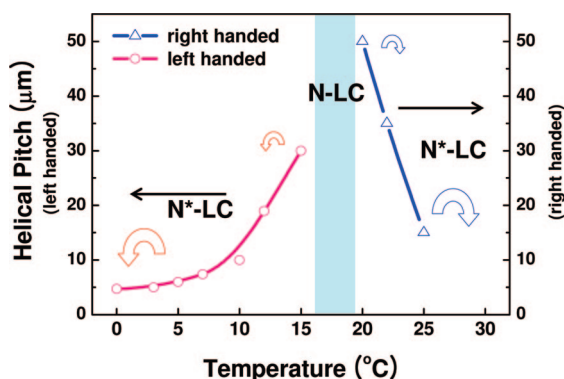


Figure 43. Temperature dependence of the helical pitch of the N*-LC with both D-1 and D-3 (System 3).

Subsequently, the helical sense of the N*-LC with both D-1 and D-3 (System 3) was examined through the miscibility test. The POM photographs of the mixing area between the N*-LC and the cholesteryl oleyl carbonate as a standard LC is also shown in Figure 44. The mixing area was continuous from 0 to 15 °C, indicating that the screw direction of the N*-LC in this temperature range is the same as that of the standard LC. However, from 16 to 19 °C, there

appeared a discontinuous boundary, showing a Schlieren texture characteristic of a nematic LC, between the N*-LC and the standard LC. The fingerprint texture reappeared in the range from 20 to 25 °C, and the screw direction was found to be opposite to that of the standard LC, i.e., right-handed. This means that the screw directions of the N*-LC below and above the compensation point (from 16 to 19 °C) are opposite each other, indicating an occurrence of helical inversion.

A schematic representation of the helical inversion in the N*-LC with both D-1 and D-3 (System 3) is shown in Figure 45. It should be noted that the temperature region above the compensation point is not entirely due to D-1 and that below the compensation point is not entirely due to D-3. At low temperature, the twisting power of D-3 is larger than that of D-1; thus, the sum of twisting power gives the same screwed direction of the N*-LC induced by D-3. The twisting power of D-1 increases with increasing temperature, and then becomes equal to that of D-3 at 16 °C. At this point (compensation point), the twisting powers with opposite directions for D-1 and D-3 cancel out each other, giving a nematic phase. With further increasing temperature, the twisting power of D-1 increases and becomes larger than that of D-3. This leads to a helical inversion in the N*-LC. Acetylene polymerization using the helical inversion-controllable N*-LC is now underway and the results are to be reported in the near future.

In summary, helical pitch and helical sense-controllable N*-LCs were prepared by using the newly synthesized two types of chiral compounds, D-1 and D-2 to D-5. Therein, D-1 is an asymmetric center-containing chiral compound and D-2 to D-5 are so-called “double chiral” compounds consisting of an axially chiral binaphthyl moiety and asymmetric center moieties, linked with methylene spacers. The N*-LC including D-1 (System 1) shows an opposite temperature dependence in helical twisting power to those of the N*-LCs including D-2 to D-5. The chiral dopant D-3, where both the binaphthyl moiety and the asymmetric center have

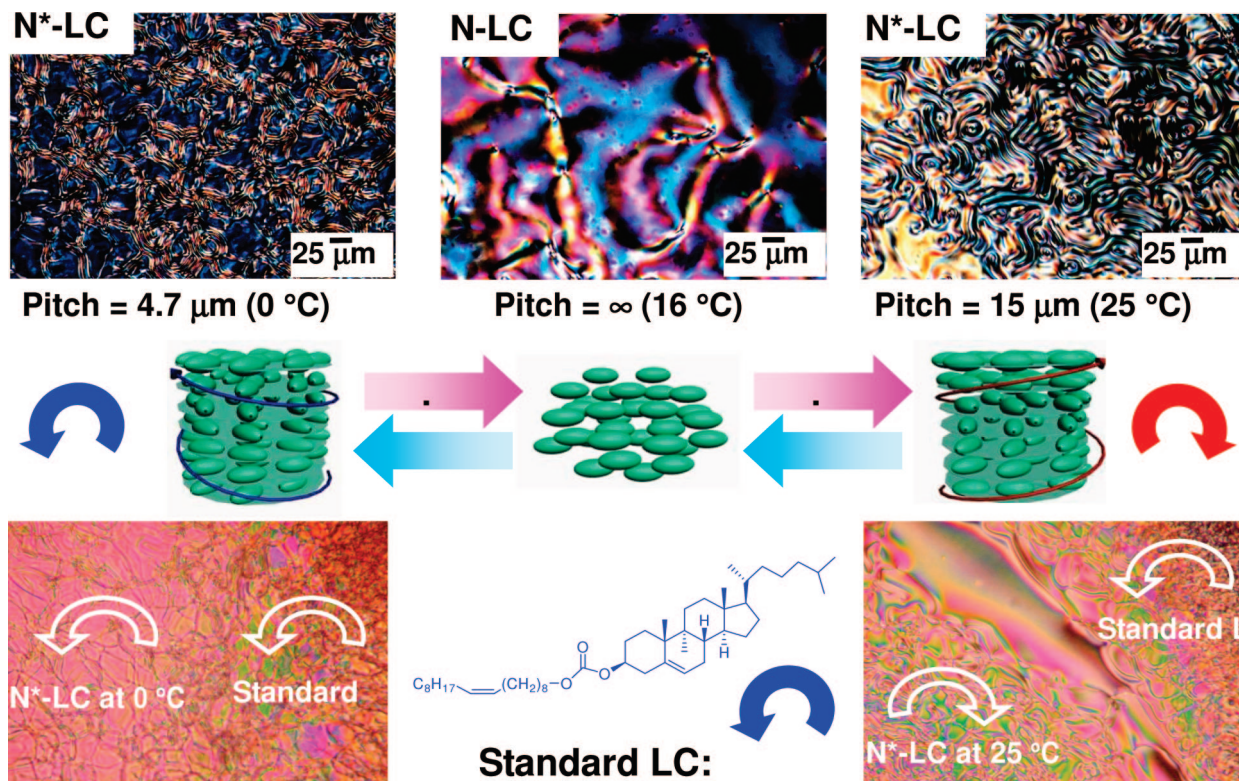


Figure 44. POM textures of N*-LC with both **D-1** and **D-3** by changing temperature (upper), and the miscibility tests between the N*-LC and standard cholesteric LC (lower). The helical sense of the N*-LC (**System 3**) was examined through the miscibility test. The observation of the mixing area between the N*-LC and a cholesteryl oleyl carbonate as a standard LC was carried out through a POM. The mixing area was continuous from 0 to 15 °C. However, from 20 to 25 °C, a discontinuous boundary appeared (a Schlieren texture characteristic of nematic LC) between the N*-LC and the standard LC.

	Screwed direction of N*-LC with D-1 (System 1)	Screwed direction of N*-LC with D-3 (System 2)	Screwed direction of N*-LC with both D-1 and D-3 (System 3)
0 °C			
↑ 17 °C			-
↓ 30 °C			

Figure 45. Schematic representation of helical inversion of N*-LC with both **D-1** and **D-3** (**System 3**). The arrows represent the screw directions of the N*-LCs, and the sizes of the arrows represent the degree of twisting powers of the chiral dopants.

(*S*)-configuration, was most effective for generating a N*-LC (**System 2**) with extraordinarily large temperature dependence. This is due to a substantial cancellation in the helical twisting power between the double chiral moieties having opposite screw directions, although both of them have the same configuration. The helical pitch-controllable N*-LC (**System 2**) enabled us to control the screw structure and the spiral morphology of H-PA by changing only the polymerization temperature. It is further elucidated that the N*-LC including the two types of chiral dopants of **D-1** and **D-3** (**System 3**) exhibited a temperature-dependent helical inversion. The changes in helical sense and helical pitch in the N*-LC were thermally reversible. It is anticipated that the helical sense-controllable N*-LC (**System 3**) may serve as the advanced asymmetric reaction field, which makes it

possible to control the screwed direction of conjugated and nonconjugated polymers through the change of the polymerization temperature.

Part 4. Extension

10. Extension of H-PA

10.1. Morphology-Retaining Carbonization for Helical Graphite

Carbon films are interesting materials because of their special physicochemical and mechanical properties. They have been used in various applications such as electrochemical energy storage,^{208,209} field-effect transistors,^{210,211} cell electrodes,^{210,212} catalyst supports,²¹³ gas-absorbent materials,²⁰⁹ and wear-resistant coating.²¹⁴ Many carbon thin films or membranes supported by substrata have been reported that consist of evaporated amorphous carbon²⁰⁹ and macroscopically aligned or random networks of carbon nanotubes.^{215–218} The freestanding carbon thin film, with a peculiar spiral structure such as hierarchical helical bundles of nanofibrils, is expected to afford novel electrical and electro-magnetic properties. However, it has been considered difficult to prepare a freestanding carbon thin film through the carbonization of an organic polymer film.^{219,220} This is because carbonization at high temperature²²¹ causes thermal decomposition and volatilization of hydrocarbon gases, destroying the morphology of the original film. On the other hand, since iodine doping of the PA film results in a remarkable increase in electrical conductivity, iodine doping has been generally

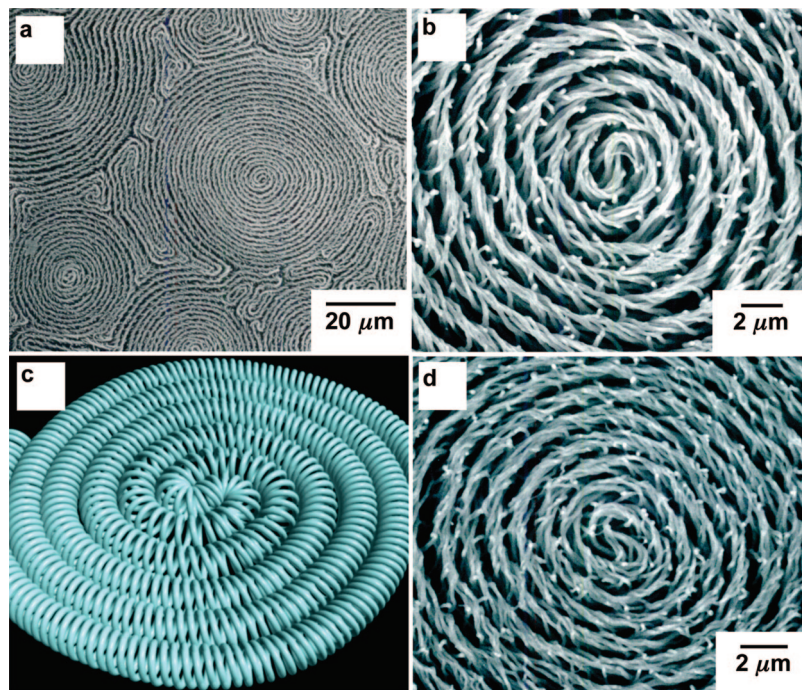


Figure 46. (a) SEM image of the H-PA film and (b) enlarged one. (c) Schematic representation of the helical morphology consisting of twisted bundles of the PA nanofibrils. (d) SEM image of helical graphitic film prepared through a morphology-retaining carbonization of iodine-doped H-PA and then heat treatment at 2600 °C.

adopted to increase the electrical conductivity of a variety of conjugated polymers.^{222–224}

This section focuses on a new aspect of the iodine doping by disclosing its indispensable role in maintaining the nanostructure and morphology of precursors during carbonization.^{225,226} The nanofibril-fabricated H-PA films (Figure 10.1a–10.1c) are used to prepare the freestanding helical carbon thin film. The H-PA film has spiral morphology in which bundles consisting of nanofibrils with diameters below 100 nm are twisted and concentrically curled.

The helical carbon thin films were prepared by carbonization of the iodine-doped H-PA film at high temperature. The atomic ratio of doped iodine-to-carbon in the PA film was about 0.25. The thermal behaviors of the undoped and doped PA films during carbonization were examined using thermogravimetry and differential thermal analysis (TG-DTA). The outgases generated during the heating of the doped PA film up to 500 °C were also examined using gas chromatography-mass spectrometry (GC-MS).

The doped PA film is almost completely carbonized at temperatures above 800 °C. The thermal behavior observed in the TG-DTA curve for the doped PA film is quite different from that of the undoped film. No indication of the thermal decomposition is observed in the DTA curve for the doped PA film. The fibrous morphology of the original structure remains unchanged even after the carbonization and then the heat treatment (Figure 46d). In addition, the weight loss of the films due to carbonization at 800 °C is very small, amounting to only 20% of the weight of the film before iodine doping. Thus, the nanofibril-fabricated carbon film is obtained through the carbonization of the doped PA film. X-ray diffraction of the carbon film prepared from the doped PA film at 800 °C has no crystalline reflection (Figure 47a). The Raman scattering spectrum of the carbon film shows a strong, broad peak at 1350 cm^{-1} attributed to the disordered structure (D-band), together with a comparable peak at 1580 cm^{-1} corresponding to the structure of the sp^2 hexagonal carbon bond network (G-band)¹ (Figure 47b).

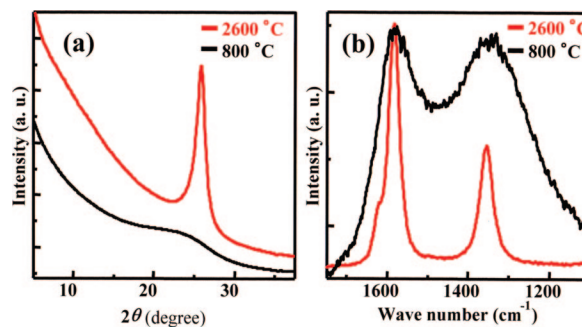


Figure 47. (a) X-ray diffraction intensity curves and (b) Raman scattering spectra for the films carbonized at 800 °C (black) and those heat-treated at 2600 °C after the carbonization (red).

It is apparent that the iodine doping prevents the PA film from thermally decomposing at high temperature. According to the structural model of the iodine-doped PA film,²²⁷ polyiodide ions such as I_3^- and I_5^- are situated between the PA chains, forming a charge transfer complex (Figure 48a). Iodine tends to react with hydrogen at high temperature.²²⁸ Since an outgassing of hydrogen iodide has been detected by GC-MS during heating of the doped PA film, it can be assumed that hydrogen contained in the doped PA is removed to some extent as hydrogen iodide from the PA chains, and that the PA chains partially cross-link between the neighboring chains (Figure 48b). Furthermore, most of the hydrogens are removed with increasing temperature. As a result, the networks of sp^2 hexagonal carbon bonds are formed during carbonization (Figure 48c). These results indicate that the carbon film prepared from the iodine-doped PA film at 800 °C exists in an almost amorphous state.

The carbon film prepared at 800 °C can be further graphitized by heat treatment at 2600 °C, as shown in Figure 47. The two peaks at 1350 and 1580 cm^{-1} become sharp in the Raman spectrum (Figure 47b). The sharp diffraction peak corresponding to the (002) face of a graphitic crystal²²⁹ indicates that the graphitic crystallization occurs in the carbon

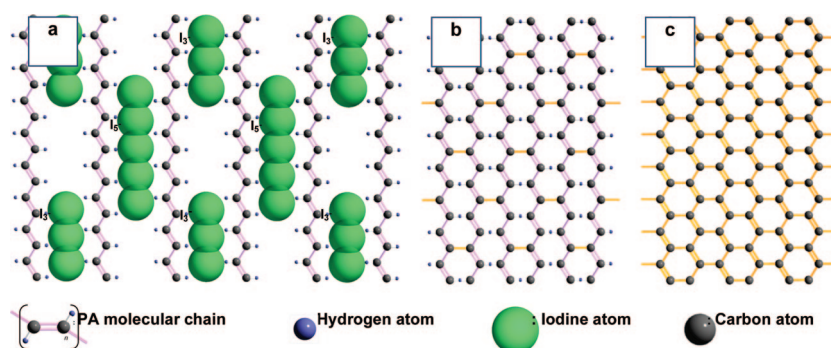


Figure 48. (a) Structural model of the iodine-doped PA. (b) Hypothetical molecular model of the specimen formed on the way to the dehydrogenation reaction from the iodine-doped PA film shown in Figure 48a. (c) Hexagonal carbon bond network formed at 800 °C after passing through the model shown in Figure 48b.

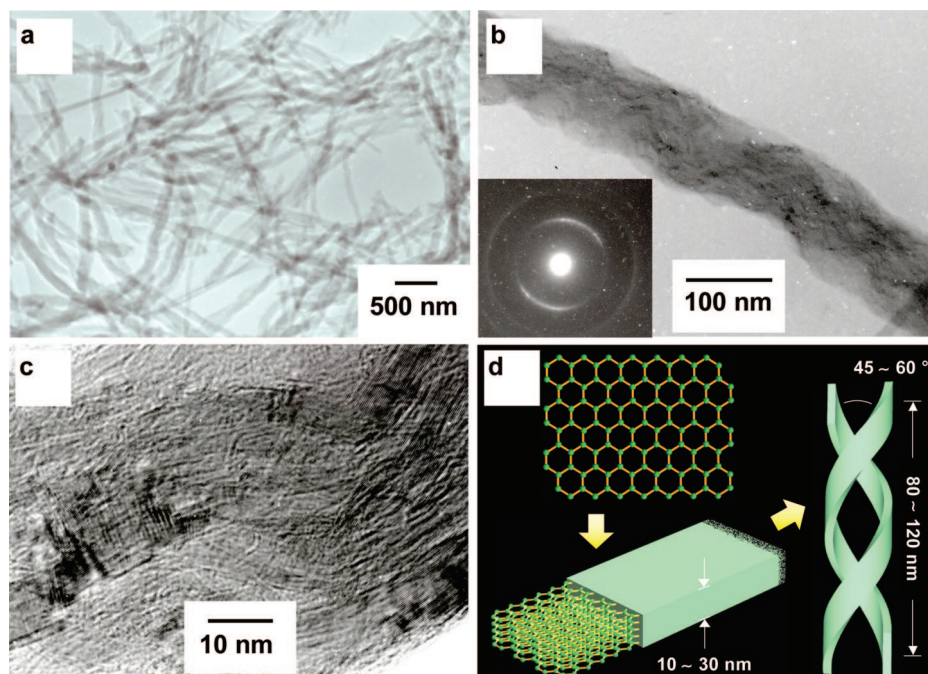


Figure 49. TEM images of (a) the dispersed helical graphitic nanofibrils and (b) a single helical graphitic nanofibril with its electron diffraction pattern (inset). (c) High-resolution TEM image of the helical graphitic nanofibril. (d) Schematic representation of the helical structure consisting of graphitic nanofibrils.

film through the heat treatment at 2600 °C (Figure 47a). It should be emphasized that the carbon film heat-treated at 2600 °C has almost the same helical structure as those of the original H-PA film and the carbon film prepared at 800 °C (Figure 46c,d).

An individual nanofibril in the carbon film can be dispersed by ultrasonication in ethanol. A TEM image of carbon nanofibril and its electron diffraction pattern (EDP) are shown in parts (a) and (b), respectively, of Figure 49. The EDP shows two pairs of the (002) reflection of the graphitic crystals, having an intersection angle in the range of 45–60° along the fibril axis (Figure 49b). From the results of the EDP and a high-resolution TEM image (Figure 47c), a schematic representation of a single helical graphitic nanofibril can be deduced (Figure 47d). The original undoped H-PA film has an electrical conductivity of less than 10^{-5} S/cm.¹¹ Meanwhile, the carbon film and the graphitic one have the conductivities on the order of 10 and 10^2 S/cm, respectively.

It is demonstrated that the iodine doping is quite effective in increasing carbon yield, and in preserving both the helical nanofibril structure and the spiral morphology of the H-PA

films. Moreover, the carbon film obtained by carbonization at 800 °C can be graphitized by heat treatment at 2600 °C while still retaining their original nanofibril-fabricated structures. As-synthesized PA film and even iodine-doped PA one are unstable under atmospheric conditions. This is the reason why the PA films are less feasible for practical use. However, the carbon and graphitic films prepared from the iodine-doped PA films are stable under atmospheric conditions. It is therefore expected that these carbonized films might exhibit intrinsic functions characteristic of the helical structure, and that they might also be used in practical carbon materials.

In summary, the carbonizations of H-PA films by way of iodine doping afford carbon and graphitic films which completely preserve morphologies and even helical nanofibril structures.

11. Conclusions

We summarize the new progress in the hierarchically controlled H-PAs synthesized in the asymmetric reaction field consisting of N*-LC.

Part 1 described the advanced asymmetric reaction field constructed with an N*-LC. The novel tetrasubstituted LC axially chiral binaphthyl derivatives with high helical twisting powers were explored to be useful for inducing a highly twisted N*-LC. The liquid crystallinity of the chiral dopant has no direct influence on the helical twisting power of the N*-LC; it plays the important role of increasing the miscibility of the chiral dopant to host N-LC, leading to an increase of the upper limit in concentration of the chiral dopant. Both the highly helical twisting power and the high miscibility of the chiral dopant are promising for highly twisted N*-LCs.

Part 2 focused on the control of fibril structure and orientation of the morphology of H-PA. It is found that the highly screwed N*-LC with a helical pitch of 270 nm depresses the formation of the bundle of fibrils of H-PA, resulting in a bundle-free fibril morphology consisting of single fibrils. This indicates that the degree of screwing in the N*-LC is a key factor to control the bundle formation and/or depression in the fibril morphology of H-PA. The orientation-controllable N*-LCs enable us to synthesize macroscopically aligned H-PAs with vertically or horizontally oriented fibril morphology. It is found that the chiral titanium complexes, having chiral center-containing groups or axially chiral binaphthyl ones as coordination ligands, not only serve as chiral dopants to N-LCs, giving induced N*-LCs, but also play the role of catalysts for acetylene polymerization.

Part 3 was concerned with the control of the helical twisting power and helical sense of the N*-LC and H-PA. The twisting power of the crown ether-type binaphthyl derivatives increases with decreasing ring size of crown ether. It is found that the bridged- and nonbridged-type binaphthyl derivatives are useful for the control of helical sense of the N*-LC and H-PA because they show oppositely screwed N*-LCs when added as chiral dopants into N-LCs, although they have the same configuration. The helical pitch and helical sense-controllable N*-LCs can be prepared by using the double chiral dopants with opposite temperature dependence in helical twisting power and opposite screw directions. It is anticipated that the helical sense-controllable N*-LC serves as the advanced asymmetric reaction field, enabling us to control the screwed direction of conjugated and nonconjugated polymers through the change of the polymerization temperature.

Part 4 described the morphology-retaining carbonization for helical graphite using H-PA as a carbonization precursor. The carbonizations by way of iodine doping afford carbon and graphitic films with completely preserved morphologies and even helical nanofibril structures of H-PA films.

It is demonstrated that the asymmetric liquid-crystal reaction field composed with N*-LC and Ziegler–Natta catalyst is promising for controlling the hierarchical structure of H-PA. It is worth noting that by using the N*-LC as an asymmetric polymerization solvent, the helix formation is possible not only for PA but also for π -conjugated polymers without chiroptical substituents in the side chains. In fact, very recently, other kinds of spiral morphology containing conjugated polymers such as polybithiophene, polyethylenedioxythiophene derivatives, and phenylene–thiophene copolymers were synthesized through chemical or electrochemical polymerizations in N*-LCs.^{80–83} The asymmetric LC reaction field should be readily applicable to producing next-generation conjugated polymers with innovative func-

tion^{230–233} and a wide range of polymeric materials through control of their chirality and hierarchy.

16. Acknowledgments

The author is grateful to Professor Emeritus Hideki Shirakawa for his invaluable advice and enormous encouragements. The author thanks Dr. Mutsumasa Kyotani for his generous and constructive help in measuring SEM photographs, and he also acknowledges Dr. Guangzhe Piao, Mr. Isao Higuchi, Dr. Shouxue Guo, Mr. Katsuhiko Kanazawa, Mr. Yashutaka Natsuka, Mr. Tetsuya Sato, Dr. Taizo Mori, Dr. Munju Goh, Mr. Satoshi Matsushita, and Mr. Takayuki Matsushita for their helpful cooperation in syntheses, polymerizations, spectroscopic measurements, and structural analyses. This work was supported by a Grant-in-Aid for Science Research (S) (No. 202250007) and that in a Priority Area “Super-Hierarchical Structures” (No. 446) from the Ministry of Education, Culture, Sports, Science and Technology, Japan.

13. References

- (1) Shirakawa, H. *Angew. Chem., Int. Ed.* **2001**, *40*, 2574.
- (2) Heeger, A. J. *Angew. Chem., Int. Ed.* **2001**, *40*, 2591.
- (3) MacDiarmid, A. G. *Angew. Chem., Int. Ed.* **2001**, *40*, 2581.
- (4) *Handbook of Conducting Polymers*; Skotheim, T. A., Ed.; Marcel Dekker: New York, 1986.
- (5) *Handbook of Organic Conductive Molecules and Polymers*; Nalwa, H. S., Ed.; Wiley: New York, 1997.
- (6) *Handbook of Conducting Polymers, Conjugated Polymers*, 3rd ed.; Skotheim, T. A., Reynolds, J. R., Eds.; CRC Press: New York, 2007.
- (7) *Electrical and Optical Polymer Systems: Fundamentals, Methods, and Applications*; Wise, D. L., Wnek, G. E., Trantolo, D. J., Cooper T. M., Gresser J. D., Eds.; Marcel Dekker: New York, 1998.
- (8) Naarmann, H.; Theophilou, N. *Synth. Met.* **1987**, *22*, 1.
- (9) Tsukamoto, J.; Takahashi, A.; Kawasaki, K. *Jpn. J. Appl. Phys.* **1990**, *29*, 125.
- (10) Akagi, K.; Piao, G.; Kaneko, S.; Sakamaki, K.; Shirakawa, H.; Kyotani, M. *Science* **1998**, *282*, 1683.
- (11) Chien, J. C. W. *Polyacetylene -Chemistry, Physics and Material Science*; Academic Press: Orlando, FL, 1984.
- (12) Shirakawa, H.; Louis, E.; MacDiarmid, A. G.; Chiang, C. K.; Heeger, A. J. *J. Chem. Soc., Chem. Commun.* **1977**, 578.
- (13) Chiang, C. K.; Fincher, C. R.; Park, Y. W.; Heeger, A. J.; Shirakawa, H.; Louis, E. J.; Gau, S. C.; MacDiarmid, A. G. *Phys. Rev. Lett.* **1977**, *39*, 1098.
- (14) Shirakawa, H.; Ikeda, S. *Polym. J.* **1971**, *2*, 231.
- (15) Ito, T.; Shirakawa, H.; Ikeda, J. *Polym. Sci., Polym. Chem. Ed.* **1974**, *12*, 11.
- (16) Tanabe, Y.; Kyotani, H.; Akagi, K.; Shirakawa, H. *Macromolecules* **1995**, *28*, 4173.
- (17) Shirakawa, H.; Masuda, T.; Takeda, T. *The Chemistry of Triple-Bonded Functional Groups, Suppl. C2*; Patai, S., Ed.; Wiley: Chichester, U.K., 1994; Vol. 2, Chapter 17, p 945.
- (18) Akagi, K.; Shirakawa, H. *The Polymeric Materials Encyclopedia. Synthesis, Properties and Applications*; Salamone, J. C., Ed.; CRC Press: Boca Raton, FL, 1996; Vol. 5, p 3669.
- (19) Akagi, K.; Shirakawa, H.; *Electrical and Optical Polymer Systems: Fundamentals, Methods, and Applications*; Wise, D. L., Eds.; Marcel Dekker, New York, 1998; Chapter 28, p 983.
- (20) Lam, J. W. Y.; Tang, B. Z. *Acc. Chem. Res.* **2005**, *38*, 745.
- (21) Akagi, K.; Suezaki, M.; Shirakawa, H.; Kyotani, H.; Shimomura, M.; Tanabe, Y. *Synth. Met.* **1989**, *28*, D1.
- (22) Cao, Y.; Smith, P.; Heeger, A. J. *Polymer* **1991**, *32*, 1210.
- (23) Shibahara, S.; Yamane, M.; Ishikawa, K.; Takezoe, H. *Macromolecules* **1998**, *31*, 3756.
- (24) Schermer, O. A.; Grubbs, R. H. *Synth. Met.* **2001**, *124*, 431.
- (25) Schermer, O. A.; Rutenberg, I. M.; Grubbs, R. H. *J. Am. Chem. Soc.* **2003**, *125*, 8515.
- (26) Schuehler, D. E.; Williams, J. E.; Sponsler, M. B. *Macromolecules* **2004**, *37*, 6255.
- (27) Gu, H.; Zheng, R.; Zhang, X.; Xu, B. *Adv. Mater.* **2004**, *16*, 1356.
- (28) Akagi, K.; Sakamaki, K.; Shirakawa, H. *Macromolecules* **1992**, *25*, 6725.
- (29) Theophilou, N.; Aznar, R.; Munardi, A.; Sledz, J.; Schue, R.; Naarmann, H. *Synth. Met.* **1986**, *16*, 337.

- (30) Oh, S. Y.; Akagi, K.; Shirakawa, H.; Araya, K. *Macromolecules* **1993**, *26*, 6203.
- (31) Oh, S. Y.; Ezaki, R.; Akagi, K.; Shirakawa, H. *J. Polym. Sci., Part A: Polym. Chem.* **1993**, *31*, 2977.
- (32) Akagi, K.; Shirakawa, H. *Macromol. Symp.* **1996**, *104*, 137.
- (33) Kuroda, H.; Goto, H.; Akagi, K.; Kawaguchi, A. *Macromolecules* **2002**, *35*, 1307.
- (34) Goto, H.; Dai, X.; Ueoka, T.; Akagi, K. *Macromolecules* **2004**, *37*, 4783.
- (35) Jin, S. H.; Choi, S. J.; Ahn, W.; Cho, H. N.; Choi, S. K. *Macromolecules* **1993**, *26*, 1487.
- (36) Choi, S. K.; Gal, Y. S.; Jin, S. H.; Kim, H. K. *Chem. Rev.* **2000**, *100*, 1645.
- (37) Tang, B. Z.; Kong, X.; Wan, X.; Peng, H.; Lam, W. Y.; Feng, X. D.; Kwok, H. S. *Macromolecules* **1998**, *31*, 2419.
- (38) Kong, X.; Lam, J. W. Y.; Tang, B. Z. *Macromolecules* **1999**, *32*, 1722.
- (39) Geng, J.; Zhao, X.; Zhou, E.; Li, G.; Lam, J. W. Y.; Tang, B. Z. *Polymer* **2003**, *44*, 8095.
- (40) Koltzenburg, S.; Wolff, D.; Stelzer, F.; Springer, J.; Nuyken, O. *Macromolecules* **1998**, *31*, 9166.
- (41) Ting, C. H.; Chen, J. T.; Hsu, C. S. *Macromolecules* **2002**, *35*, 1180.
- (42) Schenning, A. P. H. J.; Franssen, M.; Meijer, E. W. *Macromol. Rapid Commun.* **2002**, *23*, 265.
- (43) Stagnaro, P.; Conzatti, L.; Costa, G.; Gallot, B.; Valenti, B. *Polymer* **2003**, *44*, 4443.
- (44) Araya, K.; Mukoh, A.; Narahara, T.; Shirakawa, H. *Chem. Lett.* **1984**, 1141.
- (45) Akagi, K.; Shirakawa, H.; Araya, K.; Mukoh, A.; Narahara, T. *Polym. J.* **1987**, *19*, 185.
- (46) Akagi, K.; Katayama, S.; Shirakawa, H.; Araya, K.; Mukoh, A.; Narahara, T. *Synth. Met.* **1987**, *17*, 241.
- (47) Akagi, K.; Ito, M.; Katayama, S.; Shirakawa, H.; Araya, K. *Mol. Cryst. Liq. Cryst.* **1989**, *172*, 115.
- (48) Akagi, K.; Katayama, S.; Ito, M.; Shirakawa, H.; Araya, K. *Synth. Met.* **1989**, *28*, D51.
- (49) Sinclair, M.; Moses, D.; Akagi, K.; Heeger, A. J. *Phys. Rev. B* **1988**, *38*, 10724.
- (50) Montaner, A.; Rolland, M.; Sauvajol, J. L.; Galtier, M.; Almairac, R.; Ribet, J. L. *Polymer* **1988**, *29*, 1101.
- (51) Coustel, N.; Foxonet, N.; Ribet, J. L.; Bernier, P.; Fischer, J. E. *Macromolecules* **1991**, *24*, 5867.
- (52) Yamashita, Y.; Nishimura, S.; Shimamura, K.; Monobe, K. *Makromol. Chem.* **1986**, *187*, 1757.
- (53) Bozovic, I. *Mod. Phys. Lett. B* **1987**, *1*, 81.
- (54) Suh, D. S.; Kim, T. J.; Aleshin, A. N.; Park, Y. W.; Piao, G.; Akagi, K.; Shirakawa, H.; Qualls, J. S.; Han, S. Y.; Brooks, J. S. *J. Chem. Phys.* **2001**, *114*, 7222.
- (55) Aleshin, A. N.; Lee, H. J.; Park, Y. W.; Akagi, K. *Phys. Rev. Lett.* **2004**, *93*, 196601.
- (56) Lee, H. J.; Jin, Z. X.; Aleshin, A. N.; Lee, J. Y.; Goh, M. J.; Akagi, K.; Kim, Y. S.; Kim, D. W.; Park, Y. W. *J. Am. Chem. Soc.* **2004**, *126*, 16722.
- (57) Akagi, K.; Piao, G.; Kaneko, S.; Higuchi, I.; Shirakawa, H.; Kyotani, M. *Synth. Met.* **1999**, *102*, 1406.
- (58) Akagi, K. *Polym. Int.* **2007**, *56*, 1192.
- (59) Akagi, K.; Mori, T. *Chem. Record* **2008**, *8*, 395.
- (60) Akagi, K. *Bull. Chem. Soc. Jpn.* **2007**, *80*, 649.
- (61) Akagi, K. *Thermotropic Liquid Crystals: Recent Advances*; Springer: Dordrecht, The Netherlands, 2007; Chapter 9, p 249.
- (62) Akagi, K.; Goto, H.; Shirakawa, H. *Synth. Met.* **1997**, *84*, 313.
- (63) Dai, X.-M.; Goto, H.; Akagi, K.; Shirakawa, H. *Synth. Met.* **1999**, *102*, 1289.
- (64) Goto, H.; Dai, X.-M.; Ueoka, H.; Akagi, K. *Macromolecules* **2004**, *37*, 4783.
- (65) Narihiro, H.; Dai, X.-M.; Goto, H.; Akagi, K. *Mol. Cryst. Liq. Cryst.* **2001**, *365*, 363.
- (66) Dai, X.-M.; Narihiro, H.; Goto, H.; Akagi, K.; Yokoyama, H. *Mol. Cryst. Liq. Cryst.* **2001**, *365*, 355.
- (67) Goto, H.; Dai, X.-M.; Narihiro, H.; Akagi, K. *Macromolecules* **2004**, *37*, 2353.
- (68) Oguma, J.; Dai, X.-M.; Akagi, K. *Mol. Cryst. Liq. Cryst.* **2001**, *365*, 331.
- (69) Suda, K.; Akagi, K. *J. Polym. Sci., Part A: Polym. Chem.* **2008**, *46*, 3591.
- (70) Gottarelli, G.; Mariani, P.; Spada, G. P.; Samori, B.; Forni, A.; Solladie, G.; Hibert, M. *Tetrahedron* **1983**, *39*, 1337.
- (71) Semenkova, G. P.; Kutulya, L. A.; Shkol'nikova, N. I.; Khandrimailova, T. V. *Kristallografiya* **2001**, *46*, 128.
- (72) Guan, L.; Zhao, Y. *J. Mater. Chem.* **2001**, *11*, 1339.
- (73) Hatoh, H. *Mol. Cryst. Liq. Cryst. Sci. Technol., Sect A* **1994**, *250*, 1.
- (74) Lee, H.; Labes, M. M. *Mol. Cryst. Liq. Cryst.* **1982**, *84*, 137.
- (75) Kanazawa, K.; Higuchi, I.; Akagi, K. *Mol. Cryst. Liq. Cryst.* **2001**, *364*, 825.
- (76) Goh, M. J.; Kyotani, M.; Akagi, K. *Curr. Appl. Phys.* **2006**, *6*, 948.
- (77) Schnur, J. M. *Science* **1993**, *262*, 1669.
- (78) Yorozuya, S.; Osaka, I.; Nakamura, A.; Inoue, Y.; Akagi, K. *Synth. Met.* **2003**, *93*, 135.
- (79) Oh-e, M.; Yokoyama, H.; Yorozuya, S.; Akagi, K.; Belkin, M. A.; Shen, Y. R. *Phys. Rev. Lett.* **2004**, *93*, 267402.
- (80) Goto, H.; Akagi, K. *Angew. Chem., Int. Ed.* **2005**, *44*, 4322.
- (81) Goto, H.; Akagi, K. *Macromol. Rapid Commun.* **2004**, *25*, 1482.
- (82) Goto, H.; Akagi, K. *Macromolecules* **2005**, *38*, 1091.
- (83) Goto, H.; Nomura, N.; Akagi, K. *J. Polym. Sci. Part A: Polym. Chem.* **2005**, *43*, 4298.
- (84) Chen, S. H.; Katsis, D.; Schmid, A. W.; Mastrangelo, J. C.; Tsutsui, T.; Blanton, T. N. *Nature* **1999**, *397*, 506.
- (85) Broer, D. J.; Lub, J.; Mol, G. N. *Nature* **1995**, *378*, 467.
- (86) Hikmet, A. M.; Lub, J. *Prog. Polym. Sci.* **1996**, *21*, 1165.
- (87) Witte, P. V.; Brehmer, M.; Lub, J. *J. Mater. Chem.* **1999**, *9*, 2087.
- (88) Shibaev, V.; Bobrovsky, A.; Boiko, N. *Prog. Polym. Sci.* **2003**, *28*, 729.
- (89) Ozaki, M.; Kasano, M.; Kitasho, T.; Ganzke, D.; Haase, W.; Yoshino, K. *Adv. Mater.* **2003**, *15*, 974.
- (90) Cao, W. Y.; Munoz, A.; Palfy-Muhoray, P.; Taheri, B. *Nat. Mater.* **2002**, *1*, 111.
- (91) Song, M. H.; Park, B. C.; Shin, K. C.; Ohta, T.; Tsunoda, Y.; Hoshi, H.; Takanishi, Y.; Ishikawa, K.; Watanabe, J.; Nishimura, S.; Toyooka, T.; Zhu, Z. G.; Swager, T. M.; Takezoe, H. *Adv. Mater.* **2004**, *16*, 779.
- (92) Painter, O.; Lee, R. K.; Scherer, A.; Yariv, A.; O'Brien, J. D.; Dapkus, P. D.; Kim, I. *Science* **1999**, *284*, 1819.
- (93) Saeva, F. D.; Sharpe, P. E.; Oline, G. R. *J. Am. Chem. Soc.* **1975**, *97*, 204.
- (94) Pirkle, W. H.; Rinaldi, P. L. *J. Am. Chem. Soc.* **1977**, *99*, 3510.
- (95) Eskenazi, C.; Nicoud, J. F.; Kagan, H. B. *J. Org. Chem.* **1979**, *44*, 995.
- (96) Nakazaki, M.; Yamamoto, K.; Fujikawa, K.; Maeda, M. *J. Chem. Soc., Chem. Commun.* **1979**, *23*, 1086.
- (97) Hibert, M.; Solladie, G. *J. Org. Chem.* **1980**, *45*, 5393.
- (98) Kang, S. W.; Jin, S. H.; Chien, L. C.; Sprunt, S. *Adv. Funct. Mater.* **2004**, *14*, 329.
- (99) Goto, H.; Jeong, Y. S.; Akagi, K. *Macromol. Rapid Commun.* **2005**, *26*, 164.
- (100) Goto, H.; Akagi, K. *Chem. Mater.* **2006**, *18*, 255.
- (101) Goto, H.; Akagi, K. *J. Polym. Sci., Part A: Polym. Chem.* **2006**, *44*, 1042.
- (102) Coates, D.; Gray, G. W. *Phys. Lett. A* **1973**, *45*, 115.
- (103) Crooker, P. P. *Liq. Cryst.* **1989**, *5*, 751.
- (104) Renn, S. R.; Lubensky, T. C. *Phys. Rev. A* **1988**, *38*, 2132.
- (105) Srajer, G.; Pindak, R.; Waugh, M. A.; Goodby, J. W.; Patel, J. S. *Phys. Rev. Lett.* **1990**, *64*, 1545.
- (106) Eelkema, R.; Feringa, B. L. *Org. Biomol. Chem.* **2006**, *4*, 3729.
- (107) Solladie, G.; Zimmermann, R. *Angew. Chem., Int. Ed. Engl.* **1984**, *23*, 348.
- (108) Bhatt, J. C.; Keast, S. S.; Neubert, M. E.; Petschek, R. C. *Liq. Cryst.* **1995**, *18*, 367.
- (109) Suchod, B.; Renault, A.; Lajzerowicz, J.; Spada, G. P. *J. Chem. Soc., Perkin Trans. II* **1992**, 1839.
- (110) Gottarelli, G.; Hirbert, M.; Samori, B.; Solladie, G.; Spada, G. P.; Zimmermann, R. *J. Am. Chem. Soc.* **1983**, *105*, 7318.
- (111) Gottarelli, G.; Spada, G. P.; Bartsch, R.; Solladie, G.; Zimmermann, R. *J. Org. Chem.* **1986**, *51*, 589.
- (112) Gottarelli, G.; Spada, G. P. *Mol. Cryst. Liq. Cryst.* **1985**, *123*, 377.
- (113) Yoshizawa, A.; Sato, M.; Rokunohe, J. *J. Mater. Chem.* **2005**, *15*, 3285.
- (114) Heppke, G.; Lotzsch, D.; Oestreicher, F. *Z. Naturforsch. A* **1986**, *41*, 1214.
- (115) Li, Q.; Green, L.; Venkataraman, N.; Shiyonovskaya, I.; Khan, A.; Urbas, A.; Doane, J. W. *J. Am. Chem. Soc.* **2007**, *129*, 12908.
- (116) Deussen, H. J.; Shibaev, P. V.; Vinokur, R.; Bjornholm, T.; Schaumburg, K.; Bechgaard, K.; Shibaev, V. P. *Liq. Cryst.* **1996**, *21*, 327.
- (117) Akagi, K.; Guo, S.; Mori, T.; Goh, M.; Piao, G.; Kyotani, M. *J. Am. Chem. Soc.* **2005**, *127*, 14647.
- (118) Delden, R. A.; Mecca, T.; Rosini, C.; Feringa, B. L. *Chem.—Eur. J.* **2004**, *10*, 61.
- (119) Kuball, H. G.; Weiss, B.; Beck, A. K.; Seebach, D. *Helv. Chim. Acta* **1997**, *80*, 2507.
- (120) Seebach, D.; Beck, A. K.; Heckel, A. *Angew. Chem., Int. Ed. Engl.* **2001**, *40*, 92.
- (121) Neal, M. P.; Solymosi, M.; Wilson, M. R.; Earl, D. J. *J. Chem. Phys.* **2003**, *119*, 3567.

- (122) Kuball, H. G.; Höfer, T. *Chirality in Liquid Crystals*; Kitzlerow, H. S., Bahr, C., Eds.; Springer: Dordrecht, The Netherlands, 2000; Vol. 1, Chapter 3, p 67.
- (123) Goh, M.; Akagi, K. *Liq. Cryst.* **2008**, *35*, 953.
- (124) Grandjean, F. C. R. *Acad. Sci.* **1921**, *172*, 71.
- (125) Cano, R. *Bull. Soc. Fr. Mineral.* **1968**, *91*, 20.
- (126) Heppke, G.; Oestreicher, F. *Mol. Cryst. Liq. Cryst.* **1978**, *41*, 245.
- (127) Gottarelli, G.; Samori, B.; Stremmenos, C.; Torre, G. *Tetrahedron* **1981**, *37*, 395.
- (128) Yoshida, J.; Sato, H.; Yamagishi, A.; Hoshino, N. *J. Am. Chem. Soc.* **2005**, *127*, 8453.
- (129) Heppke, G.; Oestreicher, F. *Z. Naturforsch.* **1977**, *32*, 899.
- (130) Bauman, D. *Mol. Cryst. Liq. Cryst.* **1988**, *159*, 197.
- (131) Bauman, D.; Martynski, M. T.; Mykowska, E. *Liq. Cryst.* **1995**, *18*, 607.
- (132) Deussen, H. J.; Shivaev, P. V.; Vinokur, R.; Bjornholm, T.; Schaumburg, K.; Bechgaard, K.; Shivaev, V. P. *Liq. Cryst.* **1996**, *21*, 327.
- (133) Van Hecke, G. R. *J. Phys. Chem.* **1985**, *89*, 2058.
- (134) Aleshin, A. N.; Lee, H. J.; Jhang, S. H.; Kim, H. S.; Akagi, K.; Park, Y. W. *Phys. Rev. B* **2005**, *72*, 153202.
- (135) Lee, S. W.; Kim, B.; Lee, D. S.; Lee, H. J.; Park, J. G.; Ahn, S. J.; Campbell, E. E. B.; Park, Y. W. *Nanotechnology* **2006**, *17*, 992.
- (136) Ofuji, M.; Takano, Y.; Houkawa, Y.; Takanishi, Y.; Ishikawa, K.; Takezoe, H.; Mori, T.; Goh, M.; Guo, S.; Akagi, K. *Jpn. J. Appl. Phys.* **2006**, *45*, 1710.
- (137) Langeveld-Voss, B. M. W.; Janssen, R. A. J.; Christiaans, M. P. T.; Meskers, S. C. J.; Dekkers, H. P. J. M.; Meijer, E. W. *J. Am. Chem. Soc.* **1996**, *118*, 4908.
- (138) Peeters, E.; Christiaans, M. P. T.; Janssen, R. A. J.; Schoo, H. F. M.; Dekkers, H. P. J. M.; Meijer, E. W. *J. Am. Chem. Soc.* **1997**, *119*, 9909.
- (139) Bross, P. A.; Schoberl, U.; Daub, J. *Adv. Mater.* **1991**, *3*, 198.
- (140) Li, W.; Wang, H. L. *J. Am. Chem. Soc.* **2004**, *126*, 2278.
- (141) Iwaura, R.; Hoeben, F. J. M.; Masuda, M.; Schenning, A. P. H. J.; Meijer, E. W.; Shimizu, T. *J. Am. Chem. Soc.* **2006**, *128*, 13298.
- (142) Liu, J.; Rinzler, A. G.; Dai, H.; Hafner, J. H.; Bradley, R. K.; Boul, P. L.; Lu, A.; Iverson, T.; Shelimov, K.; Huffman, C. B.; Rodriguez-Macias, F.; Shon, Y.; Lee, T. R.; Colbert, D. T.; Smalley, R. E. *Science* **1998**, *280*, 1253.
- (143) Ajayan, P. M. *Chem. Rev.* **1999**, *99*, 1787.
- (144) Lee, H.; Labes, M. M. *Mol. Cryst. Liq. Cryst.* **1982**, *84*, 137.
- (145) Hatoh, H. *Mol. Cryst. Liq. Cryst. Sci. Technol., Sect. A* **1994**, *250*, 1.
- (146) Semenikova, G. P.; Kutulya, L. A.; Shkol'nikova, N. I.; Khandri-mailova, T. V. *Kristallografiya* **2001**, *46*, 128.
- (147) Guan, L.; Zhao, Y. *J. Mater. Chem.* **2001**, *11*, 1339.
- (148) Bhatt, J. C.; Keast, S. S.; Neubert, M. E.; Petschek, R. C. *Liq. Cryst.* **1995**, *18*, 367.
- (149) Proni, G.; Spada, G. P.; Lustenberger, P.; Welti, R.; Diederich, F. *J. Org. Chem.* **2000**, *65*, 5522.
- (150) Heppke, G.; Löttsch, D.; Oestreicher, F. *Naturforsch., A: Phys. Sci.* **1987**, *42*, 279.
- (151) Rokunohe, J.; Yoshizawa, A. *J. Mater. Chem.* **2005**, *15*, 275.
- (152) Goh, M.; Kyotani, M.; Akagi, K. *J. Am. Chem. Soc.* **2007**, *129*, 8519.
- (153) Friedel, G. *Ann. Phys. (Paris)* **1922**, *18*, 273.
- (154) Finkelmann, H.; Stegemeyer, H. *Ber. Bunsenges Phys. Chem.* **1978**, *82*, 1302.
- (155) Ferguson, J. L. *Mol. Cryst. Liq. Cryst.* **1966**, *1*, 293.
- (156) Saeva, F. D.; Wysocki, J. J. *J. Am. Chem. Soc.* **1971**, *93*, 5928.
- (157) Piao, G.; Otake, T.; Sato, T.; Akagi, K.; Kyotani, M. *Mol. Cryst. Liq. Cryst.* **2001**, *365*, 117.
- (158) Shirakawa, H.; Otake, T.; Piao, G.; Akagi, K.; Kyotani, M. *Synth. Met.* **2001**, *117*, 1.
- (159) Mori, T.; Sato, T.; Kyotani, M.; Akagi, K. *Synth. Met.* **2003**, *135*, 83.
- (160) Mori, T.; Sato, T.; Kyotani, M.; Akagi, K. *Macromolecules* **2009**, *42*, 1817.
- (161) Uchida, T.; Inukai, T. In *Liquid Crystal-Fundamentals*; Okano, K., Kobayashi, S., Eds.; Baifukan: Tokyo, 1985; pp 205–231.
- (162) Tsuji, T.; Negishi, M.; Yao, K.; Kubo, T.; Takezoe, H.; Fukuda, A.; Scheuble, B. S. *Jpn. J. Appl. Phys.* **1989**, *28*, L1473.
- (163) Araya, K. *Chem. Lett.* **1993**, 1547.
- (164) Matsushita, T.; Goh, M. J.; Kyotani, M.; Akagi, K. *Curr. Appl. Phys.* **2006**, *6*, 952.
- (165) Akagi, K.; Higuchi, I.; Piao, G.; Shirakawa, H.; Kyotani, M. *Mol. Cryst. Liq. Cryst.* **1999**, *332*, 463.
- (166) Piao, G.; Kawamura, N.; Akagi, K.; Shirakawa, H.; Kyotani, M. *Polym. Adv. Tech.* **2000**, *11*, 826.
- (167) Pederson, C. J. *J. Am. Chem. Soc.* **1967**, *89*, 2495–7017.
- (168) Kuhn, R.; Erni, F. *Anal. Chem.* **1992**, *64*, 2815.
- (169) Morrison, R. T.; Boyd, R. N. In *Organic Chemistry (5th edition, I)*; Tokyo Kagaku Dojin: Tokyo, 1989; pp 164–166.
- (170) Finkelmann, H.; Stegemeyer, H. *Z. Naturforsch. A* **1973**, *28*, 799.
- (171) Jacques, J.; Fouquey, C. *Org. Synth.* **1989**, *67*, 1.
- (172) Okano, M.; Kobayashi, S. *Liquid Crystal-Fundamentals*; Baifukan: Tokyo, 1985; p 209.
- (173) Akagi, K. In *Handbook of Conducting Polymers, Conjugated Polymers*, 3rd ed.; Skotheim, T. A., Reynolds, J. R., Eds.; CRC Press: New York, 2007; pp 3–14.
- (174) Sagisaka, T.; Yokoyama, Y. *Bull. Chem. Soc. Jpn.* **2000**, *73*, 191.
- (175) Mori, T.; Kyotani, M.; Akagi, K. *Macromolecules* **2008**, *41*, 607.
- (176) Sogah, G. D. Y.; Cram, D. J. *J. Am. Chem. Soc.* **1979**, *101*, 3035.
- (177) Ferrarini, A.; Moro, G. J.; Norido, P. L. *Mol. Phys.* **1996**, *87*, 485.
- (178) Ferrarini, A.; Moro, G. J.; Norido, P. L. *Phys. Rev. E* **1996**, *53*, 681.
- (179) Rosini, C.; Franzini, I.; Salvadori, P.; Spada, G. P. *J. Org. Chem.* **1992**, *57*, 6820.
- (180) Harada, H.; Nakanishi, K. *Circular Dichroic Spectroscopy Exciton Coupling in Organic Stereochemistry*; University Science Book: Mill Valley, CA, 1983; p 193.
- (181) Berova, N.; Nakanishi, K.; Woody, R. W., Eds. *Circular Dichroism: Principles and Application SE*; Wiley-VCH: New York, 2000; p 337.
- (182) Hanazaki, I.; Akimoto, H. *J. Am. Chem. Soc.* **1972**, *94*, 4102.
- (183) DeVoe, H. *J. Chem. Phys.* **1964**, *41*, 393.
- (184) Zadonmeneghi, M.; Rosini, C.; Salvadori, P. *Chem. Phys. Lett.* **1976**, *44*, 533.
- (185) Bari, L. D.; Pescitelli, G.; Salvadori, P. *J. Am. Chem. Soc.* **1999**, *121*, 7998.
- (186) Mason, S. F.; Seal, R. H.; Roberts, D. R. *Tetrahedron* **1974**, *30*, 1671.
- (187) Rosini, C.; Rosati, I.; Spada, G. P. *Chirality* **1995**, *7*, 353.
- (188) Rosini, C.; Superchi, S.; Peerlings, H. W. I.; Meijer, E. W. *J. Org. Chem.* **2000**, 61.
- (189) Gray, G. W.; McDonnell, D. G. *Mol. Cryst. Liq. Cryst.* **1979**, *40*, 178.
- (190) Rappé, A. K.; Casewit, C. J.; Colwell, K. S.; Goddard, W. A., III; Skiff, W. M. *J. Am. Chem. Soc.* **1992**, *114*, 10024.
- (191) Kuball, H. G.; Türk, O.; Kiesewalter, I.; Dorr, E. *Mol. Cryst. Liq. Cryst.* **2000**, *352*, 195.
- (192) Yashima, E.; Matsushima, T.; Okamoto, Y. *J. Am. Chem. Soc.* **1997**, *119*, 6345.
- (193) Aoki, T.; Kobayashi, Y.; Kaneko, T.; Oikawa, E.; Yamamura, Y.; Fujita, Y.; Teraguchi, M.; Nomura, R.; Masuda, T. *Macromolecules* **1999**, *32*, 79.
- (194) Lam, J. W. Y.; Tang, B. Z. *J. Polym. Sci., Part A: Polym. Chem.* **2003**, *41*, 2607.
- (195) Dierking, I.; Giesselmann, F.; Zugemaier, P.; Kuczynski, W.; Lagerwall, S. T.; Stebler, B. *Liq. Cryst.* **1993**, *3*, 399.
- (196) Mitov, M.; Dessaud, N. *Nat. Mater.* **2006**, *5*, 361.
- (197) Sackmann, E.; Meiboom, S.; Snyder, L. C.; Meixner, A. E.; Dietz, R. E. *J. Am. Chem. Soc.* **1968**, *9*, 3567.
- (198) Baessler, H.; Labes, M. M. *J. Chem. Phys.* **1970**, *52*, 631.
- (199) Baessler, H.; Malya, P. A. G.; Nes, W. R.; Labes, M. M. *Mol. Cryst. Liq. Cryst.* **1970**, *6*, 329.
- (200) Stegemeyer, H.; Siemensmeyer, K. *Naturforsch., A: Phys. Sci.* **1989**, *44*, 1127.
- (201) Dierking, I.; Giesselmann, F.; Zugemaier, P.; Mohr, K.; Zschke, H.; Kuczynski, W. *Z. Naturforsch.* **1994**, *49a*, 1081.
- (202) Slaney, A. J.; Nishiyama, I.; Styring, P.; Goodby, J. W. *J. Mater. Chem.* **1992**, *2*, 805.
- (203) Kuball, H.-G.; Müller, T.; Weyland, H.-G. *Mol. Cryst. Liq. Cryst.* **1992**, *215*, 271.
- (204) Styring, P.; Vuijk, J. D.; Nishiyama, I.; Slaney, A. J.; Goodby, J. W. *J. Mater. Chem.* **1993**, *2*, 399.
- (205) Piao, G.; Akagi, K.; Shirakawa, H.; Kyotani, M. *Curr. Appl. Phys.* **2001**, *1*, 121.
- (206) Emoto, N.; Saito, H.; Furukawa, K.; Inukai, T. *Proc. Jpn. Display* **1986**, *86*, 286.
- (207) Goh, M.; Matsushita, T.; Kyotani, M.; Akagi, K. *Macromolecules* **2007**, *40*, 4762.
- (208) *Carbon: The Future Materials for Advanced Technology Applications*; Messina, G., Santangelo, S., Eds.; Springer: Heidelberg, 2005.
- (209) Centrone, A.; Brambilla, L.; Zerbi, G. *Phys. Rev. B* **2005**, *71*, 245406.
- (210) Wu, J.; Pisula, W.; Müllen, K. *Chem. Rev.* **2007**, *107*, 718.
- (211) Gije, S.; Han, S.; Wang, M.; Wang, K. L.; Kaner, R. B. *Nano Lett.* **2007**, *7*, 3394.
- (212) Wang, X.; Zhi, L.; Müllen, K. *Nano Lett.* **2008**, *8*, 323.
- (213) Adelhelm, P.; Hu, Y.-S.; Chuenchom, L.; Antonietti, M.; Smarsly, B. M. *Adv. Mater.* **2007**, *19*, 4012.
- (214) Miyake, K.; Kusunoki, M.; Usami, H.; Umehara, N.; Sasaki, S. *Nano Lett.* **2007**, *7*, 3285.
- (215) Kocabas, C.; Shim, M.; Rogers, J. A. *J. Am. Chem. Soc.* **2006**, *128*, 4540.
- (216) Simmons, T. J.; Hashim, D.; Vajtai, R.; Ajayan, P. M. *J. Am. Chem. Soc.* **2007**, *129*, 10088.
- (217) Kaiser, A. B.; Skákalová, V.; Roth, S. *Phys. Status Solidi B* **2007**, *244*, 4199.

- (218) Ding, L.; Yuan, D.; Liu, J. *J. Am. Chem. Soc.* **2008**, *130*, 5428.
- (219) Kyotani, M.; Matsushita, S.; Nagai, T.; Matsui, Y.; Akagi, K. *Synth. Met.* **2007**, *157*, 546.
- (220) Kyotani, M.; Goto, H.; Suda, K.; Nagai, T.; Matsui, Y.; Akagi, K. *J. Nanosci. Nanotechnol.* **2008**, *8*, 1999.
- (221) *Thermal Degradation of Polymeric Materials*; Pielichowski, K., Niuguna, J., Eds.; Rapra Technology: Shropshire, 2005.
- (222) Heeger, A. J. *Rev. Mod. Phys.* **2001**, *73*, 681.
- (223) MacDiarmid, A. G. *Rev. Mod. Phys.* **2001**, *73*, 701.
- (224) Shirakawa, H. *Rev. Mod. Phys.* **2001**, *73*, 713.
- (225) Kyotani, M.; Matsushita, S.; Nagai, T.; Matsui, Y.; Shimomura, M.; Kaito, A.; Akagi, K. *J. Am. Chem. Soc.* **2008**, *130*, 10880.
- (226) Matsushita, S.; Kyotani, M.; Akagi, K. *Synth. Met.*, in press.
- (227) Roth, S.; Bleier, H. *Adv. Phys.* **1987**, *36*, 385.
- (228) *Encyclopedia of Industrial Chemical Analysis*; Snell, F. D., Ettore, L. S., Eds.; Interscience Publishers: New York, 1971.
- (229) *New Carbon: Control of Structure and Functions*; Inagaki, M., Ed.; Elsevier: Amsterdam, 2000.
- (230) Suda, K.; Yoshida, J.; Nimori, S.; Akagi, K. *Synth. Met.* **2009**, *159*, 943.
- (231) Hayasaka, H.; Tamura, K.; Akagi, K. *Macromolecules* **2008**, *41*, 2341.
- (232) Akagi, K. *J. Polym. Sci., Part A: Polym. Chem.* **2009**, *47*, 2463.
- (233) Akagi, K. In *Handbook of Thiophene-Based Material: Applications in Organic Electronics and Photonics*; Perepichka, I. F., Perepichka, D. F., Eds.; John Wiley & Sons: New York, 2009; pp 498–516.

CR900198K